A.D. MCCXXIV

Cooperative Control for Vehicle Platooning: a Complex Network approach

by
Alessandro Salvi

Thesis Supervisors:
Mario di Bernardo
Associate Professor of Automatic Control
Stefania Santini
Assistant Professor of Automatic Control

Thesis for the Degree of Doctor of Philosophy
Department of Electrical Engineering and Information Technology
University of Naples Federico II
Napoli, Italy

Submitted to the Faculty of Engineering, University of Naples Federico II, in partial fulfillment of the requirements for the degree of Doctor of Philosophy.

Copyright © 2014 by Alessandro Salvi
All rights reserved.

Printed in Italy.
Napoli, March 2014.

Acknowledgements

First of all, I would like to express my gratitude to my supervisors, Professor Stefania Santini and Professor Mario di Bernardo for their guidance and support, with helpful suggestions and references which helped me immensely in my research. I will always remember their emphasis on quality research and perseverance for years to come.

I am grateful to Professor Francesco Garofalo for his help during my Ph.D. course.

I thank also all the members from the Sincro Lab: Professor Sabato Manfredi and my collegues Achille Caldara, Michele Pugliese, Francesco Lo Iudice, Francesco Scafuti, Piero De Lellis, Daniel Alberto Burbano Lombana, Giovanni Mancini, Antonio Frezzetti, Carlos Hoyos Ildefonso Velasco, Umberto Montanaro and Giovanna D'Alonso.

Very special mention to the Mechatronics group of Chalmers University of Technology (Göteborg), that has provided a great environment to work in. I am grateful to Professor Paolo Falcone for accepting and hosting me: his endless positive attitude and contagious enthusiasm taught me how to get more and more committed to my goals. I thank Professor Jonas Sjöberg and all the Mechatronics group for let me feel at home for four months. I thank Dr. Robert Hult, Dr. Roozbeh Kianfar, Dr. Josef Nilsson and Dr. Hakan Köroglu for their support, advices and fruitful cooperation, which have enormously contributed to the experimental part of this thesis. I'm also grateful to the Volvo Car Corporation, in particular to Dr. Stefan Solyom, for his support on developing the prototype of autonomous vehicles.

Special thanks to Giuseppe Giordano and Alberto Ghione: I would like to acknowledge them for the happy period I spent in Göteborg.

I thank the colleagues and the staff from the S^2-Move project: Manuela Tufo, Pietro Marchetta, Eduard Natale, Davide De Pasquale, Antonio Tirri and Dario Di Nocera.

I also thank my dear friends Carmela Piccolo, Carla Bertapelle, Katia Piccolo and my classmates Davide Liuzza, Gianfranco Fiore and Antonio Valente.

I'll always be grateful to my parents, Salvatore and Carolina, for their undying love and support. I thank my brother Nicola and my sister in law Rosalia who have helped me at various stages in my life.

Last, but not least, very special thanks to Anna for her love and for patiently standing by me all these years.

Alessandro Salvi.
March, 2014.

Glossary

Notation	**Meaning**
$\mathcal{G}_N^*$	Directed graph of N vertices
$\mathcal{A}_N^*$	Adjacency matrix of $\mathcal{G}_N^*$
$\mathcal{V}_N^*$	Vertices set of $\mathcal{G}_N^*$
$\mathcal{E}_N^*$	Edges set of $\mathcal{G}_N^*$
∇	Incidence matrix of $\mathcal{G}_N^*$
L^*	Laplacian matrix of $\mathcal{G}_N^*$
d_i	i-th vertex degree of $\mathcal{G}_N^*$
D^*	Degree matrix of $\mathcal{G}_N^*$
L_{nm}	Normalized Laplacian matrix of $\mathcal{G}_N^*$
$\mathcal{G}_N$	Weighted directed graph of N vertices
$\mathcal{A}_N$	Adjacency matrix of $\mathcal{G}_N$
$\mathcal{V}_N$	Nodes set of $\mathcal{G}_N$
$\mathcal{E}_N$	Edges set of $\mathcal{G}_N$
L	Weighted Laplacian matrix of $\mathcal{G}_N$
$\bar{d}_i$	i-th vertex degree of $\mathcal{G}_N$
D	Degree matrix of $\mathcal{G}_N$
$\mathcal{N}_i$	i-th vertex neighbors set of $\mathcal{G}_N$
$\mathcal{V}_N^s$	Clusters of $\mathcal{G}_N$
$\mathcal{N}_{\mathcal{V}_N^s}$	Neighbors set of $\mathcal{V}_N^s$
$\bar{L}$	Normalized weighted Laplacian matrix of $\mathcal{G}_N$
$\mathcal{G}_{N+1}$	Augmented weighted directed graph
$r_i(t)$	i-th vehicle position, $\forall i \in \{1, \ldots, N\}$
$v_i(t)$	i-th vehicle velocity, $\forall i \in \{1, \ldots, N\}$
M_i	i-th vehicle mass
$u_i(t)$	Coupling protocol on the i-th node, $\forall i \in \{1, \ldots, N\}$
$\tau_{ij}(t)$	Time delays when node i obtains information from node j
h_{ij}	Constant headway time
d_{ij}^{st}	Distance at standstill between vehicles i and j
τ	Maximum delay
k_{ij}	Stiffness coefficients
b	Damping coefficient
$\bar{x}(t)$	Error state vector
$\tau^\star$	Time delay upper-bound

Acronyms

Notation	Meaning
ACC	Adaptive Cruise Control
AHS	Automated Highways System
CACC	Cooperative Adaptive Cruise Control
CAN	Controller Area Network
DGPS	Differential Global Positioning System
FSM	Front Sensing Module
GPS	Global Positioning System
HMI	Human Machine Interface
ICT	Information and Communications Technology
ITS	Intelligent Transportation Systems
IVC	Inter-Vehicular Communication
MIVC	Multi-hop IVC
RTE	Real-Time Environment
RTH	Real-Time Hardware
RTK-GPS	Real Time Kinematic Global Positioning System
SIVC	Single-hop IVC
TGW	Telematics Gateway
USB	Universal Serial Bus
UTC	Coordinated Universal Time
V2I	Vehicle-to-Infrastructure
V2V	Vehicle-to-Vehicle
WAVE	Wireless Access for Vehicular Environment
WLAN	Wireless Local Area Network

Contents

1 Introduction **1**
- 1.1 Motivation 1
- 1.2 Outline of the thesis 2

2 Mathematical preliminaries and background **5**
- 2.1 Networked Dynamical Systems: overview 5
  - 2.1.1 Definitions and notation 7
  - 2.1.2 Consensus problem 10
  - 2.1.3 Consensus in networks of dynamical systems with time-delays 11
- 2.2 Useful definitions, theorems and lemmas 12
  - 2.2.1 Signal amplification using induced norms 12
  - 2.2.2 Lyapunov-Razumikhin theorem 16

3 Problem statement **19**
- 3.1 Platooning 19
  - 3.1.1 Problem statement 19
  - 3.1.2 Evolution of platooning 20
  - 3.1.3 Problems and challenges 21
- 3.2 A networks-based approach for platooning 23
  - 3.2.1 Vehicular topologies 24
  - 3.2.2 Stability in a platoon of vehicles 26

I Distributed consensus for vehicle platooning **29**

4 Asymptotic stability of the closed loop vehicular network **31**
- 4.1 Platooning as a consensus problem 31
- 4.2 Closed-loop vehicular network 33
- 4.3 Convergence analysis 35

5 Numerical analysis **41**
- 5.1 Consensus in nominal conditions 41
- 5.2 Robustness with respect to perturbations 45
  - 5.2.1 Disturbance propagation through the string 45
  - 5.2.2 Communication failures 47

II Experimental platooning via distributed consensus strategy 53

6 Experimental setup and description of the prototype vehicles 55
  6.1 The Cooperative Driving System architecture 56
  6.2 Leader vehicle 56
    6.2.1 Hardware platform 56
    6.2.2 Software application 58
  6.3 Follower vehicle nr.1 59
    6.3.1 Hardware platform 59
    6.3.2 Software application 60
  6.4 Follower vehicle nr.2 65
    6.4.1 Hardware platform 65
    6.4.2 Software application 65
  6.5 Vehicle-to-Vehicle communication module 66
  6.6 Clock Synchronization 67

7 Experimental results 69
  7.1 Experimental characterization of the inter-vehicular delays 69
    7.1.1 Characterization of the delay on follower nr. 1 69
    7.1.2 Characterization of the delay on follower nr. 2 78
  7.2 Distributed coupling protocol validation 80
    7.2.1 Consensus validation 80
    7.2.2 Consensus in a joining maneuver 86
    7.2.3 Tracking control 91

8 Conclusions 99
  8.1 Contributions 99
  8.2 Ideas for future research 100

Bibliography 101

A Auxiliary results for Chapter 4 113
  A.1 Discussion on the spacing policy 113
  A.2 Algebraic manipulation on the distributed protocol 114

B Auxiliary results for Chapter 5 115
  B.1 String Stability analysis 115
    B.1.1 Spacing error dynamics on follower nr.1 115
    B.1.2 Spacing error dynamics on follower nr.2 116
    B.1.3 Numerical results on string stability 118
    B.1.4 Error propagation 122

C Auxiliary results for Chapter 6 - part 1 123
  C.1 Vehicle dynamics: a simulation model for the Real-Time Hardware 123

D Auxiliary results for Chapter 6 - part 2 129
  D.1 Global Positioning System: Devices and software solutions 129
    D.1.1 RTK-GPS module receiver: Trimble SPS852 129
    D.1.2 GPS module receiver: XSens MTi-G 132
  D.2 Real-Time Environment 133

D.2.1 Labview application on the leader vehicle 135

E Auxiliary results for Chapter 7 **139**

E.1 Further details on the Additional Communication module 139

E.1.1 Position reconstruction with low level accuracy measurements . . . 140

Chapter 1

Introduction

Contents

1.1 Motivation **1**
1.2 Outline of the thesis **2**

1.1 Motivation

Daily, we encounter complex systems all around us: cooperation between individuals, Internet, power grids, communication systems, are just few examples of complex networks [134], [113], [91]. Understanding the mechanisms of these complex networks is one of the major challenges in the scientific community, both to foresee their evolution in time and to manage/control them. The main elements of a network are the nodes (or vertices) and the links (or edges). In general we refer to *Complex Networks*, to indicate ensembles of different type of nodes and links interacting with each other ([134], [90], [113], [12], [19], [140], [141],[96], [157],[109], [51], [102], [37], [42]). In this framework, graph theory is used to understand the main properties of networks. In particular, networks of dynamical systems are complex networks consisting of ensemble of dynamical systems interacting with each other through edges, so as to agree upon a certain quantity of interest ([98], [96], [99], [142], [115]), dealing with applications that range from biology to computer science ([133], [117], [84], [145], [151], [33], [136], [27]).
The goal of this thesis is the control of a platoon of vehicles ([22], [144], [128]) exploiting the complex network approach ([98], [12], [19]). Consider a group of N vehicles moving along a single lane. In this scenario, vehicles are organized as a *string* with vehicles following one another along a straight line and sharing their state information (e.g., absolute position, velocity and acceleration) with all the other vehicles communicating through a Vehicle-to-Vehicle (V2V) communication paradigm [22]. An interesting arising problem is to analyze and control networks of vehicles, in the presence of time-varying communication delays and switching topologies. Specifically, the thesis addresses the problem of fleet control ([144], [22], [5], [128]): vehicle has to form and maintain a platoon that moves with an optimal spacing policy (e.g., in terms of relative distance and velocity among vehicles) in the presence of perturbations, noise and communication delays.
Commercial solution for semi-autonomous vehicles are available on the market, but still some issues must be overcome to make Automated Highways System (AHS) and

autonomous/semi-autonomous systems reliable in practice. For example, the most common and popular control approach to the problem, the so called Cooperative Adaptive Cruise Control strategy (CACC), simply relies on pairwise interactions: it is sensitive to external disturbances, especially in the case of large platoons [45], [85]. To extend the predecessor-following architecture, typical of the pairwise interactions based on sensor measurements (radar, lidar and cameras), the use of wireless communication among vehicles is considered, with respect to the other vehicles in the platoon. Clearly, the packet losses, communication failures or automated vehicle maneuvers have to be taken into account during the controller design, in order to understand how and if the control system performances may worsen by induced effects due to the communication network. In particular, data shared via V2V communication may concern (i) packet loss, (ii) time delays, (iii) data quantization, (iv) time-varying packet transmission, (v) network access competition, (vi) clock synchronization among on-board and remote nodes. Moreover, issues related to network safety and security have to be considered in order to define robust control strategies. Extensive studies have been carried out to cope with these topics, in particular the control community focuses on developing new control strategies such to overcome this network induced imperfections [78], [110], [131], [124], [100], [67]. When a group of vehicles agree on the common value of a variable of interest, they are said to reach *consensus*. Moreover, the limited communication capability of each vehicle influences consensus. To achieve consensus, each vehicle needs to manage a well defined *distributed protocol*, based on computing some shared variables of interest with neighbors.

According to the above assumption, we focus on the challenging problem of achieving consensus of both relative distance and velocity in a fleet of vehicles.

In this thesis we treat the problem of steering the platoon longitudinal dynamics as that of achieving second-order consensus in a network of multiple inertial agents in the presence of heterogeneous and time-varying delays [114], [19]. The use of the network paradigm is a promising solution suitable for exploring communication strategies alternative to pairwise interactions. The control input is acting on every vehicle in the platoon. It is designed as a coupling protocol composed by two terms: a local action depending on the state variables of the vehicle itself (measured on-board) and an action depending on the information received from the neighboring vehicles through the communication network. The resulting overall control architecture is decentralized and distributed. Moreover, the presence of time-varying heterogeneous communication delays are taken into account during control design. The platoon formation and its stability is analyzed via the Lyapunov-Razumikhin theorem [44] and numerical results are extensively used to understand the behavior of the network, for a platoon in the extra-urban technological scenario described in [22] despite rapid variations of the delays along the string. The robustness of the approach with respect to communication losses during the platoon motion considering both switching topology and time-varying delays has been addressed numerically. The control approach has been experimentally validated during on the road tests with three prototype vehicles.

1.2 Outline of the thesis

The thesis is divided in two main parts. In Part I the distributed coupling protocol to achieve consensus for a network of vehicles in the presence of time-varying and heterogeneous communication delays is proposed and its asymptotic stability is analytically

proven. Hence, results have been numerically validated, also in the presence of both periodical disturbances on the leader motion and communication failure/recovery.
In Part II we focus our attention on the development of an experimental setup to validate the distributed coupling protocol. A prototype of three vehicles equipped with both communication module and Real-Time Hardware is used for the on the road tests. Experimental results confirm the effectiveness of the consensus based strategy in creating and maintaining the platoon.
The thesis is structured as follows:

- in Chapter 2 some useful concepts and definitions are summarized for the sake of clarity.
- In Chapter 3 we provide the platooning description, focusing on autonomous vehicles applications and open issues. Here the synergy is also explored between the platooning and the framework of networked dynamical systems.
- In Chapter 4 the longitudinal control of a platoon when vehicles sharing information via V2V communication technology is investigated. Within this scenario each vehicle can communicate not only with its follower, as in the classical predecessor-following architecture, but also with a subset of vehicles in the fleet. In particular, a distributed coupling protocol to achieve the longitudinal control of the platoon is proposed and the entire closed-loop vehicular system is recast as a delayed dynamical network.
- In Chapter 5 we describe the numerical analysis to validate the proposed distributed coupling protocol in Matlab/Simulink environment.
- In Chapter 6 an overview of the experimental setup is carried out. A platoon of three prototype vehicles, equipped with specific communication and control hardware, is used to validate the platooning strategy. Details on both the hardware and software solutions are provided in this Chapter and in the Appendices at the end of the thesis.
- In Chapter 7 we show the experimental results achieved during the on the road tests. We consider a prototype of three vehicles such to validate the proposed distributed coupling protocol. Tests are performed to validate consensus both in the presence of joining maneuver and time-varying trajectory imposed by the leader vehicle.
- Some conclusions are drawn in Chapter 8.

Chapter 2

Mathematical preliminaries and background

Contents

2.1 Networked Dynamical Systems: overview 5
2.1.1 Definitions and notation 7
2.1.2 Consensus problem 10
2.1.3 Consensus in networks of dynamical systems with time-delays 11
2.2 Useful definitions, theorems and lemmas 12
2.2.1 Signal amplification using induced norms 12
2.2.2 Lyapunov-Razumikhin theorem 16

In this Chapter some useful concepts and definitions, that we will use in the rest of the thesis, are summarized for the sake of clarity.

2.1 Networked Dynamical Systems: overview

The world around us is a mixture of complex systems. The daily interactions that impose individuals to cooperate and make decisions together or the conflicts between groups of animals to promote the dominance of a group with respect to the others are two simple examples of complex systems. Familiar complex networks include the Internet, an ensemble of computers, routers and devices, linked by physical or wireless links; moreover power grids, biological networks and so on, emphasize that we are living in a networked world.

Understanding and controlling the mechanisms of these complex systems (Fig. 2.1), or complex networks, is one of the major challenges in the scientific community.

The main elements of a network are the nodes (or vertices) and the links (or edges); see Fig. 2.2. In general we refer to *Complex Networks*, as networks with more than one different type of nodes and links ([134], [90], [113], [12]).

Networks of dynamical systems are complex networks consisting of groups (i.e. ensemble) of dynamical systems, the vertices of a network, interacting with each other through edges, in order to agree, for example, upon a certain quantity of interest ([134], [90],[98]). For this reason, graph theory can be used to understand the general features of networks and the mechanisms that determine their topology. Networks of dynamical

Figure 2.1: Examples of complex systems.

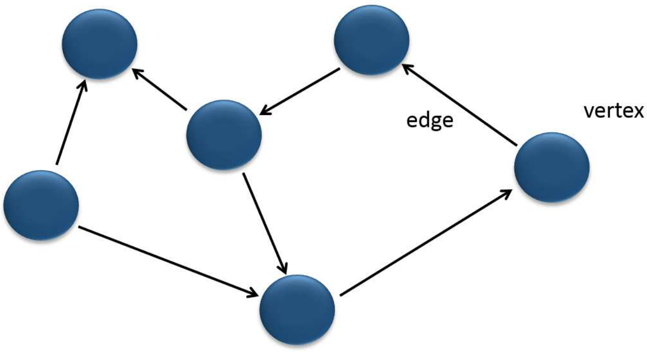

Figure 2.2: Example of a network.

systems have attracted lots of researchers recently, due to the possibility of applying control engineering tools to graph theory in order to guarantee, for instance, distributed coordination of Unmanned Air Vehicles (UAVs), Unmanned Ground Vehicles (UGVs) and Unmanned Underwater Vehicles (UUVs) ([133],[117], [84], [145], [151]), power networks (see [51], [37]), traffic control [30], multirobot control (see [33], [136]). These systems are just a few examples of networked dynamical systems applications.
To deal with the analysis and control of networked dynamical systems, in the literature we can find interesting theoretical tools used to achieve *leader-follower* coordination ([19]), *flocking* ([140], [141],[96], [157]), *consensus* ([98], [114], [158], [160], [83]), *synchronization* ([109], [51], [102] [37], [31], [42], [159]): in general, agents manage information coming from neighbors such to guarantee an agreement with each other.
Researchers have to cope with agreement problems and the theoretical tools introduced above seem to solve lots of practical problems, assuming the possibility of sharing in-

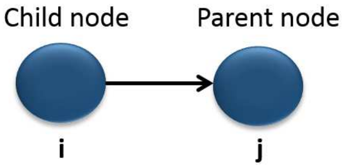

Figure 2.3: The edge (i, j), with j the *parent node* and i the *child node*. We use this notation to denote that node i can obtain information from node j.

formation between agents. If we consider the *network analysis*, the spread of emergent behaviours in networks of dynamical systems is a hot topic: interaction among non-linear dynamical systems, continuous and discontinuous coupling ([55], [87],[68], [20], [69],[60], [59]). Lots of properties can be investigated in networks: interesting topic may concern, for example, the communication delays and the link creation/failure.
Instead, about the *network control*, interesting topic concern with structural property such as, for example, the controllability or observability of the network [107].

We are interested in analysing and controlling networks with time-varying communication delays and switching topologies, with directed information flow. Time-varying communication delays and switching topologies are typical for mobile agents and they depend on links creation or failure. Directed information flow, described by directed graph (*digraph*), are more attractive than undirected graph as properties of directed graph are mostly unknown [98].

2.1.1 Definitions and notation

Now, we recall some important definitions and notation on graph theory.
We define the *adjacency matrix* $\mathcal{A}_N^* = [a_{ij}]_{N\times N}$ of directed graph (*digraph*) $\mathcal{G}_N^*$, with $\mathcal{V}_N^* = \{1, \ldots, N\}$ the set of vertices, with entries $a_{ij} = 1$ if $(i, j) \in \mathcal{E}_N^*$, with $\mathcal{E}_N^*$ the set of edges, and $a_{ij} = 0$ otherwise. Then, we consider the *incidence matrix* ∇: in order to define this matrix we assume an arbitrary but fixed orientation (i.e. direction) for each edge $e_{ij} = (i, j)$ (see Fig. 2.3). In particular, we define ∇ as a $(|\mathcal{E}_N^*| \times |\mathcal{V}_N^*|)$ matrix, whose entries $\nabla_{ex} = 1$ if x is the terminal vertex of edge e (i.e. $e = e_{ix}$), $\nabla_{ex} = -1$ if x is the initial vertex of edge e (i.e. $e = e_{xj}$), and $\nabla_{ex} = 0$ otherwise (i.e. x is not in e).
Now, we define the *Laplacian operator* from an algebraic point of view [11]:

$$L^* = \nabla^\top \nabla \tag{2.1}$$

which is the so called *Laplacian matrix* of $\mathcal{G}_N^*$. Moreover, we have that the terms in L^* are:

$$l_{ij}^* = \sum_{e\in\mathcal{E}_N^*} \nabla_{ei}\nabla_{ej} = \begin{cases} -1 & if & (i,j)\in\mathcal{E}_N^* \\ d\,(i) & if & i=j \\ 0 & otherwise & \end{cases} \tag{2.2}$$

where $d_i = |\{e = (i, j) \in \mathcal{E}_N^* | i \in e\}|$ is the *degree* of the vertex i.

Remark 2.1.1. l_{ij}^* defined in (2.2) is independent of the orientation of the edges.

We define the *degree matrix* $D^* = [D^*_{ii}]_{N\times N}$, a diagonal matrix with $D^*_{ii} = d_i$. The relationship between the Laplacian and the adjacency matrix of the graph is:

$$L^* = D^* - \mathcal{A}^*_N \tag{2.3}$$

The Laplacian matrix can be rewritten as follows:

$$L^* = \begin{bmatrix} d_1 & -a_{12} & -a_{13} & \cdots & -a_{1N} \\ -a_{21} & d_2 & -a_{23} & \cdots & -a_{2N} \\ -a_{31} & -a_{32} & \ddots & \ddots & -a_{3N} \\ \vdots & \ddots & \ddots & \ddots & \vdots \\ -a_{N1} & -a_{N2} & \cdots & -a_{N(N-1)} & d_N \end{bmatrix}. \tag{2.4}$$

with $d_i = \sum\limits_{j=1}^{N} a_{ij}$.

The following theorem from [98] is to show the spectral properties for digraphs using the *Geršgorin* disk theorem [52].

Theorem 2.1.1. *(Spectral Localization). Let $\mathcal{G}^*_N = (\mathcal{V}^*_N, \mathcal{E}^*_N, \mathcal{A}^*_N)$ be a directed graph (digraph) and L^* is the Laplacian matrix. Denote the node degree of the graph $\mathcal{G}^*_N$ by $d_i = \sum\limits_{j=1}^{N} a_{ij}$ and the maximum node degree by $d_{max}(\mathcal{G}^*_N) = max_i(d_i)$. Then, all the eigenvalues of $L^* = \mathcal{L}(\mathcal{G}^*_N)$ are located in the following disk:*

$$D(L^*) = \{z \in \mathbb{C} : |z - d_{max}(\mathcal{G}^*_N)| \leq d_{max}(\mathcal{G}^*_N)\} \tag{2.5}$$

centered at $z = d_{max}(\mathcal{G}^*_N) + 0j$ and radius $r = d_{max}(\mathcal{G}^*_N)$, in the complex plane (see Fig. 2.4).

Proof. According to the *Geršgorin* disk theorem [52], all the eigenvalues of $L^* = [l^*_{ij}]$ are located in the union of the following N disks:

$$D_i = \{z \in \mathbb{C} : |z - l^*_{ii}| \leq \sum_{\substack{j=1 \\ j\neq i}}^{N} |l^*_{ij}|\} \tag{2.6}$$

$\forall i \in \{1, \dots, N\}$. However, for the digraph $\mathcal{G}^*_N$, $l^*_{ii} = d_i$ and

$$\sum_{\substack{j=1 \\ j\neq i}}^{N} |l^*_{ij}| = d_i. \tag{2.7}$$

such to have $D_i = \{z \in \mathbb{C} : |z - d_i| \leq d_i\}$. Moreover, all these N disks are contained in the largest disk $D(L^*)$ with the radius $r = d_{max}(\mathcal{G}^*_N)$. ☐

Remark 2.1.2. The disk $D^{'}(L^*) = \{z \in \mathbb{C} : |z + d_{max}(\mathcal{G}^*_N)| \leq d_{max}(\mathcal{G}^*_N)\}$ contains all the eigenvalues of $-L^*$. In particular, $D^{'}(L^*)$ is the mirror image of $D(L^*)$ with respect to the imaginary axis.

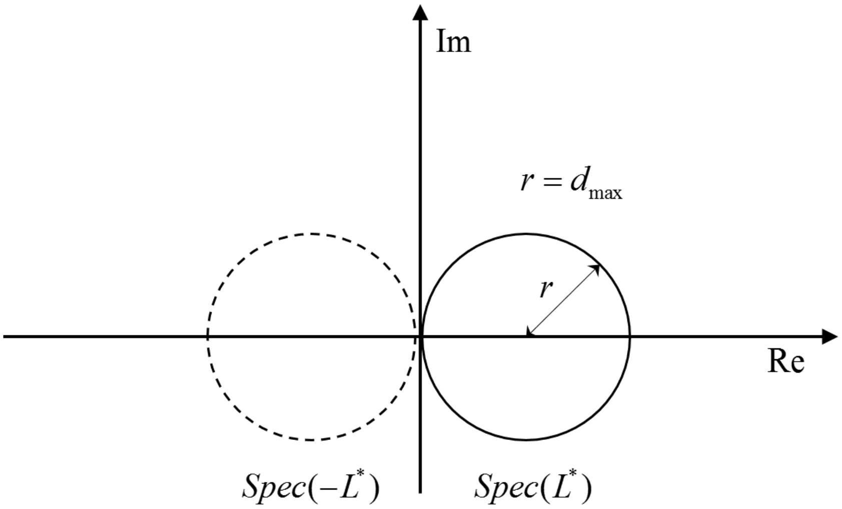

Figure 2.4: Geršgorin theorem applied to Laplacian matrix.

A normalized version of the Laplacian matrix is L_{nm}, defined according to [11]:

$$L_{nm} = (D^*)^{-1} L^* = I - (D^*)^{-1} \mathcal{A}_N^* \tag{2.8}$$

This matrix has the following structure:

$$L_{nm} = \begin{bmatrix} 1 & -\frac{a_{12}}{d_1} & -\frac{a_{13}}{d_1} & \cdots & -\frac{a_{1N}}{d_1} \\ -\frac{a_{21}}{d_2} & 1 & -\frac{a_{23}}{d_2} & \cdots & -\frac{a_{2N}}{d_2} \\ -\frac{a_{31}}{d_3} & -\frac{a_{32}}{d_3} & 1 & \ddots & \vdots \\ \vdots & \ddots & \ddots & \ddots & -\frac{a_{(N-1)N}}{d_{N-1}} \\ -\frac{a_{N1}}{d_N} & -\frac{a_{N2}}{d_N} & \cdots & -\frac{a_{N(N-1)}}{d_N} & 1 \end{bmatrix} \tag{2.9}$$

A network of N dynamical systems (i.e. nodes) can be described by a *weighted directed graph* (digraph) $\mathcal{G}_N = (\mathcal{V}_N, \mathcal{E}_N, \mathcal{A}_N)$ of order N characterized by a set of nodes $\mathcal{V}_N = \{1, \ldots, N\}$, a set of edges $\mathcal{E}_N \subseteq \mathcal{V}_N \times \mathcal{V}_N$. The topology of the graph is associated to a weighted adjacency matrix with nonnegative elements $\mathcal{A}_N = [a_{N,ij}]_{N\times N}$. In general, we assume $a_{N,ii} = 0$ (i.e., self-edges (i,i) are not allowed unless otherwise indicated). Then, we define the *weighted Laplacian matrix* as follows:

$$L = \begin{bmatrix} \bar{d}_1 & -a_{N,12} & -a_{N,13} & \cdots & -a_{N,1N} \\ -a_{N,21} & \bar{d}_2 & -a_{N,23} & \cdots & -a_{N,2N} \\ -a_{N,31} & -a_{N,32} & \ddots & \ddots & -a_{N,3N} \\ \vdots & \ddots & \ddots & \ddots & \vdots \\ -a_{N,N1} & -a_{N,N2} & \cdots & -a_{N,N(N-1)} & \bar{d}_N \end{bmatrix} \tag{2.10}$$

with $\bar{d}_i = \sum\limits_{j=1}^{N} a_{N,ij}$ and $a_{N,ij} \geq 0$.

The edge (i,j) in the edge set of a digraph denotes that node i can obtain information from node j, but not necessarily *vice versa*, being j the *parent node* and i the *child node*, as in Fig. 2.3. The set of neighbors of node i is denoted as $\mathcal{N}_i = \{i \in \mathcal{V}_N : e_{ij} = (i,j) \in \mathcal{E}_N, j \neq i\}$, $\mathcal{E}_N \subset \mathcal{V}_N \times \mathcal{V}_N$. A sequence $1, 2, ..., l$ of distinct nodes is a *directed path* if $(i-1, i) \in \mathcal{E}_N$, $i = 2, \ldots, l$. A *cycle* is a directed path that starts and ends at the same node.

A digraph is *strongly connected* if there is a path from every node to every other node. A *complete* digraph is a graph where every pair of distinct vertices is linked by a pair of unique edges, in opposite direction. A *strong component* of a digraph is an induced subgraph that is maximal, subject to being strongly connected. A *directed tree* is a digraph in which every node has exactly one parent node with the exception of one node, called the *root*, which has no parent and which has a directed path to every other node. A subgraph $(\mathcal{V}_N^s, \mathcal{E}_N^s)$ of $(\mathcal{V}_N, \mathcal{E}_N)$ is a graph such that $\mathcal{V}_N^s \subseteq \mathcal{V}_N$ and $\mathcal{E}_N^s \subseteq \mathcal{E}_N \cap (\mathcal{V}_N^s \times \mathcal{V}_N^s)$. A *rooted directed spanning tree* $(\mathcal{V}_N^s, \mathcal{E}_N^s)$ of the directed graph $(\mathcal{V}_N, \mathcal{E}_N)$ is a subgraph of $(\mathcal{V}_N, \mathcal{E}_N)$ such that $(\mathcal{V}_N^s, \mathcal{E}_N^s)$ is a directed tree and $\mathcal{V}_N^s = \mathcal{V}_N$. We say that j is *reachable* from i if there exists a path from node i to node j. A *cluster* is any subset $\mathcal{V}_N^s \subset \mathcal{V}_N$ of the nodes of the digraph. The set of neighbors of a cluster $\mathcal{V}_N^s$ is defined as $\mathcal{N}_{\mathcal{V}_N^s} = \bigcup_{i \in \mathcal{V}_N^s} \mathcal{N}_i = \{j \in \mathcal{V}_N : i \in \mathcal{V}_N^s, (i,j) \in \mathcal{E}_N\}$. Defining the *degree matrix* as $D = \text{diag}\{\bar{d}_1, \bar{d}_2, \ldots, \bar{d}_N\}$, with $\bar{d}_i = \sum_{j \in \mathcal{N}_i} a_{N,ij}$, the Laplacian of the weighted directed graph $\mathcal{G}_N$ can be defined as $L = D - \mathcal{A}_N$.

In what follows, we consider N nodes together with a leader vehicle taken as an additional agent labelled with the index zero i.e., node 0. We use an augmented weighted directed graph $\mathcal{G}_{N+1}$ to model the network topology in this case.

Definition 2.1.1. *We assume node 0 is globally reachable in $\mathcal{G}_{N+1}$ if there is a path in $\mathcal{G}_{N+1}$ from every node i in $\mathcal{G}_N$ to node 0 [52].*

Moreover, the following Lemmas hold [74], [55]:

Lemma 2.1.1. *A digraph $\mathcal{G}_N = (\mathcal{V}_N, \mathcal{E}_N, \mathcal{A}_N)$ has a globally reachable node if and only if for every pair of nonempty, disjoint subset $\mathcal{V}_N^1, \mathcal{V}_N^2 \subset \mathcal{V}_N$ satisfies $\mathcal{N}_{\mathcal{S}_i} \cup \mathcal{N}_{\mathcal{S}_j} \neq \emptyset$.*

Remark 2.1.3. Let $S_1, S_2, \ldots, S_p$ be the strong components of $\mathcal{G}_N = (\mathcal{V}_N, \mathcal{E}_N, \mathcal{A}_N)$ and $\mathcal{N}_{S_i}$ be the neighbor sets for $S_i, i = 1, \ldots, p, p > 1$.

Lemma 2.1.2. *The digraph $\mathcal{G}_N$ has a globally reachable node if and only if the Laplacian of $\mathcal{G}_N$ has a simple zero eigenvalue (with eigenvector $\mathbf{1} = (1, \ldots, 1) \in \mathbb{R}^N$).*

2.1.2 Consensus problem

Before defining consensus in an analytical way, we need to describe a network of dynamical systems, or *dynamical agents* [98], [12], [92]. We start assuming a network of N nodes (the agents); we define x_i the physical quantity describing the behavior of the $i-$th node, with $i \in \mathcal{V}_N$ (for example, position, velocity, pressure, voltage, etc.). In a network of dynamical agents, we say nodes i and j *agree* if and only if $x_i = x_j$. Moreover, the network reaches *consensus* if and only if $x_i = x_j$, for all $i, j \in \mathcal{V}_N, i \neq j$.
Now, we assume the following $i-$th dynamical system, or *dynamic agent*

$$\dot{x}_i = f(x_i, u_i), \qquad i \in \mathcal{V}_N. \tag{2.11}$$

Hence, the *network dynamics* are defined as:

$$\dot{x} = F(x, u) \tag{2.12}$$

where $F(x, u)$ is the columnwise concatenation of the elements $f(x_i, u_i)$, for $i \in \mathcal{V}_N$.
To provide a formal definition of consensus, we introduce the $\chi-$*consensus problem*, which is commonly defined in the literature [98], [86]. In particular, let $\chi : \mathbb{R}^N \to \mathbb{R}$ be a function of N variables $x_1, \ldots, x_N$ and $a = x(0)$ denote the initial state of the system. The $\chi-$*consensus problem* in a *dynamic graph* (i.e. a graph depending on the time evolution of x) is a distributed way to calculate $\chi(a)$ by applying input u_i, or *coupling protocol*, defined as follows:

$$u_i = k_i(x_{j_1}, \ldots, x_{j_{m_i}}) \tag{2.13}$$

with topology $\mathcal{G}_N$ if the cluster $\mathcal{V}_N^i = \{j_1, \ldots, j_{m_i}\}$ of nodes with indexes $j_1, \ldots, j_{m_i} \in \mathcal{V}_N$ satisfies the property $\mathcal{V}_N^i \subseteq \{i\} \cup \mathcal{N}_i$. Moreover, (2.13) is called *distributed coupling protocol* if $|\mathcal{V}_N^i| < N$, $\forall i \in \mathcal{V}_N$, .
We say protocol (2.13) asymptotically solves the $\chi-$*consensus problem* if and only if there exists an asymptotically stable equilibrium x^* of $\dot{x} = F(x, k(x))$ satisfying $x_i^* = \chi(x(0))$ for all $i \in \mathcal{V}_N$. A special case is called *average consensus*, with $\chi(x) = Ave(x) = 1/N(\sum_{i=1}^N x_i)$. Moreover, other two special cases are called *max consensus* and *min consensus*, with $\chi(x) = \max_i x_i$ and $\chi(x) = \min_i x_i$, respectively. Note that we are interested in distributed solutions of the $\chi-$*consensus problem* in the presence of nodes that are not connected to all the other nodes.
Two typical application in consensus problem are *rendezvous* and *formation control.* The *rendezvous problem* is defined as the requirement for a group of vehicles to converge on a location through local negotiation [71], [72], [118]. Interesting application can be found in [24], [35]. Moreover, the *formation problem* control objective is the relative coordination among the agents. Interesting paper are [41], [104].
Another important classification in literature on consensus problem depends on the agent dynamics. First-order dynamics are extensively used to describe agents behavior [98], [57], [73], [116]. Moreover, second-order dynamics are typical in networks of inertial agents [153], [96], [158].

2.1.3 Consensus in networks of dynamical systems with time-delays

The design of coupling protocols for the coordination of a group of agents exchanging information in the presence of limited and uncertain communication is a well-known challenging problem within the dynamical network context (see for example [98], [114] and references therein), that have been only recently theoretically addresses in the technical literature in the case of time-varying communication delays and directed network structures.
Referring to the general model of dynamical agent in (2.11) under the distributed protocol (2.13), we introduce here networks of dynamical systems with time-delays. In particular, delay affects the state inside the protocol (2.13): for that reason, its action has to be considered in the network dynamics. We can write the following coupling protocol:

$$u_i = k_i(x_{j_1}, \ldots, x_{j_{m_i}}; \tau_{ij_1}(t), \ldots, \tau_{ij_{m_i}}(t)) \tag{2.14}$$

where $\tau_{ij_1}, \ldots, \tau_{ij_{m_i}}$ are the time delays for information communicated from vehicle j_1 to vehicle i, from vehicle j_2 to vehicle i and so on.

Usually, the consensus problem in the presence of communication time delays is solved by designing coupling protocols under the assumption of a constant delay affecting communication among agents. Such a delay can be homogeneous or heterogeneous

along the network [55], [83], [18], [19] (i.e. homogeneous $\tau_{ij_1}(t) = \tau_{ij_{m_i}}(t) = \tau$ and heterogeneous $\tau_{ij_1}(t) = \tau_{ij_{m_i}}(t) = \tau_i$). In particular, in [158] a second-order consensus algorithm is derived for the multi-agent system in the presence of an homogeneous coupling delays. Authors investigate networks with directed and fixed interconnection graph.
In [55] authors discuss the consensus problem of second-order multiagent systems considering time-varying coupling delays for directed graph ($\tau_{ij_1}(t) = \tau_{ij_{m_i}}(t) = \tau(t)$), with both fixed and switched topology. In particular they consider an homogeneous time-varying delay all over the network and demonstrate stability of the networked systems under some constraints on the maximum allowable time-varying delay for networks with both (i) fixed and (ii) switching and balanced topologies.

Fewer approaches have been only recently proposed to cope with time-varying heterogeneous communication delays for first and second order linear systems [137] [160], [80], [75], [79] (i.e. heterogeneous $\tau_{ij_1}(t) = \tau_{ij_{m_i}}(t) = \tau_i(t)$). Moreover, in [160] a leader-following consensus problem is investigated considering heterogeneous time-varying delays, both for fixed and switching topologies. In particular, consensus is solved for fixed and switching topologies (under a particular condition). In [76] consensus problem of second-order multi-agent systems in the presence of velocity damping term is studied. They consider both heterogeneous input and communication delays obtaining conditions to achieve consensus on both undirected and directed graphs with fixed topologies. Then, in [77] are considered, in addition to results previous described in [76], the switching topologies with a common time-invariant communication delay.
Furthermore, although the relevance of theoretical results, the control theory applied to networks of dynamical systems with time-delays have not been extensively validated solving technological problems inspired by real world applications.

2.2 Useful definitions, theorems and lemmas

2.2.1 Signal amplification using induced norms

Useful norms are detailed in the following Paragraphs.

Norms of Vectors - The n-dimensional Euclidean space $\mathbb{R}^n$ is the set of all n-dimensional vectors $x = [x_1, \dots, x_n]$, with $x_i \in \mathbb{R}$, for $i = 1, \dots, n$. An $m \times n$ matrix A of real elements defines a linear mapping $y = Ax$ from $\mathbb{R}^n$ into $\mathbb{R}^m$.
The norm $\|x\|$ of a vector x is a real-valued function with the properties [62]:

(i) $\|x\| \geq 0$ for all $x \in \mathbb{R}^n$, with $\|x\| = 0$ if and only if $x = 0$;

(ii) $\|x + y\| \leq \|x\| + \|y\|$, for all x, $y \in \mathbb{R}^n$ (triangle inequality);

(iii) $\|\alpha x\| = |\alpha| \, \|x\|$, for all $\alpha \in \mathbb{R}$ and $x \in \mathbb{R}^n$.

We define the class of p-norms as follows:

$$\|x\|_p = \left(|x_1|^p + \cdots + |x_n|^p\right)^{1/p}, 1 \leq p < \infty \tag{2.15}$$

and

$$\|x\|_\infty = \max_i |x_i| \tag{2.16}$$

The Euclidean norm is:

$$\|x\|_2 = \left(|x_1|^2 + \cdots + |x_n|^2\right)^{1/2} = \left(x^\top x\right)^{1/2}. \tag{2.17}$$

p-norms equivalence - If $\|\cdot\|_\alpha$ and $\|\cdot\|_\beta$ are two different p-norms, then there exist positive constants c_1 and c_2 such that:

$$c_1 \|x\|_\alpha \leq \|x\|_\beta \leq c_2 \|x\|_\alpha \tag{2.18}$$

for all $x \in \mathbb{R}^n$. For the 1-, 2-, and ∞-norms, these inequalities become:

$$\|x\|_2 \leq \|x\|_1 \leq \sqrt{n}\,\|x\|_2 , \quad \|x\|_\infty \leq \|x\|_2 \leq \sqrt{n}\,\|x\|_\infty , \quad \|x\|_\infty \leq \|x\|_1 \leq n\,\|x\|_\infty . \tag{2.19}$$

Hölder inequality -

$$|x^\top y| \leq \|x\|_p \|y\|_p , \quad \frac{1}{p} + \frac{1}{q} = 1 \tag{2.20}$$

for all $x, y \in \mathbb{R}^n$.

Norms of Matrices - The induced p-norm of A is defined by:

$$\|A\|_p = \sup_{x \neq 0} \frac{\|Ax\|_p}{\|x\|_p} = \max_{\|x\|_p = 1} \|Ax\|_p \tag{2.21}$$

being *sup* the supremum, i.e. the least upper bound and *inf* the infimum, i.e. the greatest lower bound. In particular, we have that:

- $\|A\|_1 = \max_j \sum_{i=1}^m |a_{ij}|$ with $p = 1$;
- $\|A\|_2 = [\lambda_{max}]$ with $p = 2$;
- $\|A\|_\infty = \max_i \sum_{j=1}^n |a_{ij}|$ with $p = \infty$;

with $\lambda_{max}\left(A^\top A\right)$ the maximum eigenvalue of $A^\top A$.

Induced p-norms properties -

$$\frac{1}{\sqrt{n}} \|A\|_\infty \leq \|A\|_2 \leq \sqrt{m}\,\|A\|_\infty , \quad \frac{1}{\sqrt{m}} \|A\|_1 \leq \|A\|_2 \leq \sqrt{n}\,\|A\|_1 \tag{2.22}$$

$$\|A\|_2 \leq \sqrt{\|A\|_1 \|A\|_\infty}. \tag{2.23}$$

Assuming matrix B of dimensions $n \times l$, we have:

$$\|AB\|_p \leq \|A\|_p \|B\|_p \tag{2.24}$$

Norms of Signals - The size of an error signal is useful to evaluate the performance of a tracking system. We consider signals mapping $[0,\infty)$ to $\mathbb{R}$, assumed to be piecewise continuous. According to [38], we recall the following properties for signals:

(i) $\|u\| \geq 0$;

(ii) $\|u\| = 0 \Leftrightarrow u\left(t\right) = 0$, $\forall t$;

(iii) $\|ax\| = |a| \left\|u\right\|$, $\forall a \in \mathbb{R}$;

(iv) $\|u+y\| \leq \|u\| + \|y\|$;

The following norms of signals are defined [38]:

1. $1-$**norm** - The $1-$norm of a signal $u(t)$ is the integral of its absolute value:

$$\left\|u\right\|_1 = \int\limits_0^\infty |u\left(t\right)| dt \tag{2.25}$$

2. $2-$**norm** - The $2-$norm of $u(t)$ is:

$$\left\|u\right\|_2 = \left[\int\limits_0^\infty \left|u\left(t\right)\right|^2 dt\right]^{1/2} \tag{2.26}$$

3. $p-$**norm** - The $p-$norm of $u(t)$ is:

$$\left\|u\right\|_p = \left[\int\limits_0^\infty \left|u\left(t\right)\right|^p dt\right]^{1/p} \tag{2.27}$$

4. $\infty-$**norm** - The $\infty-$norm of a signal $u(t)$ is the least upper bound of its absolute value:

$$\left\|u\right\|_\infty = \sup_t \left|u\left(t\right)\right| \tag{2.28}$$

Norms of Systems - We consider a linear time-invariant system. In the time domain we describe the input-output model as a convolution equation:

$$y\left(t\right) = g\left(t\right) * u\left(t\right) \tag{2.29}$$

that is,

$$y\left(t\right) = \int\limits_0^t g\left(t-\tau\right) u\left(\tau\right) d\tau \tag{2.30}$$

Let $G(s)$ denote the Laplace transform of $g(t)$, with $g\left(t\right) = \mathcal{L}^{-1}\left\{G\left(s\right)\right\}$ the impulse response of the system; we have in the $s-$domain that:

$$Y\left(s\right) = G\left(s\right) U\left(s\right) \tag{2.31}$$

We define the $\infty-$norm for the transfer function $G(s)$ [38]:

$$\|G(s)\|_{\infty} = \sup_{\omega} |G(j\omega)| \tag{2.32}$$

The $\infty-$norm appears as the peak value on the Bode magnitude plot of $G(s)$. Then, the $1-$norm of the impulse response is:

$$\|g\|_1 = \int_0^{\infty} |g(t)|\, dt \tag{2.33}$$

In order to relate the input and the output of the system with the signals and systems norms defined above, we have that [38],[111]:

$$\|g\|_1 = \sup_{u \in L_{\infty}} \frac{\|y\|_{\infty}}{\|u\|_{\infty}} \tag{2.34}$$

$$\|G(s)\|_{\infty} = \sup_{u \in L_2} \frac{\|y\|_2}{\|u\|_2} \tag{2.35}$$

where L_{∞} is the set of signals with ∞-norm and L_2 is the set of signals with 2-norm. In order to study signal amplification in vehicle platoons, a performance-oriented approach can be used to characterize string stability [89], [111], [152], [110]. In general, a desirable feature for attenuation in upstream direction of either distance error, velocity or acceleration is specified as:

$$\|y\|_{\infty} \leq \|u\|_{\infty} \tag{2.36}$$

with y the scalar output (i.e. distance error, velocity or acceleration) of the i-th vehicle, u the scalar output (i.e. distance error, velocity or acceleration) of the $(i-1)$-th vehicle and the following transfer function:

$$\hat{H}(s) = \frac{Y(s)}{U(s)} \tag{2.37}$$

that relates both the Laplace transform of y and u, i.e. $Y(s)$ and $U(s)$, respectively. Then, string stability is guaranteed if :

$$\left\|\hat{H}(s)\right\|_{\infty} \leq 1 \tag{2.38}$$

Remark 2.2.1. According to (2.38) we have that $\|y\|_2 \leq \|u\|_2$ is satisfied., i.e. the energy in signal y is less than energy in signal u. However, $\|y\|_{\infty} \leq \|u\|_{\infty}$ is a stronger condition to be guaranteed, i.e. $\|h\|_1 \leq 1$.

A useful lemma from [26] is the following:

Lemma 2.2.1. *If $h(t) > 0$, then all the input-output induced norms are equal.*

Proof. Let γ_p be the generic p-th induced norm from input to output, i.e.

$$\gamma_p = \sup_{u \in L_p} \frac{\|y\|_p}{\|u\|_p} \tag{2.39}$$

From linear system theory [34] we have that:

$$\left|\hat{H}(0)\right| \leq \left\|\hat{H}(j\omega)\right\|_{\infty} \leq \gamma_p \leq \|h\|_1 \tag{2.40}$$

If $h(t) > 0$, then $\left|\hat{H}(0)\right| = \|h\|_1$. Indeed:

$$\left|\hat{H}(0)\right| = \left|\int_0^\infty h(t)\,dt\right| \leq \int_0^\infty |h(t)|\,dt \tag{2.41}$$

if and only if $h(t) > 0$. □

Remark 2.2.2. We underline that if $\hat{H}(s)$ is designed such that $\left\|\hat{H}(s)\right\|_\infty \leq 1$, then $\|y\|_2 \leq \|u\|_2$; moreover, if the extra condition $h(t) > 0$ holds, then $\|y\|_\infty \leq \|u\|_\infty$.

2.2.2 Lyapunov-Razumikhin theorem

Let $C([-r,0],\mathbb{R}^n)$ be a Banach space of continuous functions defined on an interval $[-r,0]$, taking values in $\mathbb{R}^n$ with a norm $||\varphi||_c = \max_{\theta\in[-r,0]}||\varphi(\theta)||$, $||\cdot||$ being the Euclidean norm. Given a system of the form:

$$\begin{aligned} \dot{x} &= f(x_t), t > 0, \\ x_0(\theta) &= \varphi(\theta), \forall\theta \in [-r,0], \end{aligned} \tag{2.42}$$

where $x_t(\theta) = x(t+\theta), \forall\theta \in [-r,0]$ and $f(0) = 0$, the following results holds:

Theorem 2.2.1. *(Lyapunov-Razumikhin) [44]. Given system (2.42), suppose that the function* $f : C([-r,0],\mathbb{R}^n) \to \mathbb{R}^n$ *maps bounded sets of* $C([-r,0],\mathbb{R}^n)$ *into bounded sets of* $\mathbb{R}^n$*. Let* ψ_1, ψ_2*, and* ψ_3 *be continuous, nonnegative, nondecreasing functions with* $\psi_1(s) > 0, \psi_2(s) > 0, \psi_3(s) > 0$ *for* $s > 0$ *and* $\psi_1(0) = \psi_2(0) = 0$*. If there is a continuous function* $V(t,x)$ *(Lyapunov-Razumikhin function) such that:*

$$\psi_1(||x||) \leq V(t,x) \leq \psi_2(||x||), t \in \mathbb{R}, x \in \mathbb{R}^n, \tag{2.43}$$

and there exists a continuous non decreasing function $\psi_4(s)$ *with* $\psi_4(s) > s, s > 0$ *such that :*

$$\begin{aligned} &\dot{V}(t,x) \leq -\psi_3(||x||) \\ &if \quad V(t+\theta, x(t+\theta)) < \psi_4(V(t,x(t))), \theta \in [-r,0], \end{aligned} \tag{2.44}$$

then the solution $x = 0$ *is uniformly asymptotically stable.*

Definition 2.2.1. *A complex square matrix is said to be negative stable [positive stable] if its spectrum lies in the open left [right] half plane [48].*

Definition 2.2.2. *The square matrix* $\tilde{A} = [\tilde{a}_{ij}]$ *of order* $N \times N$*, has property SC if for every pair of distinct integers p,q, with* $1 \leq p$ *and* $q \leq N$*, there is a sequence of distinct integers* $p = o_1, o_2, o_3, \ldots, o_{m-1}, o_m = q, 1 \leq m \leq N$ *such that all of the matrix entries* $\tilde{a}_{o_1o_2}, \tilde{a}_{o_2o_3}, \ldots, \tilde{a}_{o_{m-1}o_m}$ *are non-zero [52].*

Lemma 2.2.2. *(Schur's formula). Let* $A_{11}, A_{12}, A_{21}, A_{22} \in \mathbb{R}^{n\times n}$ *and* $M = \begin{bmatrix} A_{11} & A_{12} \\ A_{21} & A_{22} \end{bmatrix}$. *Then* $\det(M) = \det(A_{11}A_{22} - A_{12}A_{21})$*, where* $\det(\cdot)$ *denotes the determinant of a matrix, if* A_{11}, A_{12}, A_{21} *and* A_{22} *commute pairwise, i.e.* $A_{ij}A_{lm} = A_{lm}A_{ij}$ *for all possible pairs of indices* i,j *and* l,m *[15].*

Lemma 2.2.3. *Given a complex-coefficient polynomial,*

$$f(s) = s^2 + (a + ib)s + c + id, \tag{2.45}$$

where $a, b, c, d \in \mathbb{R}$*,* $f(s)$ *is Hurwitz stable if and only if* $a > 0$ *and* $abd + a^2c - d^2 > 0$ *[106].*

Chapter 3

Problem statement

Contents

3.1 Platooning 19
  3.1.1 Problem statement 19
  3.1.2 Evolution of platooning 20
  3.1.3 Problems and challenges 21
3.2 A networks-based approach for platooning 23
  3.2.1 Vehicular topologies 24
  3.2.2 Stability in a platoon of vehicles 26

This Chapter provides the platooning description. In particular, we focus on both describing autonomous vehicles applications and the open issues related with them. Finally, we explore the synergy between the platooning and the framework of networked dynamical systems.

3.1 Platooning

3.1.1 Problem statement

Platooning is an innovative, automated way of driving a fleet of vehicles on a freeway in order to reduce fuel consumption and their overall environmental impact [5], [22] (see Fig. 3.1). It consists of the coordinated motion of groups of vehicles cooperating with each other so as to reach the same destination with a common velocity [46], [112]. It has been shown that platooning can effectively improve safety, efficiency and travel time while decreasing traffic congestion, pollution and stress for passengers [16]. In general, platooning depends on several factors, for example GPS signal quality, infrastructure and inter-vehicular communication [6], [10], [94]. From a control viewpoint, the main goal is to form the platoon and then maintain an optimal spacing policy (e.g., in terms of their relative distance and velocity) in the presence of perturbations, noises and communication delays. Platooning requires the full longitudinal control of the vehicle motion (lateral control can be also considered in a more wide mobility scenario).

Usually, vehicles are equipped with on-board sensors (radar, camera, lidar) in order to measure the predecessor relative position and velocity. In general, for safety reasons each vehicle in the platoon is equipped with (i) on-board sensors monitoring the state of its neighbors and (ii) its own control system.

Figure 3.1: Vehicle platooning applications. Top-left panel: SARTRE project [22]. Top-right panel: Energy ITS project [144]. Down-left panel: Scania platooning [5]. Down-right panel: PATH program [128].

Dedicated Short-Range Communication (DSRC), which uses radio waves at 5.9 GHz frequency, enable more enlarged information exchange between vehicles through wireless Vehicle-to-Vehicle (V2V) and Vehicle-to-Infrastructure (V2I) communication [105], [95]. Standards such as IEEE 802.11p and SAE J2735 are used to select the kind, the meaning and the structure of the messages to share via V2V [56]: they guarantee both low latency, high reliability, privacy and security.

In this emerging technological scenario platooning can be guaranteed exploiting the features of wireless communication network through which every vehicle transmits its state (for example position and velocity) to the neighboring vehicles. The reference behavior is dispatched to all vehicles in the network by either *a leader vehicle* belonging to the platoon (typically the first vehicle in the group) [22], or some *road infrastructure* (acting as a virtual leader) [129], [156], [103] [154]. Note that, although the presence of V2V technology, sensor-based solutions will need to coexist in order to guarantee safety and a certain degree of redundancy, for example in the presence of sudden obstacles.

3.1.2 Evolution of platooning

One of the first and most popular platooning application was developed within the California Partners for Advanced Transit and Highways (PATH) program [127], and described in [27] and [26] (see Fig. 3.1, down-right panel). The proposed solution is based on an Automated Highways System (AHS) structure [46], that implements a hierarchical structure including different layers of control (each layer is responsible for performing a specific task). To automate the longitudinal control, sensor-based adaptive control strategies are used, such to guarantee the convergence of the relative distance to a desired inter-vehicular spacing policy. Strategies are aimed to achieve [27] *string stability*, e.g. the uniform boundedness of all the states of a group of interconnected system for all time under specific condition on the initial states of the interconnected system (see Sec. 3.2.2). In [65] a longitudinal control strategy through two different traction force controllers, an adaptive fuzzy logic control and an adaptive sliding mode control, is proposed and numerically validated.

More recently, the Cooperative Adaptive Cruise Control (CACC) (an extension of the more classic Adaptive Cruise Control (ACC) [82], [61], [23], including information via Vehicle-to-Vehicle technology), can be applied to solve platooning. For example, in [89] a CACC solution is analyzed and experimentally validated to coordinate a vehicle with respect to the predecessor, including in the controller design the acceleration of the preceding vehicle collected via Vehicle-to-Vehicle communication. Moreover, a solution of CACC including the leader vehicle acceleration can be found in [70].

In 2011 the competition Grand Cooperative Driving Challenge (GCDC) took place in Helmond, Netherlands, with the aim of testing cooperative systems in different platoon scenarios, such as innovative solutions to control the longitudinal motion of vehicles with respect to the neighbors [146].

The problem has been also addressed during the activities of many research projects. The Energy ITS project [144] (see Fig. 3.1, top-right panel) is a Japanese project that aims at controlling both longitudinal and latitudinal control in truck platoon; Scania worked on distributed control of a heavy duty vehicle platoon, in particular with the application of the automatic longitudinal control (see Fig. 3.1, down left panel).

In SARTRE project [22] both longitudinal and lateral control techniques are applied to control a platoon of vehicles. An expert driver is responsible for the management of the platoon and to control the platoon with respect to path-following goal (see Fig. 3.1 top-left panel).

Nowadays, an higher degree of cooperation due to V2V technology and the increasing number of autonomous vehicles is capturing the interest of the scientific community in solving platooning. An interesting graph showing platooning with respect to the other applications in the autonomous driving framework is in Fig. 3.2.

3.1.3 Problems and challenges

Currently stability and robustness of the platoon are guaranteed by implementing a local cooperative adaptive control action (usually a Cooperative Adaptive Cruise Control or CACC): common CACC strategies rely on pairwise interactions. Namely, each vehicle only uses proximity information transmitted from its preceding vehicle in the platoon and local measurement by on-board sensors [101],[89]. Then, besides the convergence of the platoon to a common velocity and a well defined relative distance with respect to the neighbors, a typical aim of the theoretical analysis is to prove robustness i.e., that perturbations on the leader vehicle are not amplified when propagating downstream through the follower vehicles (see for example [70], [89], [43] and references therein). This property is also known in the technical literature with the name of string stability [27], [26]. Note that, as recently shown in literature, this predecessor-following architecture based on pairwise interactions can be highly sensitive to external disturbances along the string, that may lead to string instability, [45], [85]. Moreover, the complexity of the controller and the performance of the closed-loop system worsens as the number of vehicles increases.

Moreover, the presence of a distributed communication system allows to overcome sensors limitations [43], but new challenges arise due to uncertainties and time-varying

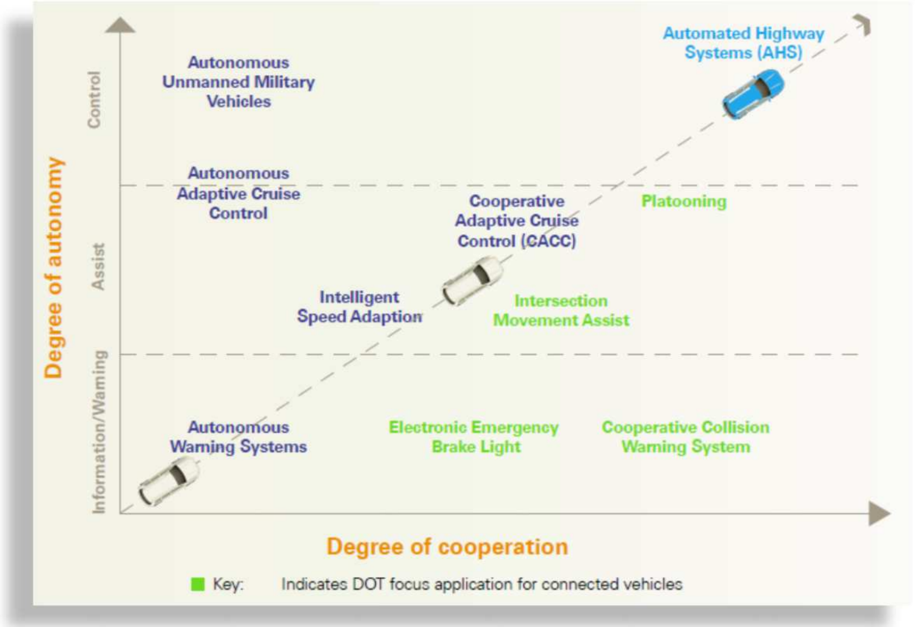

Figure 3.2: Self-driving applications plotted along two dimensions: the degree of autonomy and the degree of cooperation [130].

communication delay, in the presence of queueing, contention, transmission and propagation of the information via Vehicle-to-Vehicle. Indeed, a performance evaluation of the standard Wi-Fi communication protocol (for example IEEE 802.11p) and the way the protocol affects V2V environment can be found in [39], [6], [88], [149] in term of Quality of Service (QoS: packet loss, delay, jitter, throughput and available bandwidth; see also [14] for a deep study of the behaviour of QoS parameters in heterogeneous wireless/wired networks). In order to guarantee the IEEE 802.11p robustness in the vehicular environment, adaptive parameters strategies are used in V2V communication systems to alleviate network performance degradation due to high mobility, in particular in the presence of a non-zero relative speed and frequent network topology changes. For example, in [6], the service priority in V2V communication is based both on the number of neighbors and relative speed: in particular the deviation of the node speed with respect to the average speed of the neighbors is proportional to the level of channel access priority. As a consequence, the number of vehicles and their motion affect the communication in the wireless network and these effects have to be considered during the controller design. Moreover, the network induced effects have to be taken into account during the platooning performance evaluation. Indeed, in [78] authors analyze the robustness of the control strategy based on [27] with respect to communication delay. They focus on string stability, underling that the latter is influenced by communication delays. Moreover, bounds exists for communication delays such to guarantee string stability, in the presence of synchronized controllers.

Recent works address this problem within the CACC framework investigating the effect of constant delays on string stability within a Networked Control System prospective

(NCS) [100], [101], but considering interaction with the predecessor only.
Then, the importance of GPS receivers is becoming more and more essential for considering an absolute framework both for (i) positioning and (ii) clock synchronization.
All these issues have to be taken into account during the controller design.

3.2 A networks-based approach for platooning

Consider a group of N vehicles moving along a single lane. In the scenario under investigation, vehicles are organized as a *string* with vehicles following one another along a straight line sharing their state information (e.g., absolute position, velocity and acceleration) with all the other agents communicating through a V2V communication paradigm, as described in [22]. The on-board integration of inertial sensors with a Global Positioning System (GPS) receiver allows each vehicle to know, for example, absolute position, velocity and UTC (i.e. Coordinated Universal Time) [121]. Vehicles are also equipped with *communication modules* configured as receiving and transmitting hosts.

The platoon is usually in a leader-following structure, as is schematically depicted in Fig. 3.3 in the case of an extra urban scenario. Here the leader communicates in a broadcast mode with all followers, while each vehicle in the string only shares information with its neighbors. Referring to this scenario the reference trajectory according to the required spacing policy can be provided by the first vehicle in the platoon.
According to the paradigm of dynamical networks, the platoon is represented as a network where: (i) each *vehicle*, with its own dynamics, is a *node*; (ii) the presence of information flow through the *communication links* between neighboring vehicles is represented by the *edges*, and (iii) the structure of the inter-vehicle communication is encoded in the network topology. Note that the use of network paradigm is a promising solution suitable for exploring communication strategies alternative to pairwise interactions. For example, the possibility of vehicles communicating in cluster can be investigated because of conditions due to their proximity and practical communication constraints. Furthermore, switching topologies in network control design can be exploited to consider the effect of packet losses, communication failures or maneuvers of autonomous vehicles, like for example joining/leaving the platoon. Note that, although the string of vehicles is usually in a leader-predecessor configuration, i.e. a vehicle receives information both from the leader and predecessor, different topologies may arise depending on the communication technology and its specific transmission ranges [10].

Note that other attempts to solve platooning within the dynamical networks approaches have been recently independently presented in the literature. For example in [150] authors consider mobile robots (for example, small cars) to analyze and solve leader-following consensus without considering time-delays; moreover, in [45] a network of double integrators used to model vehicle dynamics is assumed with a nearest neighbor interaction, without considering time-delays. In [139], a leaderless strategy is proposed for three autonomous vehicles ideally moving in a circle and sharing information across an all-to-all configuration via V2V communication affected by a constant and common delay. Results on platooning as a consensus problem within the context of switching stochastic Markovian networks in absence of delay will appear in the literature [147] (see also [148] for preliminary results). Synchronization among agents has been also applied to vehicle platooning, but again in the absence of time delays [81].
Hence, the main idea of this thesis is to solve the longitudinal control problem for vehicle platoons with new solution in the field of networks of dynamical systems. The aim is thus to exploit the new paradigm of the dynamical networks, and its recent theoretical

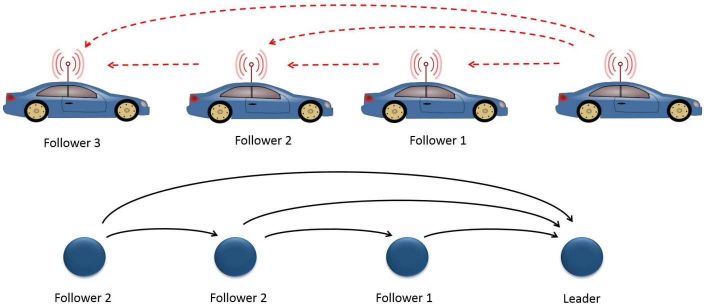

Figure 3.3: Schematics of representative platoon configurations. A leader and three followers $F1 - F2 - F3$. Note that the red dashed arrows in the top panel denote the V2V communication link among vehicles and with the leader, while those in the associated network graphs indicate edges directed according to the definition given in Section 2.1.1.

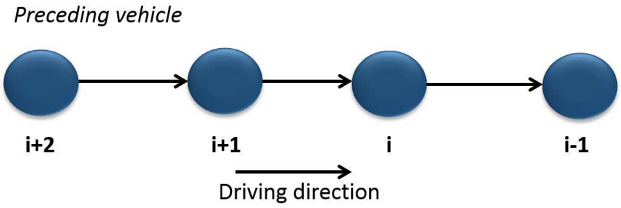

Figure 3.4: Vehicular topology: Preceding vehicle.

tools, to analyze and solve the platoon problem by treating it as the problem of achieving consensus in a network of dynamical systems [32], [120], [118], [119]. This new approach allows to guarantee platooning in the presence of heterogeneous time-varying delays, thus ensuring robustness with respect to uncertain wireless communication among vehicles. Furthermore, the formation and maintaining of the platoon can then be treated as the problem of finding conditions for the existence and stability of some emerging collective behavior at the network level induced by delocalized and decentralized control action.

3.2.1 Vehicular topologies

Now, we use graphs to describe all the possible topologies in vehicular networks: in our notation, each arrow in the figures below means that a specific vehicle receives the information flow from the linked vehicle through a V2V communication.
The most common emerging topologies are now discussed. In Fig. 3.4 we have the communication with respect to the *preceding vehicle* only, i.e. there is a V2V communication between the predecessor vehicle $i - 1$ and its follower i.
If the i-th vehicle receives information from N predecessors, we have the topology described in Fig. 3.5. In Fig. 3.6, we have that the i-th vehicle receives both information

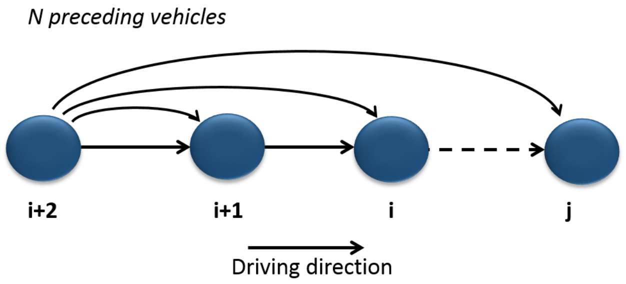
N preceding vehicles
i+2
i+1
i
j
Driving direction

Figure 3.5: Vehicular topology. N preceding vehicles.

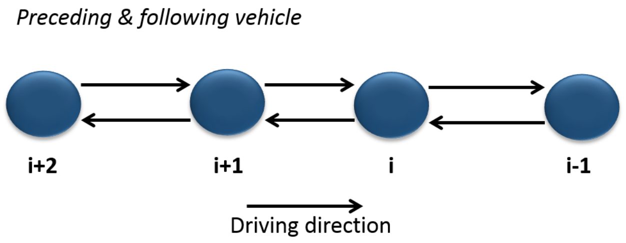
Preceding & following vehicle
i+2
i+1
i
i-1
Driving direction

Figure 3.6: Vehicular topology. Bidirectional.

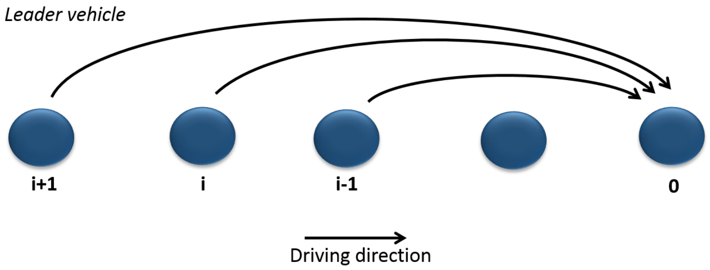
Leader vehicle
i+1
i
i-1
0
Driving direction

Figure 3.7: Vehicular topology. Leader.

from predecessor and follower via V2V. Then, Fig. 3.7 shows that i-th vehicle receives information from the leader vehicle only, while Fig. 3.8 means that i-th vehicle receives information from both the predecessor and the leader vehicle.

One of all the possible interactions of all the previous topology is depicted in Fig. 3.9.

Depending on whether the Inter-Vehicular Communication (IVC) is retransmitted at intermediate hops or not, we have either Single-hop IVC (SIVCs) or Multi-hop IVCs (MIVCs) [129]. SIVCs systems are useful for applications requiring short-range communications; instead, MIVC systems can also support applications that require long-range communications. Indeed, in a MIVCs system, a vehicle B can forward a received message from a vehicle A to another vehicle C, with C outside the transmission range of the

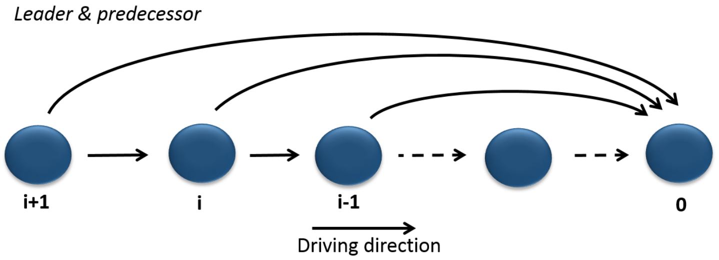

Figure 3.8: Vehicular topology. Leader-predecessor.

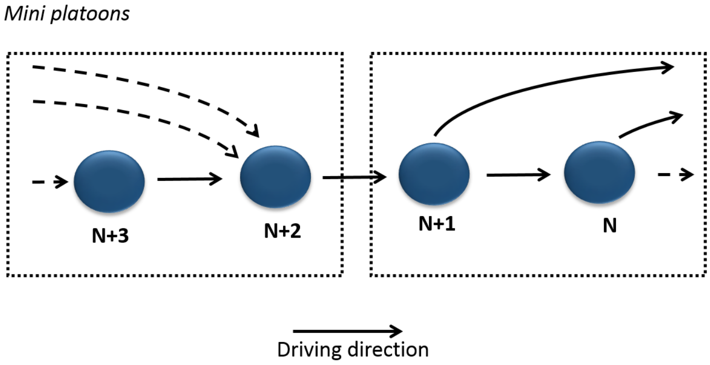

Figure 3.9: Vehicular topology. Mini platoons.

vehicle A. In so doing, vehicle C receives the information flow from the vehicle A.

3.2.2 Stability in a platoon of vehicles

Platooning has to satisfy the following criteria:

- **individual vehicle stability** - the closed-loop of the platoon of vehicles is asymptotically stable;
- **string stability** - any perturbation of the position or velocity due to any maneuver of the leading vehicle is not an amplified fluctuation to the following vehicle position and velocity.

Individual vehicle stability. We define $\epsilon_i = (x_i(t) - x_r(t) - L_{i,r})$, with $x_i, x_r \in \mathbb{R}$, the spacing error of the $i-$th vehicle with respect to the reference vehicle indexed by r, with $r = 0$ if we consider the leader or $r = i - 1$ [111] if we consider the predecessor, $x_i(t)$ is the position of the $i-$th vehicle with respect to an inertial reference, and $L_{i,r}$ the desired distance with respect to the reference vehicle. In general, individual vehicle stability means that if the reference vehicle had a constant velocity, the spacing error of the vehicle should converge to zero. In particular the control strategy provides individual vehicle stability if the following condition is satisfied [111]:

$$\ddot{x}_r \longrightarrow 0 \qquad \Rightarrow \qquad \epsilon_i \longrightarrow 0 \tag{3.1}$$

Instead, the spacing error is non-zero if the reference vehicle velocity is not constant.

String Stability. In a platoon of vehicles, the spacing error is expected to be non-zero only if preceding vehicle velocity is not constant, according to Paragraph 3.2.2. In order to describe the behaviour of the spacing error, velocity and acceleration about disturbance attenuation along a string of vehicles equipped with the same control strategy and spacing policy, we consider *string stability* (see Subsection 2.2.1).
The term *string stability* was used in [21],[108], applied for the first time in the vehicle-following framework. According to [27], string stability indicates the uniform boundedness of all the states of the interconnected system for all time if the initial states of the interconnected system are uniformly bounded. In [27] the authors generalized the concept of string stability to a class of interconnected systems: *sufficient condition* has been sought to guarantee the string stability of these systems, such that system cascading is made stable by ensuring that the error attenuates as it propagates downstream the platoon. In particular, string stability has been considered as a tool useful to demonstrate asymptotic stability of interconnected vehicles, focusing on initial condition perturbation [26]. In [78] authors consider the effects of communication delays on string stability. The relationship between string stability and spacing policies has been investigated in (see [152] and reference therein). Heterogeneous strings of vehicles have been analyzed in [126].
A performance-oriented approach is frequently used to evaluate string stability of interconnected systems [89]. This approach indicates that either distance error, velocity or acceleration do not amplify as they propagate in upstream direction [89]. In particular, any perturbation of the position or velocity of the lead vehicle will not be amplified resulting as following vehicle position or velocity fluctuation. In [101] a discrete-time interconnected system model and the corresponding discrete-time frequency response analysis are provided: in particular, authors define for the first time the string stability in frequency domain for discrete-time vehicle interconnected systems; then, there is a numerical analysis approach for the simplest interconnected vehicle string (i.e. two vehicles platoon), with respect to constant time delay τ. In [100] authors focus, deeper than in [101], the propagation of disturbances through the interconnected vehicle string by using string stability in terms of an $\mathscr{L}_2-$ gain requirement from disturbance inputs to controlled outputs. They consider sensitivity of NCS to perturbations, employing $\mathscr{L}_p-$ stability results for NCS developed in [47].

Note that another interesting tool to analyze the robustness in mobile agent is described in [143]. Here, authors investigate the stability properties of mobile agent formations which are based on leader-following, introducing the so called Leader-to-Formation Stability (LFS). Moreover, they use the input-to-state stability tool and its invariance properties under cascading to quantify error amplification during signal propagation (see [143] and references therein).

Part I

Distributed consensus for vehicle platooning

Chapter 4

Asymptotic stability of the closed loop vehicular network

Contents

4.1 Platooning as a consensus problem 31
4.2 Closed-loop vehicular network 33
4.3 Convergence analysis 35

In this Chapter the longitudinal control of a platoon when vehicles communicate via V2V communication technology is investigated. Within this scenario each vehicle can communicate not only with its follower, as in the classical predecessor-following architecture, but also with a subset of vehicles in the fleet. In particular, a distributed coupling protocol to achieve the longitudinal control of the platoon is proposed in Section 4.1. The proposed solution aims to guarantee the second order consensus to a target velocity defined on the leader vehicle motion. Moreover, a pre-defined inter-vehicle distance to satisfy the distributed control guarantees safety constrains. In Section 4.2 the entire closed-loop vehicular system is recast as a delayed dynamical network whose convergence analysis is provided in Section 4.3.

4.1 Platooning as a consensus problem

Consider the generic platoon scenario in Fig. 3.3. Within our framework, the behavior of the generic i-th vehicle is mathematically described as the following inertial agent ($i = 1, \ldots, N$):

$$\begin{aligned} \dot{r}_i(t) &= v_i(t) \\ \dot{v}_i(t) &= \frac{1}{M_i} u_i(t), \end{aligned} \tag{4.1}$$

where $r_i(t)$ [m] and $v_i(t)$ [m/s] are the i-th vehicle position and velocity, measured with respect to a given reference framework, M_i [kg] is the i-th vehicle mass assumed to be constant and $u_i(t)$ denotes the control input to be appropriately chosen to achieve the desired position, speed keeping and braking maneuvers (see Fig. 4.1). Note that the vehicle linear model (4.1) can be derived by applying input–output (I/O) feedback linearization to simplify the complexity of the model describing the longitudinal vehicle dynamics and without considering parasitic time delays and lags [152], [17]. Furthermore, we remark that the cooperative platoon control provides an high level control action. Hence, following a hierarchal approach, the specific throttle/brake commands necessary to track the desired acceleration trajectory are imposed by the standard on-board vehicle control strategies. Finally, we define the state vector of the $i-$th vehicle as $\eta_i(t) = [\eta_i^{(1)}(t), \eta_i^{(2)}(t)]^\top = [r_i(t), v_i(t)]^\top \in \mathbb{R}^2$. In the leader-following architecture [93], the spacing policy is determined according to the reference dynamics provided by the leader (see Fig. 4.1). Assuming platoon has to move with a reference constant velocity, say v_0, the leader reference dynamics can be described as:

$$\begin{aligned} \dot{r}_0(t) &= v_0; \\ \dot{v}_0 &= 0. \end{aligned} \tag{4.2}$$

We label as $\eta_0(t) = [r_0(t), v_0]^\top \in \mathbb{R}^2$ the leader state vector.

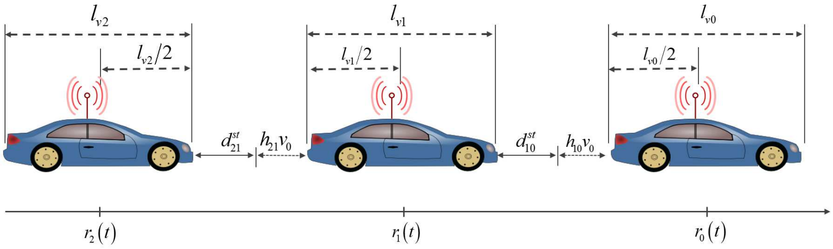

Figure 4.1: Schematics of the spacing policy. Leader and two followers $F1 - F2$.

Given equations (4.1) - (4.2), the problem of maintaining a desired inter-vehicle spacing policy and a common velocity of the platoon of vehicles under limited communication in the presence of delays can be rewritten as a second order consensus problem with the aim of driving the positions and velocities of all vehicles towards the following desired steady-state values:

$$\begin{aligned} & r_i(t) \to \frac{1}{d_i} \left\{ \sum_{j=0}^{N} a_{ij} \cdot (r_j(t) + d_{ij}) \right\} \\ & v_i(t) \to v_0. \end{aligned} \tag{4.3}$$

where d_{ij} are the desired spacing vehicle separation between vehicles i and j [28], a_{ij} (for $i = 1, \dots, N$ and $j = 0, \dots, N$) are the nonnegative elements (i.e. $a_{ij} = 0/1$) that models the network topology emerging from the presence/absence of the information flow through the communication links (see Subsection 2.1.1 for definitions and further mathematical details) and $d_i = \sum_{j=0}^{N} a_{ij}$ is the degree of vehicle/agent i. In so doing, we consider N follower vehicles (agents or nodes) together with a leader vehicle taken as an additional agent labelled with the index zero i.e., node 0. Furthermore, we assume $a_{0j} = 0$ ($\forall j = 0, \dots, N$), since the leader could not be interested in receiving data from any other vehicle. The desired spacing vehicle separation d_{ij} can be expressed in terms of the *constant time headways* h_{ij} (e.g., the time that the $i-$th vehicle takes to arrive at the position of its predecessor, for constant velocity) and their distance at standstill, say d_{ij}^{st}, as $d_{ij} = h_{ij}v_0 + d_{ij}^{st}$ [29] (see Figure 4.1 and Appendix A.1 for further details). Setting $h_{ij} = -h_{ji}$ (in order to increase safety, for example, with respect to the vehicles following the $i-$th agent as done in [8]), the consensus target (4.3) can be easily rewritten, after some algebraic manipulations, in a more compact form as:

$$\begin{aligned} &r_i(t) \to r_0(t) + d_{i0} \\ &v_i(t) \to v_0. \end{aligned} \tag{4.4}$$

where d_{i0} is the desired spacing vehicle separation with respect to the leader. Consensus (4.4) can be achieved using an appropriate distributed strategy that takes explicitly into account the information exchange through the communication layer as:

$$u_i = u_i\left(\eta_i\left(t\right), \eta_j\left(t, \tau_{ij}\left(t\right)\right), \eta_0\left(t, \tau_{i0}\left(t\right)\right)\right), \tag{4.5}$$

where $\tau_{ij}(t)$ and $\tau_{i0}(t)$ are the unavoidable time-varying communication delays affecting the i-th agent when information is transmitted from its neighbor j and from the leader, respectively. Note that communication is assumed to be such that in general the delay $\tau_{ij}(t) \neq \tau_{ji}(t)$. In so doing different communication links, based on different communication tools/technologies may be considered. Focusing on the road segment close to the receiver-vehicle, the time delay $\tau_{ij}(t)$ can be assumed to be bounded between a maximum and minimal value, e.g. $0 \leq \tau_{ij}(t) \leq \tau$ [14], [6] ($\tau_{ij}(t)$ is a *piecewise continuous function*). Note that if some of the network information, like the state of the preceding vehicle, is available from on-board sensor measurements they results to be not affected by sensible delay and, hence, this link can be also modeled with $\tau_{ij}(t) = 0$. Furthermore, although the delay $\tau_{ij}(t)$ is unknown, it is detectable and it can be evaluated on-board from all agents when they receive information, since all neighbor vehicles transmits not only their absolute position and velocity information to the i-th vehicle, but also the relative timestamp $\bar{t}$, representing the time instant at which the information are measured [19], [49]. Note that the clock synchronization is guaranteed across all the string via GPS [40] (see Section 6.6 for details).

In what follows, the platoon consensus problem (4.4) is solved by the following distributed coupling protocol embedding the spacing policy information as well as the time-varying communication delay:

$$u_i = -b\left[v_i\left(t\right) - v_0\right] - \frac{1}{d_i}\sum_{j=0}^{N} k_{ij}a_{ij}\left[r_i\left(t\right) - r_j\left(t - \tau_{ij}\left(t\right)\right) - \tau_{ij}\left(t\right)v_0 - h_{ij}v_0 - d_{ij}^{st}\right], \tag{4.6}$$

where k_{ij} and b are stiffness and damping coefficients to be opportunely tuned to regulate the mutual behavior among the neighboring inertial agents (i.e. the distributed coupling protocol parameters).

4.2 Closed-loop vehicular network

To prove consensus (4.4) of system (4.1)-(4.2) under the action of the coupling protocol (4.6), we define the following position and velocity errors with respect to the reference signals $r_0(t), v_0$ $(i = 1, \ldots, N)$ as:

$$\begin{aligned} &\bar{r}_i = (r_i(t) - r_0(t) - h_{i0}v_0 - d_{i0}^{st}); \\ &\bar{v}_i = (v_i(t) - v_0), \end{aligned} \tag{4.7}$$

and the position and velocity error vectors as $\bar{r} = \left[\bar{r}_1, ..., \bar{r}_i, ..., \bar{r}_N\right]^\top$, $\bar{v} = \left[\bar{v}_1, ..., \bar{v}_i, ..., \bar{v}_N\right]^\top$ respectively.

To derive the expression of the closed-loop vehicular network, in what follows we first rewrite the coupling protocol (4.6) in terms of the state error (4.7). Expressing both the headway constants h_{ij} and the standstill distances between vehicles i and j, d_{ij}^{st}, with respect to the leading vehicle, namely $h_{ij} = h_{i0} - h_{j0}$ and $d_{ij}^{st} = d_{i0}^{st} - d_{j0}^{st}$ (see Appendix A.1), the distributed coupling protocol (4.6) can be at first easily rewritten as:

$$\begin{aligned} u_i\left(t\right) =& -b(v_i(t) - v_0) - \tfrac{1}{d_i} \sum_{j=1}^{N} k_{ij} a_{ij} \left[r_i\left(t\right) - r_0\left(t\right) - h_{i0} v_0 - d_{i0}^{st}\right] \\ & - \tfrac{1}{d_i} \sum_{j=1}^{N} k_{ij} a_{ij} \left[-r_j\left(t - \tau_{ij}\left(t\right)\right) + r_0\left(t - \tau_{ij}\left(t\right)\right) + h_{j0} v_0 + d_{0j}^{st}\right] + \\ & - \tfrac{1}{d_i} k_{i0} a_{i0} \left[r_i\left(t\right) - r_0\left(t - \tau_{i0}\left(t\right)\right) - \tau_{i0}\left(t\right) v_0 - h_{i0} v_0 - d_{i0}^{st}\right] \\ & - \tfrac{1}{d_i} \sum_{j=1}^{N} k_{ij} a_{ij} \left[r_0\left(t\right) - r_0\left(t - \tau_{ij}\left(t\right)\right) - \tau_{ij}\left(t\right) v_0\right]. \end{aligned} \tag{4.8}$$

Since $r_0(t) = r_0\left(t - \tau_{ij}\left(t\right)\right) + \tau_{ij}(t) v_0$ $(j = 0, \ldots, N)$, from (4.8), after some algebraic manipulations (see Appendix A.2 for details), we obtain:

$$u_i\left(t\right) = -b\bar{v}_i - \frac{1}{d_i} \sum_{j=1}^{N} k_{ij} a_{ij} \left[\bar{r}_i\left(t\right) - \bar{r}_j\left(t - \tau_{ij}\left(t\right)\right)\right] - \frac{1}{d_i} k_{i0} a_{i0} \bar{r}_i. \tag{4.9}$$

Hence, the closed-loop dynamics of the error variables under the coupling protocol (4.9) can be written for a generic i-th vehicle in the platoon $(i = 1, \ldots, N)$ as

$$\left\{ \begin{array}{lcl} \dot{\bar{r}}_i & = & \bar{v}_i, \\ M_i \dot{\bar{v}}_i & = & -\frac{1}{d_i}(k_{i0} a_{i0} + \sum_{j=1}^{N} k_{ij} a_{ij}) \bar{r}_i - b\bar{v}_i + \frac{1}{d_i} \sum_{j=1}^{N} k_{ij} a_{ij} \left[\bar{r}_j\left(t - \tau_{ij}\left(t\right)\right)\right]. \end{array} \right. \tag{4.10}$$

Recasting the closed-loop network dynamics in the presence of the time-varying delays associated to the different links in a compact form, we now define the error state vector as $\bar{x}\left(t\right) = \left[\begin{array}{cc} \bar{r}^\top\left(t\right) & \bar{v}^\top\left(t\right) \end{array}\right]^\top$ and $\tau_p(t) \in \{\tau_{ij}(t) : i, j = 1, 2, ..., N, i \neq j)$ for $p = 1, 2, ..., m$ with $m \leq N(N-1)$ $(0 \leq \tau_p(t) \leq \tau)$.

Remark 4.2.1. m is the total number of different time delays and it is equal to its maximum, $N(N-1)$, if the network is represented by a directed complete graph and all time delays are different.

From (4.10), the dynamics of the closed loop vehicular network is:

$$\dot{\bar{x}}\left(t\right) = A_0 \bar{x}\left(t\right) + \sum_{p=1}^{m} A_p \bar{x}\left(t - \tau_p\left(t\right)\right), \tag{4.11}$$

where

$$A_0 = \left[\begin{array}{cc} 0_{N\times N} & I_{N\times N} \\ -M\widetilde{K} & -M\widetilde{B} \end{array}\right] \quad \text{and} \quad A_p = \left[\begin{array}{cc} 0_{N\times N} & 0_{N\times N} \\ M\widetilde{K}_p & 0_{N\times N} \end{array}\right] \tag{4.12}$$

being

$$M = \operatorname{diag}\left\{\frac{1}{M_1}, \ldots, \frac{1}{M_N}\right\} \in \mathbb{R}^{N\times N}; \qquad \widetilde{B} = \operatorname{diag}\{b, \ldots, b\} \in \mathbb{R}^{N\times N}; \tag{4.13}$$

$$\widetilde{K} = \operatorname{diag}\left\{\tilde{k}_{11}, \ldots, \tilde{k}_{NN}\right\} \in \mathbb{R}^{N\times N}, \text{ with } \tilde{k}_{ii} = \frac{1}{d_i} \sum_{j=0}^{N} k_{ij} a_{ij}; \tag{4.14}$$

and $\widetilde{K}_p = [\bar{k}_{pij}] \in \mathbb{R}^{N\times N}$ $(p = 1, \dots, m)$ is the matrix defined, according to the formalism adopted in [155], as:

$$\bar{k}_{pij} = \begin{cases} \frac{k_{ij}a_{ij}}{d_i}, & j \neq i, \tau_p(\cdot) = \tau_{ij}(\cdot), \\ 0, & j \neq i, \tau_p(\cdot) \neq \tau_{ij}(\cdot). \\ 0, & j = i. \end{cases} \tag{4.15}$$

Remark 4.2.2. Matrix $\widetilde{K}$ in (4.14) can be recast as follows:

$$\widetilde{K} = K + \bar{K} \tag{4.16}$$

where

$$K = \mathrm{diag}\{k_1, \dots, k_N\}, \quad \text{being} \quad k_i = \frac{k_{i0}a_{i0}}{d_i} \qquad (i = 1, \dots, N), \tag{4.17}$$

and

$$\bar{K} = \mathrm{diag}\{\bar{l}_{11}, \dots, \bar{l}_{NN}\}, \tag{4.18}$$

being $\bar{l}_{ii}$ the diagonal elements of the normalized weighted Laplacian matrix $\bar{L}$ associated to the weighted graph $\mathcal{G}_N$ [97] defined as:

$$\bar{l}_{ii} = \frac{1}{d_i} l_{ii} = \frac{1}{d_i} \sum_{j=1}^{N} k_{ij}a_{ij} \qquad (i = 1, \dots, N), \tag{4.19}$$

where l_{ii} are the diagonal elements of the weighted Laplacian matrix L of $\mathcal{G}_N$ (see Subsection 2.1.1).

Remark 4.2.3. From the definition of $\widetilde{K}_p$ and $\bar{K}$ given in (4.15) and (4.18), respectively, the normalized weighed Laplacian $\bar{L}$ can also be recast as:

$$\bar{L} = \left[\bar{l}_{ij}\right]_{N\times N} = \bar{K} - \sum_{p=1}^{m} \widetilde{K}_p \quad (i, j = 1, \dots, N;\ j \neq 0). \tag{4.20}$$

4.3 Convergence analysis

Now, before solving the consensus problem in the presence of time-varying communication delays, we introduce a model transformation. From the Leibniz-Newton formula is known that [135]:

$$\bar{x}\left(t - \tau_p(t)\right) = \bar{x}\left(t\right) - \int_{-\tau_p(t)}^{0} \dot{\bar{x}}\left(t + s\right) ds. \tag{4.21}$$

Hence, substituting expression (4.11) in (4.21) we have:

$$\bar{x}\left(t - \tau_p(t)\right) = \bar{x}\left(t\right) - \sum_{q=0}^{m} A_q \int_{-\tau_p(t)}^{0} \bar{x}\left(t + s - \tau_q\left(t + s\right)\right) ds, \tag{4.22}$$

where matrices $A_0, A_1, \dots, A_m$ are defined in (4.12) and $\tau_0\left(t + s\right) \equiv 0$.

Expressing the delayed state as in (4.22), the time-delayed model (4.11) can be transformed into:

$$\dot{\bar{x}}\left(t\right) = A_0\bar{x}\left(t\right) + \sum_{p=1}^{m} A_p\bar{x}\left(t\right) - \sum_{p=1}^{m}\sum_{q=0}^{m} A_pA_q \int_{-\tau_p(t)}^{0} \bar{x}\left(t + s - \tau_q\left(t + s\right)\right) ds. \tag{4.23}$$

From definition (4.12) it follows that $A_pA_q = 0$ when $p = 1, \dots m$ and $q = 1, \dots, m$ $(q \neq 0)$. Hence system (4.11) can be rewritten as:

$$\dot{\bar{x}}(t) = F\bar{x}(t) - \sum_{p=1}^{m} C_p \int_{-\tau_p(t)}^{0} \bar{x}(t+s)\, ds \tag{4.24}$$

where

$$C_p = A_pA_0 = \begin{bmatrix} 0_{N\times N} & 0_{N\times N} \\ 0_{N\times N} & M\widetilde{K}_p \end{bmatrix}, \tag{4.25}$$

and

$$F = A_0 + \sum_{p=1}^{m} A_p = \begin{bmatrix} 0_{N\times N} & I_{N\times N} \\ -M\widehat{K} & -M\widetilde{B} \end{bmatrix}, \tag{4.26}$$

with

$$\widehat{K} = -\sum_{p=1}^{m} \widetilde{K}_p + \widetilde{K}. \tag{4.27}$$

Before giving the proof of convergence we introduces some preliminary Lemmas.

Lemma 4.3.1. *Supposing $k_i \geq 0$ in (4.17) $(i = 1, \dots, N)$, the matrix $\widehat{K}$ in (4.27) is positive stable if and only if node* 0 *is globally reachable in $\mathcal{G}_{N+1}$.*

Proof. (*Sufficiency*). Firstly, substituting expression (4.16) into (4.27), from (4.20) we have $\widehat{K} = \bar{L} + K$. According to *Geršgorin* disk theorem [52], all eigenvalues of $\widehat{K}$ are located in the union of N discs, the so-called *Geršgorin region* given by:

$$D(\widehat{K}) = \bigcup_{i=1}^{N} \{z \in \mathbb{C} : |z - \bar{l}_{ii} - k_i| \leq \sum_{\substack{j\neq i\\ j\neq 0}}^{N} |\bar{l}_{ij}|\} \tag{4.28}$$

From the assumptions $k_i \geq 0$ and the protocol gains $k_{ij} > 0, (i = 1, \dots, N$ and $j = 0, \dots, N)$, therefore each *Geršgorin disc* is located in the right-hand side of the complex plane and matrix $\widehat{K}$ has either zero eigenvalue or eigenvalue with positive real-part. Furthermore, from the assumption that node 0 is globally reachable in $\mathcal{G}_{N+1}$, there exists at least one $k_i > 0$, and therefore at least one *Geršgorin circle* bounding a corresponding *Geršgorin disc*, that does not pass through the origin of the complex plane.

Now to prove the sufficient condition we consider the following two cases.
Case(a): *$\mathcal{G}_N$ has a globally reachable node.* Let $S_1, \dots, S_q$ $(q \in \mathbb{Z}^+)$ be the strong components of $\mathcal{G}_N$. If we consider $q = 1$, $\mathcal{G}_N$ is strongly connected and its weighted adjacency matrix $\left(\sum_{p=1}^{m} \widetilde{K}_p\right)$ has also property *SC* (see Def. 2.2.2). Since $\left(K + \bar{K}\right)$ is a diagonal matrix with nonnegative diagonal entries, also the matrix $\widehat{K}$ has property SC. According to [52], if zero is a simple eigenvalue of $\widehat{K}$, then every *Geršgorin circle* of $\widehat{K}$ passes through 0, which leads to a contradiction. It follows that zero cannot be an eigenvalue of $\widehat{K}$. Then, if we consider $q > 1$, according to Lemma 2.1.1, there is one strong component, say S_1, having no neighbor set. We can then rewrite the normalized weighted Laplacian matrix $\bar{L}$ in the following block form:

$$\bar{L} = \begin{pmatrix} \bar{L}^{(11)} & 0 \\ \bar{L}^{(21)} & \bar{L}^{(22)} \end{pmatrix} \tag{4.29}$$

with $\bar{L}^{(11)} \in \mathbb{R}^{\iota\times\iota}$ ($\iota < N$) the normalized weighted Laplacian matrix of S_1. From Lemma 2.1.2, it follows that zero is a simple eigenvalue of $\bar{L}^{(11)}$ (and therefore $\bar{L}$), while $\bar{L}^{(22)}$ is nonsingular. Node 0 is globally reachable, hence the block corresponding to $\bar{L}^{(11)}$ in the matrix K, say K_1 is not null. As done for the case when $q = 1$, it follows that zero is not an eigenvalue of $\bar{L}^{(11)} + K_1$ and therefore it is not an eigenvalue of $\widehat{K}$.
Case(b): *$\mathcal{G}_N$ has no globally reachable node.* Let $S_1, \ldots, S_q$ ($q \in \mathbb{Z}^+$) be the strong components with $\mathcal{N}_{S_\xi} = \emptyset$ for $\xi = 1, \ldots, q$ being $q > 1$. As $\bigcup\limits_{\xi=1}^{q} \mathcal{V}(S_\xi) \subset \mathcal{V}(\mathcal{G}_N)$, the matrix $\bar{L}$ associated to $\mathcal{G}_N$ can be recast in the following form:

$$\bar{L} = \begin{pmatrix} \bar{L}^{(11)} & 0 & \cdots & \cdots & 0 \\ \vdots & \bar{L}^{(22)} & \ddots & \ddots & \vdots \\ \vdots & \ddots & \ddots & \ddots & \vdots \\ \vdots & \ddots & \ddots & \bar{L}^{(qq)} & \vdots \\ \bar{L}^{(q+1,1)} & \cdots & \cdots & \bar{L}^{(q+1,q)} & \bar{L}^{(q+1,q+1)} \end{pmatrix} \tag{4.30}$$

where $\bar{L}^{(\xi\xi)}$ is the normalized weighted Laplacian matrix of S_ξ ($\xi = 1, \ldots, q$); $\bar{L}^{(q+1,q+1)}$ is nonsingular. Node 0 is globally reachable in $\mathcal{G}_{N+1}$, then the blocks K_ξ in K corresponding $\bar{L}^{(\xi\xi)}$ are non-null. Following the same steps taken to prove *Case (a)*, we can conclude that zero is not an eigenvalue of $\bar{L}^{(\xi\xi)} + K_\xi$ or equivalently $\widehat{K}$.
(*Necessity*). If node 0 is not globally reachable in $\mathcal{G}_{N+1}$, then $\mathcal{G}_N$ may have or not a globally reachable node. Consider first the case when $\mathcal{G}_N$ has a globally reachable node. Following the approach used to prove *Case(a)* above, assuming $\mathcal{V}_1$ has no neighbor set, we can derive again (4.29) with $\bar{L}^{(11)} \in R^{\iota\times\iota}$ ($\iota < N$) being the weighted Laplacian matrix corresponding to $\mathcal{V}_1$. Again from Lemma 2.1.2, it follows that zero is an eigenvalue of $\bar{L}^{(11)}$ and $\bar{L}$ while $\bar{L}^{(22)}$ is nonsingular. Now, since node 0 is not globally reachable in $\mathcal{G}_{N+1}$, we have $K_1 = 0$, hence zero is a simple eigenvalue of $\bar{L}^{(11)} + K_1$ and a simple eigenvalue of $\widehat{K}$, leading to a contradiction.
Instead, when $\mathcal{G}_N$ has no globally reachable node, we consider (4.30) as in *Case(b)*. Node 0 is not globally reachable in $\mathcal{G}_{N+1}$, hence, there exist at least one $K_\xi = 0$ (corresponding to $\bar{L}^{(\xi\xi)}$) for $\xi = 1, \ldots, q$. Thus $\bar{L}^{(\xi\xi)} + K_\xi$ and, correspondingly, $\widehat{K}$ have more than one zero eigenvalues and this implies a contradiction. In so doing the Lemma is proven. ☐

Remark 4.3.1. Notice that according to Lemma 4.3.1 the following matrix

$$\widehat{K}_M = M\widehat{K} \tag{4.31}$$

is also positive stable since $M > 0$ (4.13).

Lemma 4.3.2. *Let F be the matrix defined in (4.26). F is Hurwitz stable if and only if $\widehat{K}_M$ (4.31) in Lemma 4.3.1 is positive stable and*

$$b > \max_i \left\{ \frac{|Im(\mu_i)|}{\sqrt{Re(\mu_i)}} M_i \right\} \tag{4.32}$$

being μ_i the i-th eigenvalue of $\widehat{K}_M$ ($i = 1, \ldots, N$).

Proof. According to Lemma 4.3.1 select gains $k_i \geq 0$ ($i = 1, \ldots, N$), so that the matrix $\widehat{K}_M$ defined as in (4.31) is positive stable i.e., $Re(\mu_i) > 0$ for any $\mu_i \in \Lambda(\widehat{K}_M)$[48], with

$\Lambda(\widehat{K}_M)$ the spectrum of the matrix $\widehat{K}_M$. Exploiting Schur's formula (see Lemma 2.2.2), the characteristic polynomial of F can be computed as:

$$\begin{aligned} \det(sI_{2N\times 2N} - F) &= \det\left(\begin{bmatrix} sI_{N\times N} & -I_{N\times N} \\ \widehat{K}_M & \left(M\widetilde{B} + sI_{N\times N}\right) \end{bmatrix}\right) = \\ = \det\left(\begin{bmatrix} sI_{N\times N} & -I_{N\times N} \\ \widehat{K}_M & (bMI_{N\times N} + sI_{N\times N}) \end{bmatrix}\right) &= \det(s^2 I_{N\times N} + bMI_{N\times N}s + \widehat{K}_M). \end{aligned} \tag{4.33}$$

From (4.33), we have:

$$\det(sI_{2N\times 2N} - F) = \prod_{i=1}^{N}(s^2 + \frac{b}{M_i}s + \mu_i) \tag{4.34}$$

where μ_i is the i-th eigenvalue of $\widehat{K}_M$. Since the polynomial $\pi(s,\mu_i) = s^2 + \frac{b}{M_i}s + \mu_i$ is Hurwitz stable if and only if $Re(\mu_i) > 0$ and $b > (|Im(\mu_i)|/\sqrt{Re(\mu_i)})M_i$ [52], it follows that all eigenvalues of F have negative real parts if and only if inequality (4.32) is fulfilled. In so doing the Lemma is proved. ☐

The consensus of the vehicular network in the presence of heterogeneous time-varying delays can be guaranteed under the hypothesis of the following theorem.

Theorem 4.3.1. *Consider system (4.11) and take the control parameters in (4.6) as* $k_{ij} > 0$ *and* b *such that*

$$b > b^* = \max_i \left\{ \frac{|Im(\mu_i)|}{\sqrt{Re(\mu_i)}} M_i \right\} \tag{4.35}$$

where $\widehat{K}_M$ *is defined in (4.31). Then, there exists a constant* $\tau^\star > 0$ *such that, when* $0 \leq \tau_p(t) \leq \tau < \tau^\star$ $(p = 1, \ldots, m)$,

$$\lim_{t\to\infty} \bar{x}(t) = 0, \tag{4.36}$$

if and only if node 0 *is globally reachable in* $\mathcal{G}_{N+1}$.

Proof. (*Sufficiency*). Since node 0 is globally reachable in $\mathcal{G}_{N+1}$, from Lemma 4.3.1 it follows that the matrix $\widehat{K}_M$ is positive stable. Setting b as in (4.35), the hypothesis of Lemma 4.3.2 is satisfied, hence the matrix F defined in (4.26) is Hurwitz stable and from Lyapunov theorem there exists a positive definite matrix $P \in \mathbb{R}^{2N\times 2N}$ such that

$$PF + F^\top P = -Q; \quad Q = Q^\top > 0. \tag{4.37}$$

Consider the following Lyapunov-Razumikhin candidate function (e.g. satisfying condition (2.43) of Lyapunov-Razumikin in Section 2.2.1)

$$V(\bar{x}) = \bar{x}^\top P\bar{x}. \tag{4.38}$$

Then, according to the Lyapunov-Razumikhin theorem in Section 2.2.1, we have:

$$\psi_1(\|x\|) \leq x^\top Px \leq \psi_2(\|x\|) \tag{4.39}$$

where, according to the Rayleigh inequality [52] $\psi_1(s) = \lambda_{min}(P)s^2$ and $\psi_1(s) = \lambda_{max}(P)s^2$, being $\lambda_{\min}(P)$ and $\lambda_{\max}(P)$ the minimun and the maximum eigenvalue of

P, respectively. Note that $\psi_1(s)$ and $\psi_2(s)$ are continuous, nonnegative, nondecreasing functions with $\psi_1(s) > 0$, $\psi_s(s) > 0$ for $s > 0$ and $\psi_1(0) = \psi_2(0) = 0$.
From equation (4.24), taking the derivative of V along (4.11) gives:

$$\dot{V}(\bar{x}) = \bar{x}^\top (PF + F^\top P)\bar{x} - \sum_{p=1}^{m} 2\bar{x}^\top PC_p \int\limits_{-\tau_p(t)}^{0} \bar{x}(t+s)ds. \tag{4.40}$$

Now, according to [52], for any positive definite matrix $\Xi \in \mathbb{R}^{m\times m}$ and $a, c \in \mathbb{R}^m$, it is possible to show that $2a^\top c \leq a^\top \Xi a + c^\top \Xi^{-1} c$. Therefore, setting $a^\top = -\bar{x}(t)^\top PC_p$, $c = \bar{x}(t+s)$, $\Xi = P^{-1}$, and integrating both sides of the inequality, we can write:

$$\begin{aligned}\dot{V}(\bar{x}) \quad \leq \quad & \bar{x}^\top (PF + F^\top P)\bar{x} + \sum_{p=1}^{m} \int\limits_{-\tau_p(t)}^{0} [\bar{x}^\top PC_p] P^{-1} [C_P^\top P\bar{x}] ds \\ & + \sum_{p=1}^{m} \int\limits_{-\tau_p(t)}^{0} \bar{x}^\top (t+s) P\bar{x}(t+s) ds.\end{aligned} \tag{4.41}$$

such that:

$$\begin{aligned}\dot{V}(\bar{x}) \quad \leq \quad & \bar{x}^\top (PF + F^\top P)\bar{x} + \sum_{p=1}^{m} \tau_p(t) \bar{x}^\top PC_p P^{-1} C_P^\top P\bar{x} \\ & + \sum_{p=1}^{m} \int\limits_{-\tau_p(t)}^{0} \bar{x}^\top (t+s) P\bar{x}(t+s) ds.\end{aligned} \tag{4.42}$$

Choosing the following continuous, nondecreasing function $\psi_4(s) = qs$ (for some constant $q > 1$), when:

$$V(\bar{x}(t+\theta)) = \bar{x}(t+\theta)^\top P\bar{x}(t+\theta) < \psi_4(V(\bar{x})) = qV(\bar{x}(t)) = q\bar{x}(t)^\top P\bar{x}(t), \; -\tau \leq \theta \leq 0, \tag{4.43}$$

then, inequality (4.42) becomes:

$$\begin{aligned}\dot{V}(\bar{x}) \quad \leq \quad & \bar{x}^\top (PF + F^\top P)\bar{x} + \sum_{p=1}^{m} \tau_p(t) \bar{x}^\top PC_p P^{-1} C_P^\top P\bar{x} \\ & + q \sum_{p=1}^{m} \int\limits_{-\tau_p(t)}^{0} \bar{x}^\top (t) P\bar{x}(t) ds\end{aligned} \tag{4.44}$$

Hence, the integral term in (4.44) becomes:

$$\int\limits_{-\tau_p(t)}^{0} \bar{x}^\top (t) P\bar{x}(t) ds = \tau_p(t)\bar{x}(t)^\top P\bar{x}(t) \leq \tau\bar{x}(t)^\top P\bar{x}(t). \tag{4.45}$$

Substituting (4.45) in (4.44), after simple algebraic manipulation, equation (4.42) becomes:

$$\dot{V}(\bar{x}) \leq -\psi_3(||\bar{x}||), \tag{4.46}$$

being $\psi_3(s) = (\lambda_{\min}(Q) - \tau\lambda_{\max}(H))s^2$ a continuous, nonnegative, nondecreasing function (as required by the Lyapunov-Razumikhin theorem) and $\lambda_{\max}(H)$ the maximum eigenvalue of the matrix H defined as $H = \sum_{p=1}^{m} (PC_p P^{-1} C_P^\top P + qP)$. Then, $\psi_3(s)$ is a positive function for $s > 0$ and null for $s = 0$ if:

$$\tau < \tau^\star := \frac{\lambda_{\min}(Q)}{\lambda_{\max}(H)}. \tag{4.47}$$

In so doing, the sufficient condition is proven.

(*Necessity*). System (4.11) is asymptotically stable for any time delay $\tau_p(t) \leq \tau < \tau^\star (p = 1, \ldots, m)$. Letting $\tau_p(t) \equiv 0$ $(p = 1, \ldots, m)$ in (4.11), from (4.24) it follows that system $\dot{\bar{x}} = F\bar{x}$, with F defined in (4.26), is asymptotically stable. As all the eigenvalues of F have negative real parts, Lemma 4.3.2 implies that $\widehat{K}_M$ is positive stable. Now, applying Lemma 4.3.1, the theorem is proven. □

Chapter 5

Numerical analysis

Contents

5.1 Consensus in nominal conditions 41
5.2 Robustness with respect to perturbations 45
5.2.1 Disturbance propagation through the string 45
5.2.2 Communication failures 47

In this Chapter we describe the numerical analysis used to validate the proposed distributed coupling protocol (4.6) in the Matlab/Simulink environment. Numerical results showing consensus are reported in Section 5.1, while robustness in the presence of sudden disturbances due to the leader motion and communication failures can be found in Section 5.2.

5.1 Consensus in nominal conditions

As a first attempt for the validation of platoon consensus, some numerical investigations have been performed by using the Matlab/Simulink platform. As a representative example, we refer to a platoon of two vehicles and a leader as depicted in Fig. 5.1. According to the ITS extra-urban scenario described in [22], the leader communicates with all the vehicles in a broadcast mode, while every vehicle shares information with its neighbors through wireless technology [22], [39]. Note that this scenario will be considered also for the on the road tests (as discussed in Chapter 7). Simulations results are related to a single lane road, where the leader vehicle imposes a common and constant fleet velocity equal to 20 [m/s] (i.e., 72 [km/h]). The spacing policy requires a constant time headway $h_{01} = h_{12} = 0.8$ [s] for all vehicles in the platoon with $h_{ij} = -h_{ji}$. Note that the simulation scenario has been set according to [88], where it is shown that for this specific choice of parameters (mean speed and headway time) the effect of packet losses during communication is negligible. Furthermore, without loss of generality we consider the case of homogeneous traffic i.e., $M_i = M$ $(i = 0, 1, 2)$. To accomplish the time-varying nature of the different delays, in the simulation runs all delays vary randomly with a uniform discrete distribution, $\tau_{ij}(t) \leq \tau^\star; \tau_{ij}(t) \in [\tau_{\min}, \tau_{\max}]$, with $\tau_{\min} = 0$ [s] and $\tau_{\max} \leq \tau^\star = 154 \cdot 10^{-3} [s]$, where the theoretical upper bound $\tau^\star$ is computed as in Theorem 4.3.1 (choosing $q = 1.02 > 1$). Note that $\tau^\star$ is greater than the average end-to-end communication delay typical of IEEE802.11p vehicular networks which is of the order of hundredths of a second (i.e., 10^{-2} [s]) as reported in [89], [10], [6]. Furthermore, to test

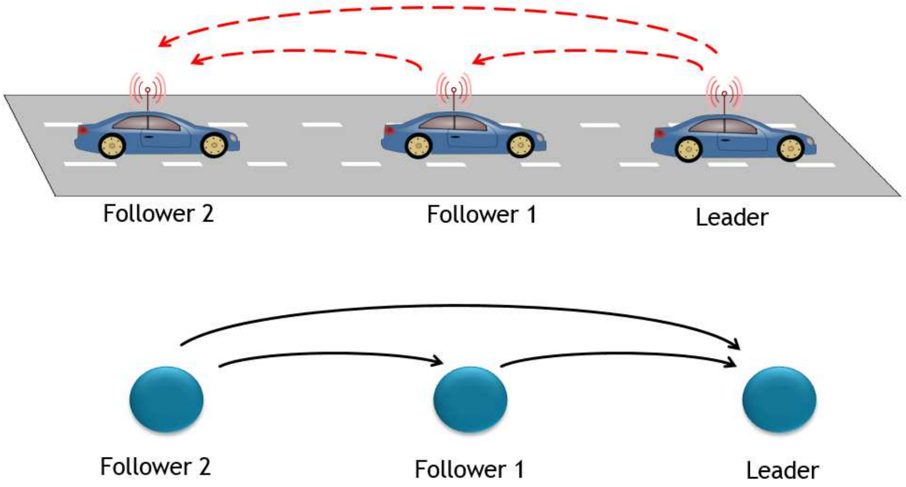

Figure 5.1: Schematics of representative platoon configurations. Top panel: a leader and two followers $F1 - F2$. Down panel: dynamical network of the above platoon.

the ability of the platooning protocol of rejecting variations of the communication delays $\tau_{ij}(t)$, we select $\tau_{ij}(t)$ as a piecewise-continuous function whose value is selected with uniform probability between 0 and $\tau^\star$, e.g., once every millisecond. Control parameters values, for both k_{ij} and b, belong to the gain region that ensures the stability of the closed-loop vehicular network according to Theorem 4.3.1. Note that node 0, i.e., the leader, is globally reachable as required in Theorem 4.3.1. Moreover, for the sake of simplicity, we select a unique value for all the gains $k_{ij} = k = 800$, tuned to achieve acceptable transient performance. Under this choice the matrix $\widehat{K}$ is

$$\widehat{K} = \begin{bmatrix} 800 & 0 \\ -400 & 800 \end{bmatrix}. \tag{5.1}$$

Since all μ_i are real (the matrix $\widehat{K}_M$ is positive stable), in this case it suffices to choose $b > 0$ (according to Theorem 4.3.1). We choose $\widetilde{B} = \text{diag}\{1800, 1800\}$ to fulfill the conditions of Lemma 4.3.2.

First numerical results show the algorithm performance in the simple case of heterogeneous, but constant, communication delays (i.e., $\tau_{10}(t) = \tau_1$, $\tau_{20}(t) = \tau_2$ and $\tau_{21}(t) = \tau_3$). Results in Fig. 5.2 show the convergence to the desired consensus values.

Simulation results, depicted in Fig. 5.3, confirm platooning formation and maintaining in the more realistic case of different time-varying delays, $\tau_{ij}(t)$. As expected from the theoretical analysis, the consensus in the platoon is achieved and both position and speed errors go to zero. Note that the presence of noise in position and velocity error signals (see Fig. 5.3 - top and down panel) is simply originated from the rapid switching nature of the time-varying delay during the simulation run.

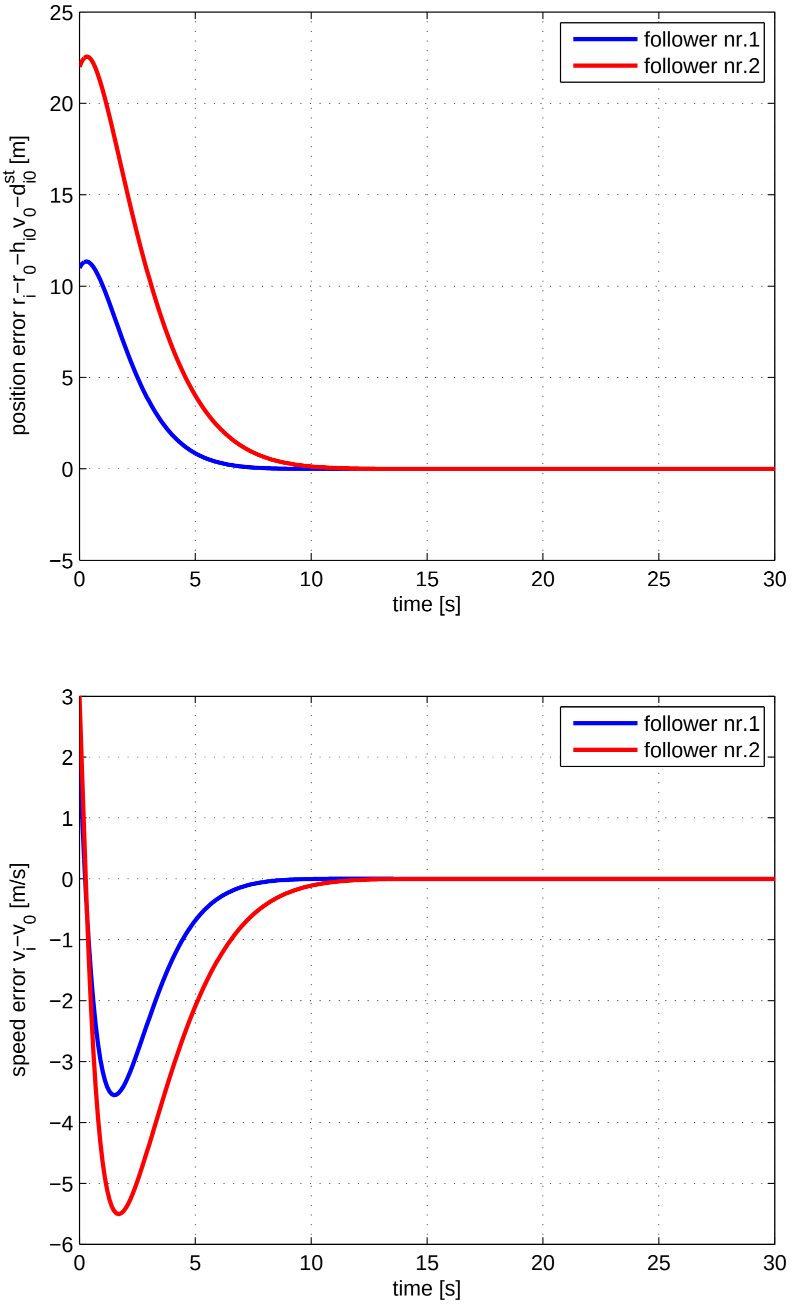

Figure 5.2: Platooning in the presence of different *constant* delays. Top panel: Time history of the position error. Down panel: Time history of the velocity error.

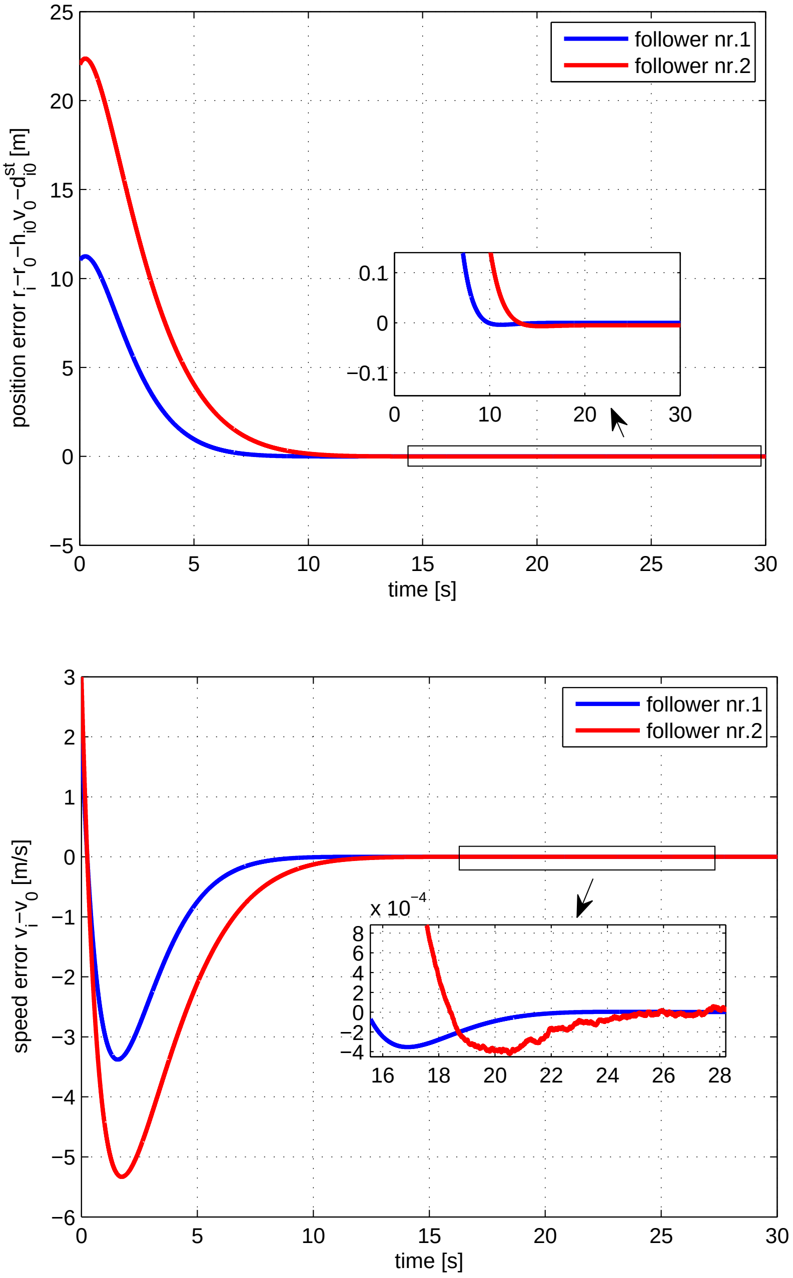

Figure 5.3: Platooning in the presence of *time-varying* heterogeneous delays $\tau_{ij}(t)$. Top panel: Time history of the position error. Down panel: Time history of the velocity error.

5.2 Robustness with respect to perturbations

The numerical analysis have been also devoted to investigate the robustness of the consensus achieved by the distributed coupling protocol (4.6) in the presence of perturbations or communication losses (and recovery). The first issue addressed is to understand, once the platoon is formed and consensus among vehicles is established, if and how spacing errors, velocity or acceleration fluctuation are amplified upstream the traffic flow. Specifically, the platoon is said to be string stable if any sudden perturbation on the speed of the leading vehicle (or leading signal) is attenuated along the the rest of the string [27] (see Subsection 2.2.1 for details about string stability). The second issue is to analyze the behaviour in the presence of communication failure and recovery.

5.2.1 Disturbance propagation through the string

A common issue in platooning is to ensure string stability. The key idea is to avoid that spacing errors are amplified upstream the traffic flow. Specifically, the platoon is string stable if any sudden perturbation on the position or speed of the leading vehicle (or leading signal) is attenuated along the the rest of the string [27].

Consider the platoon *leader-predecessor* topology described in Fig. 5.1: here we analyze the propagation of the position error back through the string (i.e., between following vehicles) due to the presence of a periodical perturbation acting on the leader motion. The analysis is carried out in the Laplace domain. Furthermore, we assume the time-varying delays to be set to their maximum admissible value $\tau_{ij}(t) = \tau \leq \tau^{\star}$.

According to the model described in Section 4.1, the i-th vehicle dynamics can be recast as:

$$\ddot{r}_i = \frac{1}{M_i} u_i \tag{5.2}$$

or equivalently using the Laplace transform $\mathcal{L}(\cdot)$:

$$X_i(s) = H_i(s) U_i(s) + \frac{x_i(0)}{s}, \tag{5.3}$$

with $X_i = X_i(s) = \mathcal{L}(r_i)$, $U_i(s) = \mathcal{L}(u_i)$, $H_i(s) = \frac{1}{M_i s^2}$ and $x_i(0)$ the initial condition. Note that under the assumption of homogeneous traffic $M_i = M$ (i=0,..., N), we have $H_i(s) = H(s) = \frac{1}{Ms^2}$.

The Laplace transform of the distributed coupling protocol (4.6) for the leader-predecessor topology is:

$$U_1(s) \quad = \quad k_{10} E_1(s) + b(X_0 s - X_1 s) \tag{5.4}$$

where

$$E_1(s) = X_0 e^{-\tau s} - X_1 + \tau X_0 s + h_{10} X_0 s + \frac{d_{10}}{s} \tag{5.5}$$

and

$$U_i(s) = \frac{k_{i0}}{d_i}(X_0 e^{-\tau s} - X_i + \tau X_0 s + h_{i0} X_0 s + \frac{d_{i0}}{s}) + \frac{k_{i,i-1}}{d_i} E_i(s) + b(X_0 s - X_i s) \tag{5.6}$$

when i= $2, ..., N$; the spacing error dynamics with respect to the preceding vehicle is:

$$E_i(s) = X_{i-1} e^{-\tau s} - X_i + \tau X_0 s + h_{i,i-1} X_0 s + \frac{d_{i,i-1}}{s}. \tag{5.7}$$

Note that d_{ij} is the desired spacing vehicle separation, defined in Section 4.1. Consider now the first vehicle following the leader along the platoon, namely $i = 1$. From (5.4), according to the expression (5.3), for an homogeneous string of vehicles, i.e. $H_i(s) = H(s)$, we have:

$$X_1 = k_{10} H E_1 + bH \left(X_0 - X_1\right) s + \frac{x_1(0)}{s} \tag{5.8}$$

thus the corresponding spacing error dynamics (5.5) can be written in terms of the sensitivity function, say $W_1(s)$, after the substitution of (5.8) in (5.5):

$$E_1(s) = W_1(s) X_0(s) + S_1(s) \frac{d_{10}}{s}, \tag{5.9}$$

where

$$W_1\left(s\right) = \frac{e^{-\tau s} + \tau s + h_{10} s - b\bar{H} s}{1 + k_{10}\bar{H}} \tag{5.10}$$

$$S_1(s) = \frac{1}{1 + k_{10}\bar{H}} \left(1 - \frac{1}{1 + bHs}\right) \tag{5.11}$$

with

$$\bar{H}(s) = \frac{H(s)}{1 + bH(s)s}. \tag{5.12}$$

See Appendix B.1.1 for the mathematical derivation of (5.9).
Analogously for $i = 2, \ldots, N$, (5.6) in (5.3) lets us to have:

$$\begin{aligned} X_i(s) \quad = \quad & \tfrac{k_{i0} H(s)}{d_i} [X_0 e^{-\tau s} - X_i + \tau X_0 s + h_{i0} X_0 s + \tfrac{d_{i0}}{s}] \\ & + \tfrac{k_{i,i-1} H(s)}{d_i} E_i(s) + bH(X_0 - X_i)s + \tfrac{x_i(0)}{s} \end{aligned} \tag{5.13}$$

and thus the spacing error can be computed in terms of the complementary sensitivity function, say $T_i(s)$, as:

$$E_i(s) = T_i(s) E_{i-1}(s) + S_i(s) \frac{d_{i,i-1}}{s} \tag{5.14}$$

where

$$\begin{aligned} T_i\left(s\right) \quad = \quad & \tfrac{1}{(-1-D_i)} \left[C_i + \left(C_i - e^{-\tau s}\right) k_{i-1,0} \bar{H}\right] \\ & + \tfrac{1}{(-1-D_i)} \left[W_1^{-1} F_i s + W_1^{-1} \left(C_i - e^{-\tau s}\right) b\bar{H} s\right] \end{aligned} \tag{5.15}$$

$$\begin{aligned} S_i\left(s\right) \quad = \quad & \tfrac{1}{(-1-D_i)} \left[\tfrac{\left(C_i - e^{-\tau s}\right)}{1 + bHs} - 1 + C_i + \tfrac{2}{B_i}\right] \\ & + \tfrac{1}{(-1-D_i)} \left[-W^{-1} \left(F_i s + \left(C_i - e^{-\tau s}\right) b\bar{H} s\right) S_{i-1}\right] \end{aligned} \tag{5.16}$$

with

$$C_i = \frac{k_{i0} H}{d_i B_i} \tag{5.17}$$

$$D_i = \frac{k_{i,i-1} H}{d_i B_i} \tag{5.18}$$

$$B_i = 1 + \frac{k_{i0} H}{d_i} + bHs \tag{5.19}$$

$$F_i = -\tau - h_{i,i-1} + C_i h_{i,i-1} + \frac{bH}{B_i} \tag{5.20}$$

See Appendix B.1.2 for the mathematical derivation of (5.14).
Propagating errors along the string are attenuated when $|T_i(j\omega)| < 1$ for all frequencies of interest (see Subsection 2.2.1 and [125]).
It is worth to note here that control gains can be tuned inside the wide parameter region in which consensus is guaranteed so to satisfy additional string stability condition, e.g. $|T_i(j\omega)| < 1$.

Note that numerical simulation aimed to show string stability are in Appendix B.1.3.

Remark 5.2.1. Under the assumption of neglecting the communication delay (i.e. $\tau = 0$) and considering a classical proportional controller on the position error with respect to both the leader and the predecessor (i.e. $b = 0$), our analysis on string stability is similar to that described in [125] and [126]; indeed, we have that expression (5.10) becomes:

$$W_1(s) = \frac{1}{1 + k_{10}H} \tag{5.21}$$

and (5.11) is:

$$S_1(s) = 0 \tag{5.22}$$

Moreover, for $i = 2$, expression (5.15) is:

$$T_2(s) = \frac{k}{2} \cdot \frac{H}{1 + Hk} \tag{5.23}$$

with the assumption of $k_{10} = k_{20} = k$. Finally, (5.16) is:

$$S_2(s) = 0 \tag{5.24}$$

Note that the transfer function $W_1(s)$ and $T_2(s)$ described in (5.21) and (5.23) respectively, are the well known sensitivity and the complementary sensitivity function, derived for a vehicle platoon in [125] and [126]. See Appendix B.1.4 for details.

In what follows, we analyze both propagation velocity and acceleration back through the string (i.e., between following vehicles) in the classical presence of a sinusoidal perturbation acting on the leader motion (due, for example, to the human leader driver), namely $\delta(t) = A\sin\omega t$ being $A = 4$ and $\omega = \pi/5$ according to [70].
Simulations results in Fig. 5.4 show how our control gains choice, tuned within the wide region consensus, ensure the string stable behavior both on velocity and acceleration for a particular frequency of interest.

Moreover, we consider in Fig. 5.5 both velocity and acceleration as a consequence of another sudden variation in the leader motion, such to guarantee string stability.

5.2.2 Communication failures

We now validate the robustness of our approach with respect to communication losses during the platoon motion. Specifically we investigate the effect of a sudden loss in the information flow due to communication failure, and its subsequent recovery, among the leader and some of the followers, as well as the presence of losses during the inter-vehicles communication. Note that communication loss and its subsequent recovery can be modeled in terms of switching of the network topology.

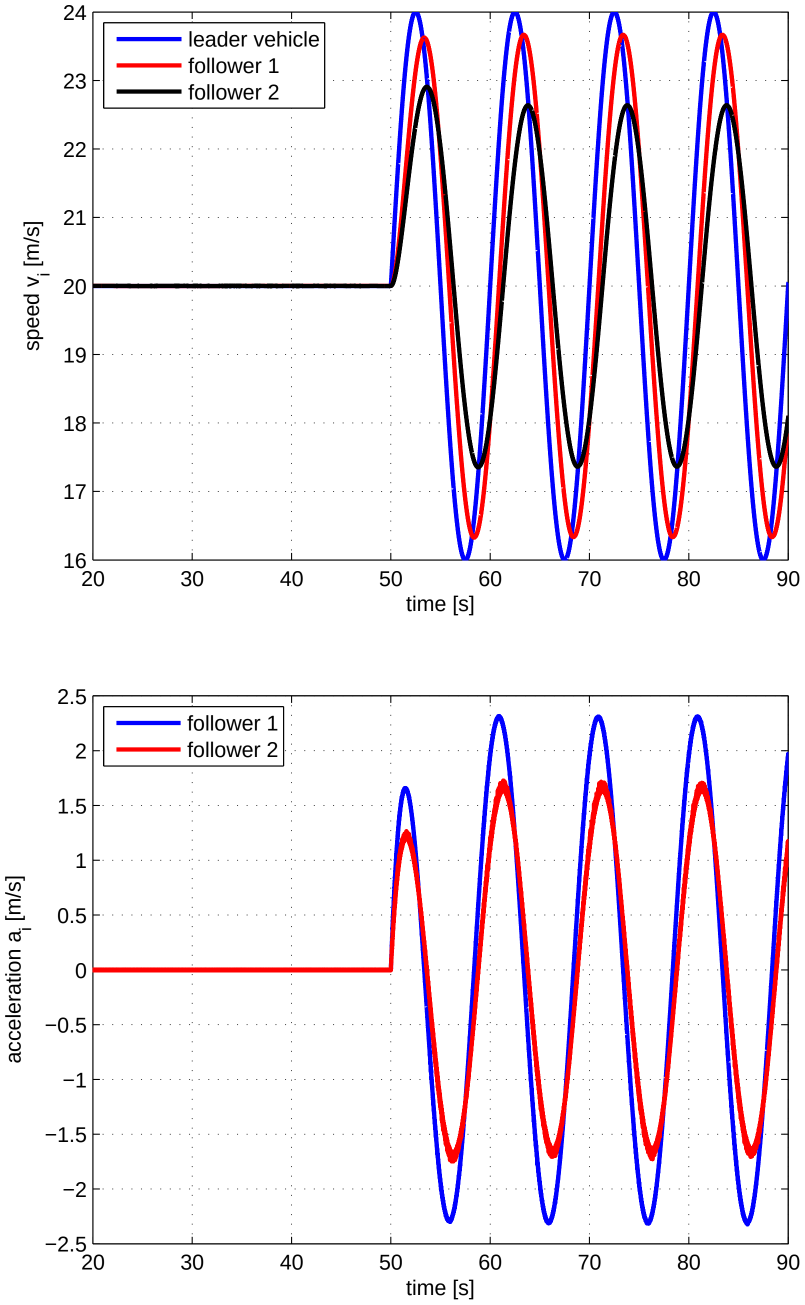

Figure 5.4: Performance of the platooning algorithm in the presence of a fluctuation in the leader dynamics. Time history of the velocity (top) and acceleration (down) attenuating along the string.

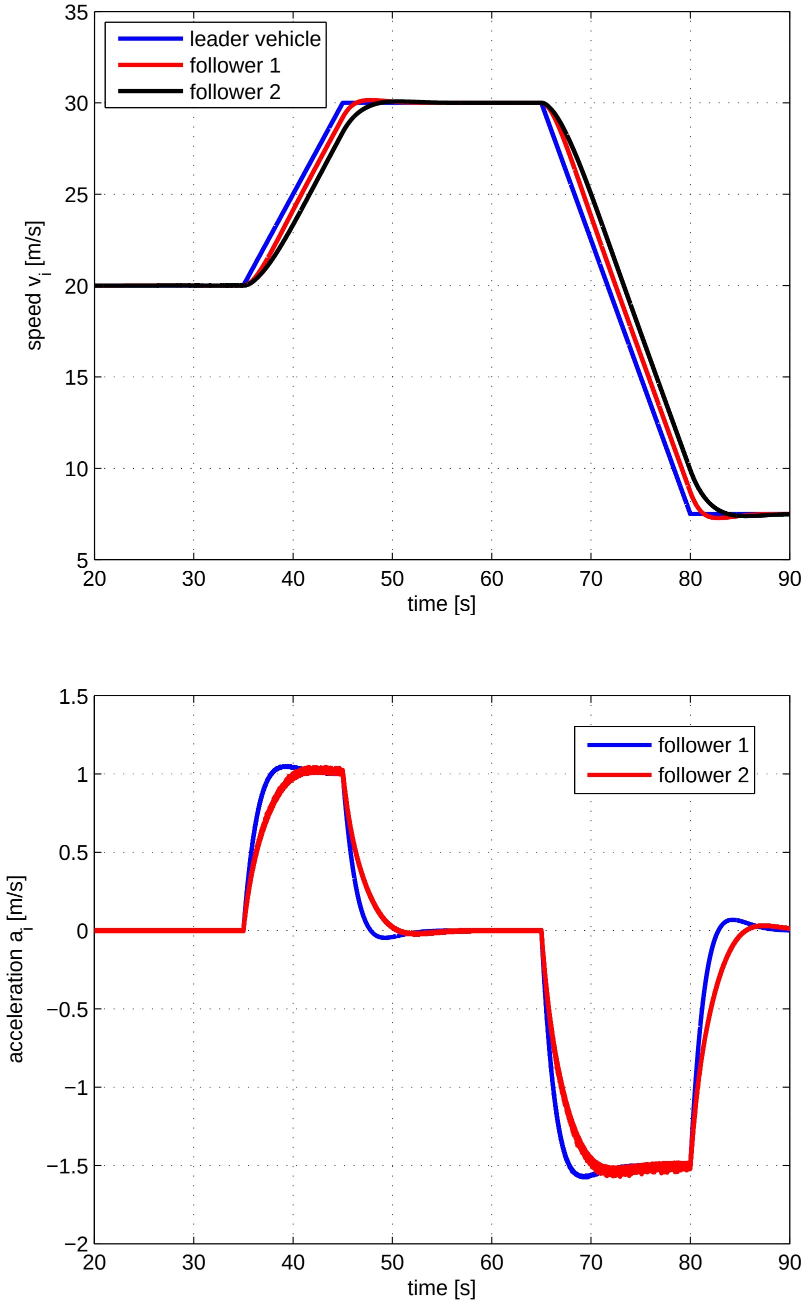

Figure 5.5: Performance of the platooning algorithm in the presence of a fluctuation in the leader dynamics. Time history of the velocity (top) and acceleration (down) attenuating along the string.

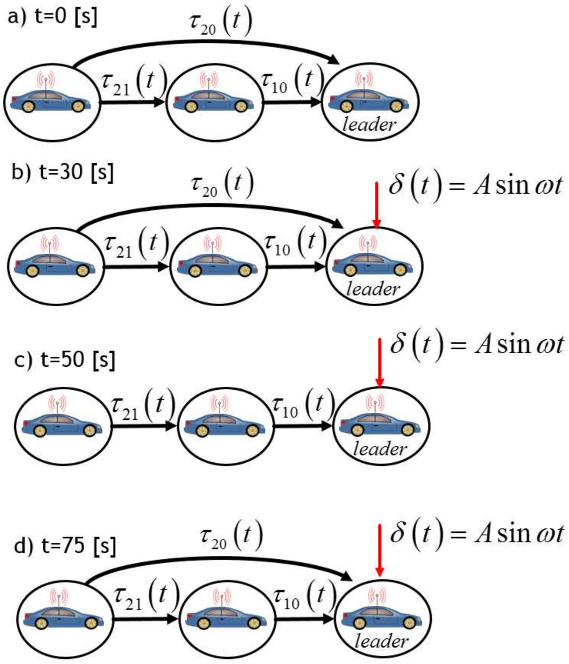

Figure 5.6: Performance of the platooning algorithm in the presence of communication losses between the leader and the follower 2. Switching topologies.

To this aim, as a representative case of study, we analyze the performance of the strategy when follower 2 in the platoon (see the platoon topology depicted in Fig. 5.6.a) looses connection with the leader at time instant $t = 50$ [s] (see Fig. 5.6.c), recovering it at $t = 75$ [s] (see Fig. 5.6.d). Moreover, to better test the effectiveness of the approach, the periodic disturbance $\delta(t)$ is added again to the leader dynamics at $t = 30$ [s] (see Fig. 5.6.b). Results in Fig. 5.7 show the effectiveness of the approach in guaranteeing disturbance attenuation along the string. Note that the network switches among different string topologies, that are still globally reachable.

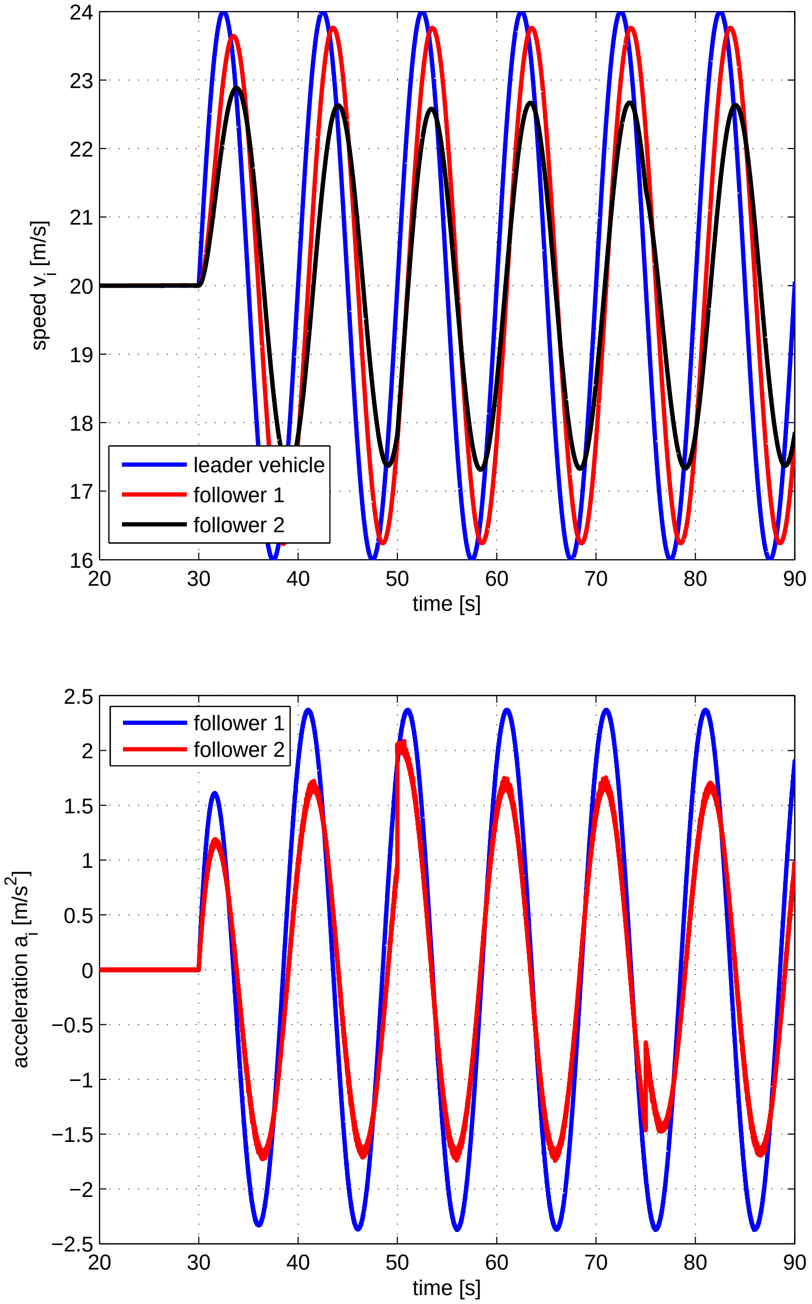

Figure 5.7: Performance of the platooning algorithm in the presence of communication losses between the leader and the follower 2. Time history of the velocity (top) and acceleration (down) attenuating along the string.

Part II

Experimental platooning via distributed consensus strategy

Chapter 6

Experimental setup and description of the prototype vehicles

Contents

6.1 The Cooperative Driving System architecture 56
6.2 Leader vehicle 56
6.2.1 Hardware platform 56
6.2.2 Software application 58
6.3 Follower vehicle nr.1 59
6.3.1 Hardware platform 59
6.3.2 Software application 60
6.4 Follower vehicle nr.2 65
6.4.1 Hardware platform 65
6.4.2 Software application 65
6.5 Vehicle-to-Vehicle communication module 66
6.6 Clock Synchronization 67

In this Chapter an overview of the experimental setup is carried out. A platoon of three prototype vehicles, equipped with specific communication and control hardware, is used to validate the platooning strategy defined in Chapter 4. The three vehicle platoon is depicted in Fig. 6.1. Details about the general Cooperative Driving System architecture used to develop the setup on each vehicle of the platoon is given in Section 6.1. Then, we focus on the leader vehicle experimental setup in Section 6.2. More precisely, we start introducing the hardware and the main application used on the leader in Subsections 6.2.1 and 6.2.2, respectively. Then, in Section 6.3 and Section 6.4 we describe the experimental setup for both followers, focusing on the main differences of the proposed solution for the follower nr.1 with respect to the follower nr.2. A description of the Vehicle-to-Vehicle technology used to establish inter-vehicular communication is in Section 6.5 and, finally, we motivate the use of *Coordinated Universal Time-UTC* to achieve clock synchronization in a platoon of vehicles in Section 6.6.

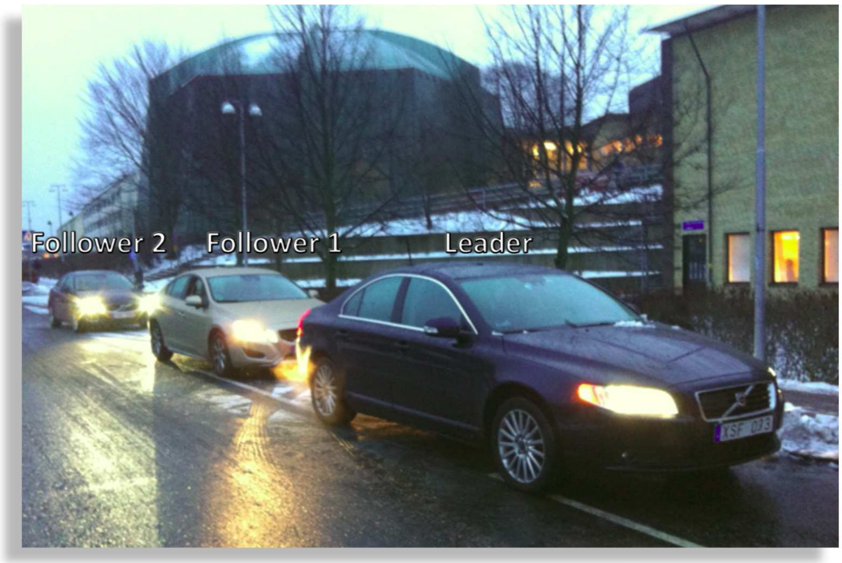

Figure 6.1: Platoon of vehicles: the leader vehicle (Volvo S80), the follower nr.1 and nr.2 (Volvo S60)

6.1 The Cooperative Driving System architecture

In our framework, the platooning strategy has to guarantee the following main functions: (i) fully automated longitudinal control of the followers and (ii) management of the driver requests during joining/leaving the platoon maneuvers. The latter function can be achieved introducing a modular Cooperative Driving System architecture, as depicted in Fig. 6.2. Each module in Fig. 6.2 is a *software functional module*, connected each other by arrows to indicate the data flow. This architecture is inspired by that used in the *Cooperative Autonomous Car Train - CoAct* project [36], sponsored by Chalmers University of Technology (Göteborg, Sweden). Starting on the latter solution, the main architecture has been extended to manage the data collected through the V2V communication module and their fusion with the on-board sensor measurements for computing the distributed coupling protocol (4.6). According to the architecture in Fig. 6.2, the proposed solution is described in Sections 6.3 and 6.4.

6.2 Leader vehicle

In this Section we describe both hardware and software used to develop the experimental setup on the leader vehicle. The leader vehicle is a Volvo $S80$, provided by the Volvo Car Corporation (see Fig. 6.1, leader vehicle). The leader is 4820 [mm] length, 1861 [mm] width and 1490 [mm] height, with a 6-speed automatic gear.

6.2.1 Hardware platform

The hardware platform on the leader vehicle has the structure depicted in Fig. 6.3. The Real-Time Environment (RTE) is used to run a main software application, developed in

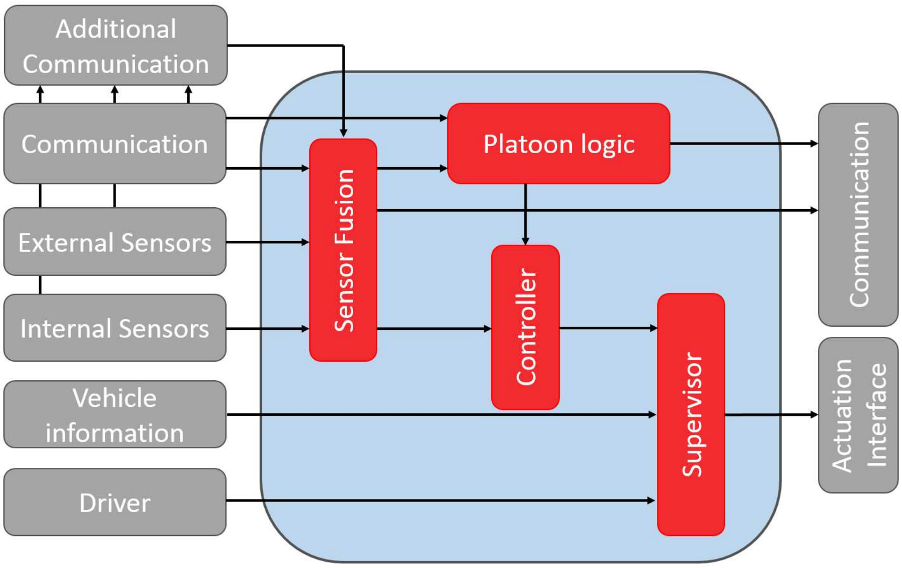

Figure 6.2: The modular Cooperative Driving system architecture

Labview. In our setup the latter software application running on RTE works on a laptop with the Windows Operative System. Since the laptop is fairly fast it can still handle communication broadcast, forcing the tasks execution as if it were acting in real-time [36]. The *CAN to Ethernet* gateway in Fig. 6.3, called also Telematics Gateway - TGW, lets the RTE to collect information from on-board car sensors, as for example vehicle steering, gear, speed, acceleration and other signals. The TGW is a read-only interface with respect to the vehicle Controller Area Network (CAN) BUS and it is provided by the Volvo Car Corporation. A high precision *Real Time Kinematic-GPS* receiver (RTK-GPS) equips the leader vehicle: in our setup we consider a Trimble $SPS852$ GNSS Modular Receiver wired to the laptop via a serial-to-USB cable. In general, the accuracy that we expect out of GPS receivers is in meters (around $10-15$ [m]). Differential and Real-Time Kinematic (RTK) can be used to improve the precision: in particular Differential-GPS introduces a precision level up 2 meters; instead, RTK-GPS improves accuracy up centimeter level, using RTK-base stations. In our experimental setup we use the RTK-GPS, due to the high position accuracy requests (see Subsection 6.3.1). The *Communication Box* is an Alix embedded system board (see Section 6.5 for details), used to send data to the following vehicles via V2V communication. An extra battery and a DC/DC power converter of $12-5$ [V] is used for power supplying the Ethernet switch and the Communication Box. An Ethernet switch is used to connect all the platform devices. In particular, the TGW sends out the laptop UDP messages that can be read such to collect the desired information. Then, the laptop shares data with the Communication Box. The assigned IP subnet for the leader is 192.168.0.x: the IP addresses (and ports) are in Table 6.1.

In Fig. 6.4 a picture of the leader setup is depicted.

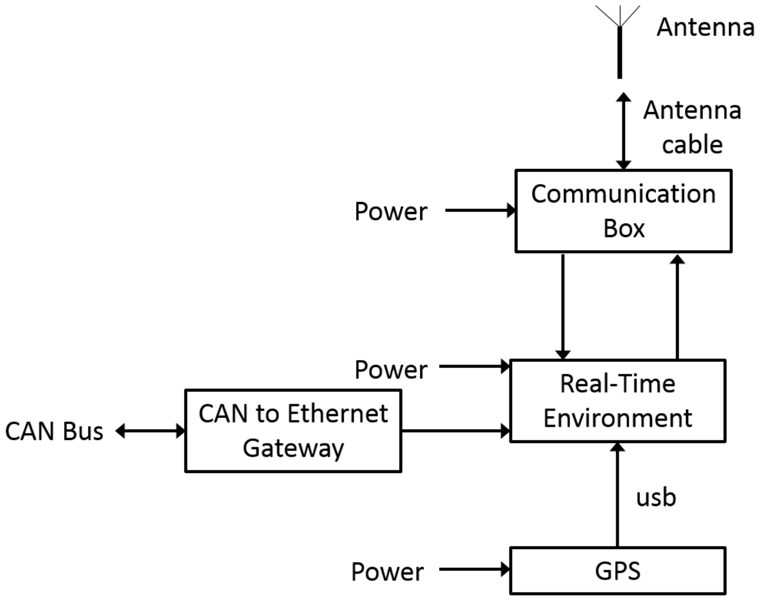

Figure 6.3: The hardware platform on the leader vehicle. Modular architecture.

Device	Address	Receive port	Send port
Laptop	42	26001, 50020, 50005	26003
Comm. Box	137	26003	26001
TGW	5	-	50020
GPS	20(not used)	-	50005

Table 6.1: Addresses and ports on devices - Leader vehicle.

6.2.2 Software application

The main application running on the RTE is called *main.vi* Labview file. An application overview (i.e. a schematic of the Block Diagram) is in Fig. 6.5; in particular, the software is able to:

- *Read TGW UDP* messages: the application collects the measurements from on-board sensors (see Table 6.2(a) for signals).
- *Read GPS via Serial-to-USB cable*: the RTK-GPS receiver sends the laptop information about UTC and absolute position (see Table 6.2(b) for signals). The *GPS.vi* Labview file is described in Appendix D.1.1.
- *Read Communication Box UDP messages*: there are nr.6 *classes* for messages that the Communication Box forwards to the RTE; in Table 6.3 we classify all the classes we use in our experimental setup.
- *Create an UDP packet structure* with the collected data from TGW and GPS: the

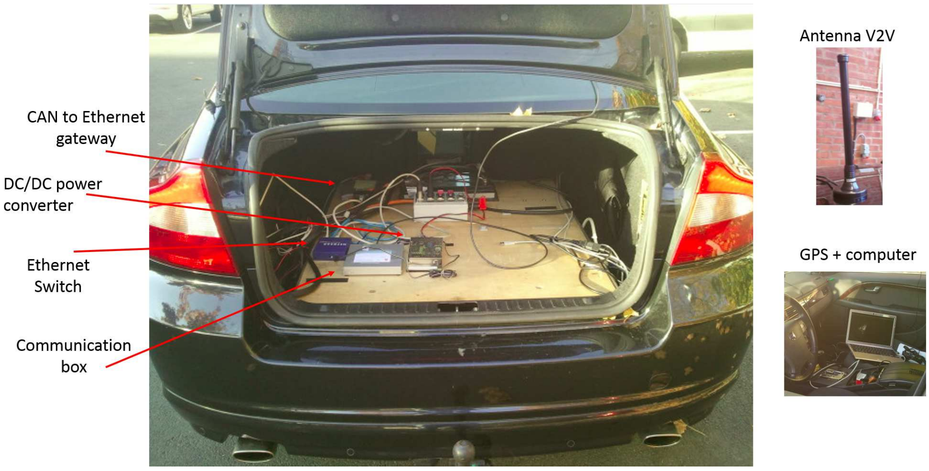

Figure 6.4: The experimental setup on the leader vehicle.

real-time data that the RTE shares with the Communication Box are structured in an UDP packet, such as described in Table 6.4.

- *Fleet management*: the leader vehicle replies to the requests from followers to join and to leave the platoon.
- *Write and send an UDP packet* to Communication Box.

In general, the *main.vi* application collects and packages information from on-board devices. Then, it forwards messages to the Communication Box, that is responsible to transmit messages via wireless. The front panel overview of the *main.vi* file is in Appendix D.2.1.

6.3 Follower vehicle nr.1

The follower vehicle nr.1 is a Volvo $S60$, with a six cylinder turbo charged engine with three liters displacement, 304 [hp] and is equipped with a six-speed geartronic transmission. The vehicle is 1484 [mm] height, 4628 [mm] length and 2097 [mm] width. Moreover, Volvo $S60$ is equipped with a Front Sensing Module (FSM) consisting of a camera, a radar unit and an infra-red sensor as standard equipment. This vehicle has a read/write interface with the CAN BUS, such to control directly the vehicle motion and read information provided by internal sensors, i.e. speed, steering, braking and other states.

6.3.1 Hardware platform

The hardware platform is described in Fig. 6.6. The Real-Time Hardware (RTH) is a dSpace MicroAutobox 2. This is the most important difference with respect to the leader vehicle experimental setup described in Subsection 6.2.1: indeed, we can both read and write messages on the CAN BUS with a RTH. A functional module inside the

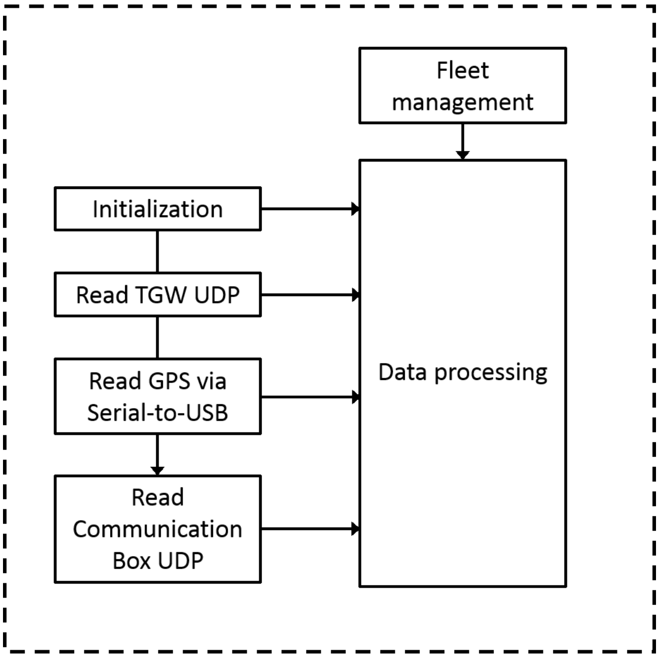

Figure 6.5: *main.vi* Labview file overview

main software application running on the RTH interacts directly with the CAN BUS. A laptop is used to manage the entire software running on the RTH. In particular, with an *Human Machine Interface-HMI* running on the laptop we can (i) monitor the signals from any devices cabled in the experimental setup both off-line and on-line, (ii) tune any parameter on-line (for example, controller parameters, sensor fusion, communication protocol, CAN BUS) and (iii) record all the signals of interest. Another difference with respect to the experimental setup described in Subsection 6.2.1 is the use of the *compass*. In particular, an Arduino Uno equipped with a compass is used to have better performances at standing still than using the GPS compass information.

The IP-addresses and ports number are in Table 6.5, with the assigned IP subnet 192.168.188.x. There is an Ethernet switch to cable all the devices used in the experimental setup. Moreover, CAN BUS is wired with the RTH by a 78-pin, male sub-D I/O Connector that grants access to various I/O signals (i.e LIN, CAN and other signals). A picture of the experimental setup is in Fig. 6.7.

6.3.2 Software application

According to the modular architecture described in Section 6.1, we used the Simulink file developed in [36] to build a new software application to validate the distributed coupling protocol (4.6). The compiled version of this Simulink file runs on the dSpace Microautobox 2, i.e. the Real-Time Hardware (RTH), used to compute the main action to be performed by the experimental setup. According to the modular approach depicted in Fig. 6.2, the final application can be decoupled in three main part: the (i) *input modules*, the (ii) *management and control modules* and the (iii) *output modules*. The *input modules* read and pre-process data from both on-board sensors and V2V. The

(a)

Signals from TGW	**Units**
Gear, brake and door status	-
Lateral and longitudinal accel.	[m/s^2]
Speed	[m/s]
Steering angle	[deg]
Yaw rate	[deg/s]
Vehicle length and width	[mm]

(b)

Signals from GPS	**Units**
UTC	[hhmmss.mmm]
Latitude	[ddmm.mmmm]
Longitude	[ddmm.mmmm]
Magnetic variation	[deg]
Speed over ground	[knots]
Course over ground	[deg]
Horizontal accuracy	[m]

Table 6.2: Labview *main.vi* application. Input signals.

input modules are:

- *Communication receive*: this module lets the RTH to receive information from neighbors in a platoon. In particular, it takes care of establishing a reliable connection through the Ethernet UDP Interface, used to receive data from the Communication Box. Moreover, before decoding the received packets, this module determines the *message class* (see Table 6.3); then it verifies the packet reliability and refreshes memory according to the new information.

- *Additional communication*: we use this module for computing the *packet delay* $\tau_{ij}(t)$ in (4.6) with respect to both the leader and the followers information from the communication receive module.

Class	**Purpose**
DynamicVehicleInfo ($10Hz$)	Dynamic Vehicle Information (DVI), including platoon state and "request-to-join"; see Tab. 6.4
StaticVehicleInfo ($1Hz$)	Static Vehicle Information (SVI); see Tab. 6.4
PlatoonAction (on demand)	Reply from a platoon leader to a follower request for joining the platoon (PA); see Tab. 6.4
ManeuverRequest ($10Hz$)	Request to maneuver (MR); see Tab. 6.4
ManeuverState ($10Hz$)	The current maneuver state (MS); see Tab. 6.4
ManeuverOffsetActive ($10Hz$)	Maneuver active (MA); see Tab. 6.4

Table 6.3: Class of messages from the communication box to laptop.

Array Index	Message	Parameter	Value Range
0	DVI	seconds_header	0...4294967295
1	DVI	msecs_header	0...999
2	DVI	Vehicle_Id	0...255
3	DVI	Node_Type	0...3
4	DVI	seconds_payload	0...4294967295
5	DVI	msecs_payload	0...999
6	DVI	Accuracy	−32768...32767
7	DVI	Longitude	−1440000000...1440000000
8	DVI	Latitude	−720000000...720000000
9	DVI	Velocity	−32768...32767
10	DVI	Vehicle_Heading	0...65535
11	DVI	Acceleration	−2000...2000
12	DVI	Yaw_Rate	−32768...32767
13	DVI	Platoon_Id	0...255
14	DVI	Platoon_State	0...3
15	SVI	Vehicle_Width	0...1023
16	SVI	Vehicle_Length	0...16383
17	SVI	toNodeId	0...255
18	PA	Platoon_Action	0...2
19	MR	sourceVehicleID	0...255
20	MR	maneuverId_seconds	0...4294967295
21	MR	maneuverId_msec	0...999
22	MR	destinationvehicleId	0...255
23	MR	referencevehicleId	0...255
24	MR	longitudinaloffset	0...65535
25	MR	laneoffset	0...2
26	MS	maneuverstate	0...2
27	MA	triggerManeuverState	0 or 1

Table 6.4: UDP packet structure.

Device	Address	Receive port	Send port
Comm. Box	136	26003	26001
RTH	41	26001, 50389, 50390	26003
GPS	21	-	50389
Compass	100	-	50390

Table 6.5: Addresses and ports on devices - follower nr.1.

- *Internal and external sensors*: there is a software module to read the GPS messages (see Appendix D.1.1 for GPS configuration details); as well as done in the communication module, this module establishes a reliable connection through the Ethernet UDP Interface with the GPS; then, the GPS data processing starts unpacking UDP messages and analysing them in order to select $\$GPRMC$ messages (i.e. recommended minimum specific GPS/transit data). Then another software module is to collect messages from compass; the first step is to establish a reliable connection through the Ethernet UDP Interface with the Arduino Uno microprocessing board that let the compass to be used. We underline the importance

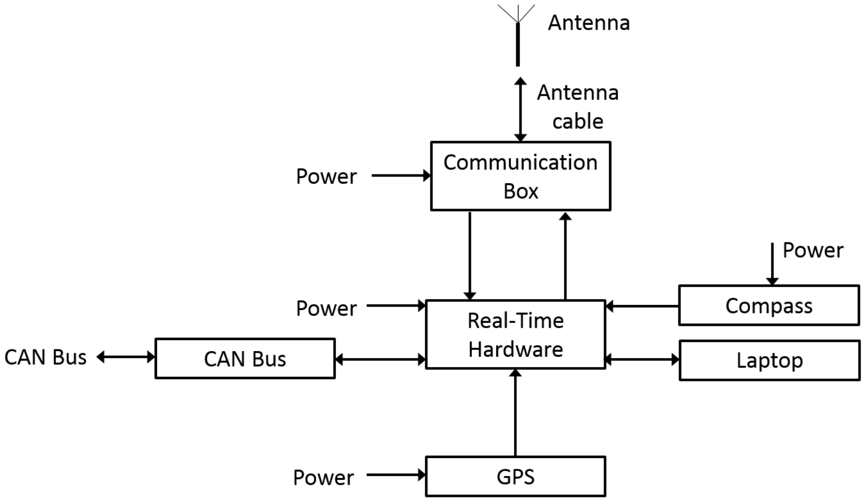

Figure 6.6: The hardware platform on the follower nr.1. Modular architecture.

of compass in measuring a more accurate heading signal than GPS heading measurement at standing still.

- *Vehicle information*: all the vehicle CAN BUS messages can be read with this module. In particular, S60 has a FSM, including a camera, a radar and an infrared sensor and a software sub-unit for processing. The latter is inside a main software module provided by the Volvo Car Corporation, such to let the RTH of reading with the best degree of accuracy signals like the vehicle longitudinal speed, acceleration, relative distance with respect to the previous vehicle, the steering angle and the gear status.

- *Driver*: this module lets the driver to select vehicular parameter with an user friendly HMI. In this way, the driver decides, for example, the platoon to join (leader ID), the safety degree (by setting the max speed and the headway time; by enabling/disabling the cooperative control).

The *management and control* modules are responsible of supervising the main software application, such to guarantee the effectiveness of all the main tasks to be executed as expected. These modules are:

- *Sensor fusion*: all processes dealing with system data (i.e. FSM, RTK GPS, Communication Box, compass) are linked to sensor fusion module, to obtain a robust estimate of the states information to be used by the distributed coupling protocol (4.6). In order to guarantee the data coherence and reliability, sensor fusion applies Kalman filters to reconstruct the state of both the S60, the predecessor, and the leader. Moreover, the output of the sensor fusion are used to perform platoon logic and supervision. The proposed solution is described in [63].

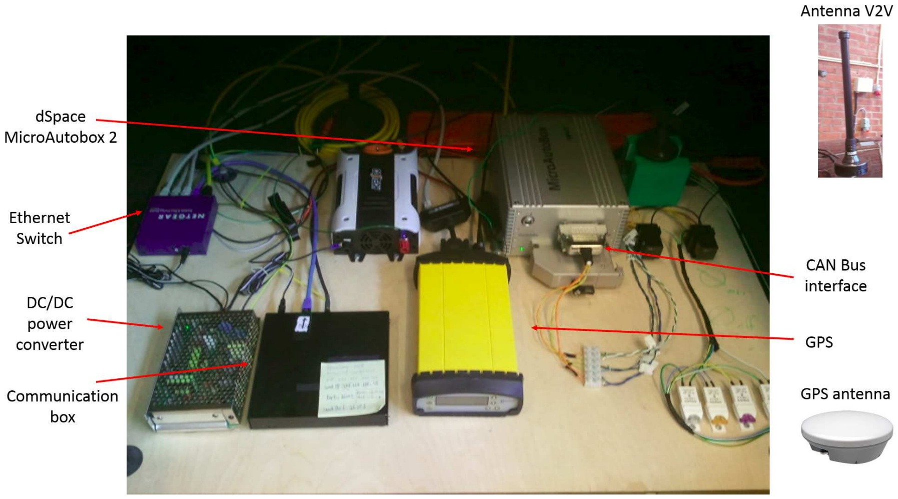

Figure 6.7: The experimental setup on the follower nr.1.

- *Platoon logic*: this software module is responsible of interaction between the S60 and the other vehicles in the platoon.

- *Controller*: according to the distributed coupling protocol (4.6), this module computes the target acceleration to achieve the desired longitudinal motion of the S60 in terms of relative distance with respect to the predecessor and leader, with a common velocity. In order to compute the coupling protocol strategy, the main software application uses either signals from the sensor fusion or directly the measured information. Note that the controller depends on the parameter selected by the driver on HMI, i.e. headway time and safety distance with respect to predecessor).

- *Supervision*: this module manages the interaction of different systems (the main software application and the vehicle). Applying event based algorithms, the supervision module guarantees safety, ensuring to avoid errors in the main application execution [63].

The *output modules* forward the processed signals to on-board actuators and share them with the other vehicles in the platoon. The output modules are:

- *Communication send*: this module collects the information computed on RTH, encodes them and builds the UDP message according to the structure defined in Table 6.4. Then this module establishes a connection through the Ethernet UDP Interface with the Communication Box. Then the latter will send this message via V2V.

- *Actuation interface*: this module is responsible of interfacing the vehicle CAN BUS in order to write over that the target acceleration computed on the RTH: in particular, this signal is the reference for a low-level controller (i.e. the engine control) equipping the S60.

Moreover, the HMI running on a laptop is used to interact with the RTH via an Ethernet port.
The whole experimental setup has been validated within the COACT project [36]. Moreover, the modified functional module have been tested both separately and inside the main functional application.

6.4 Follower vehicle nr.2

In this Section we describe the follower vehicle nr.2. This vehicle is a Volvo S60 and it's similar to the follower nr.1 (see Section 6.3 for technical parameters).

6.4.1 Hardware platform

The hardware platform on the follower nr.2 is similar to that described in Fig. 6.6, with the exception of the GPS used to perform experiments. The latter is a XSens MTi-G model, an inertial sensor equipped with an integrated GPS receiver. A laptop is used to wire the GPS receiver via a Serial-to-Universal Serial Bus (USB) cable. Moreover, a Labview application running on the laptop has been developed in order to read messages from the GPS receiver and forward them to the RTH via an Ethernet UDP interface. A detailed description of both the Xsens sensor and the Labview application is in Appendix D.1.2. The IP-addresses and ports number are in Table 6.6 (IP subnet 192.168.188.x.) and in Fig. 6.8 an overview of the experimental setup is depicted.

Device	Address	Receive port	Send port
Comm. Box	40	26003	26001
RTH	41	26001, 50389, 50390	26003
GPS	22 (laptop)	-	50389
Compass	103	-	50390

Table 6.6: Addresses and ports on devices - follower nr.2.

6.4.2 Software application

The main application used to control the follower nr.2 and running on the RTH (i.e. the compiled version of the Simulink file that contains all the software modules described in Section 6.3) is similar to that developed on follower nr.1. The main difference is a more accurate *additional communication* module, faster and easier than on follower nr. 1 such to manage the multi-source messages collected via V2V communication in order to compute with higher precision the heterogeneous time-varying delays $\tau_{ij}(t)$ used in (4.6). Note that the on-board GPS receiver cannot be used in RTK mode: in order to guarantee the best accuracy in measuring the vehicle position, a model of vehicle dynamics has been developed such to run in real-time on the RTH during the experiments. In so doing, we succeed to manage the experimental setup in order to validate the distributed coupling protocol (4.6).

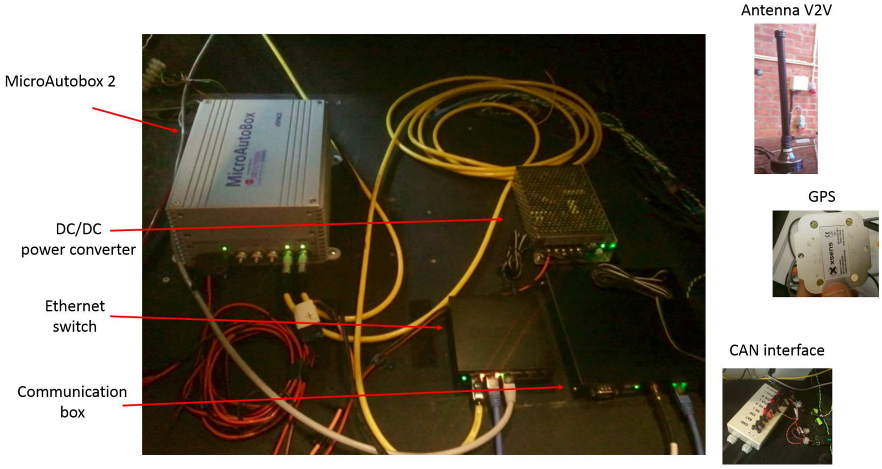

Figure 6.8: The experimental setup on the follower nr.2.

6.5 Vehicle-to-Vehicle communication module

The *communication module* depicted in Fig. 6.2 is described in this Section. It drops out the V2V communication, according to the message exchange format and transmission frequency defined in [2]. The hardware used to enable the platform for vehicle to vehicle (V2V) communication is depicted in Fig. 6.9 and consists of:

- Atheros-based (Wireless Local Area Network) WLAN card (Mikrotik R52H High Power (350mW) 2.4/5GHz IEEE 802.11a, for use with IEEE 802.11p Linux driver).
- Alix embedded system board (3D2) with casing and SMA connector, Ethernet, 2xmini-PCI, serial-port (DB9), usb, compact flash socket.
- Solid state CF memory card 4GB where OpenWrt - x86 image is loaded.
- ECOM6-5500 Omni-Directional Magnetic Mount Antenna 6dBi for 802.11p (5-6GHz), with SMA connector for direct connection to Alix-board casing.

The communication stack development follows the guidelines in [1], supported by the inclusion of drivers used to enable WLAN. The CALM/FAST protocol is the high level protocol (Network and Transport layers), while IEEE 802.11p protocol is the low level protocol (PHY and MAC layers). CALM/FAST protocol can be used to send both in broadcast and unicast messages to a particular vehicle, identified by an unique IPv4 address. A block diagram of the hardware interfaces is depicted in Fig. 6.10.

As well as described in Section 6.2, Section 6.3 and Section 6.4, the Communication Box interfaces with RTH via UDP protocol. The data received from RTH are managed via a *createMessage* process and sent over the wireless channel encoded in Packaged Encoding Rules (PER) unaligned format messages. On the other side, the received messages over the wireless link are decoded, managed via a *receiveMessage* process and sent to the RTH. For a more detailed description, see [36] and reference therein. Note that V2V communication has been extensively tested within the GCDC competition [146].

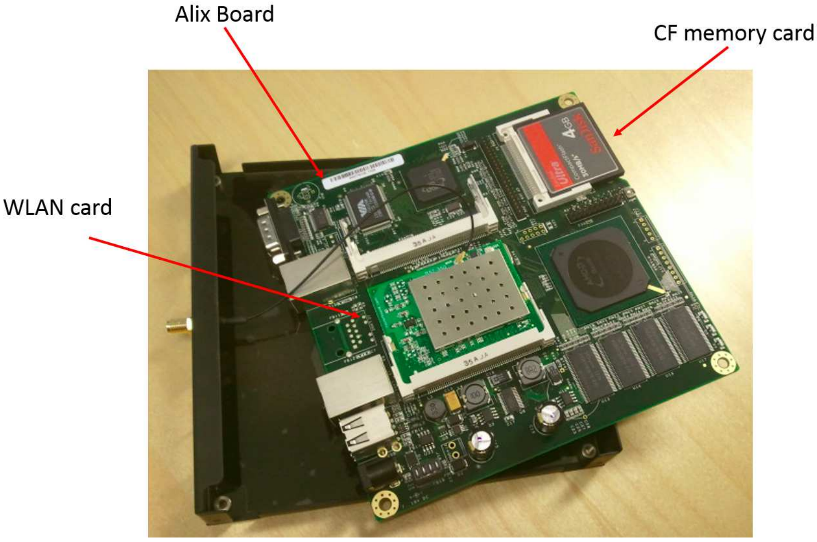
Alix Board
CF memory card
WLAN card

Figure 6.9: V2V Communication Box.

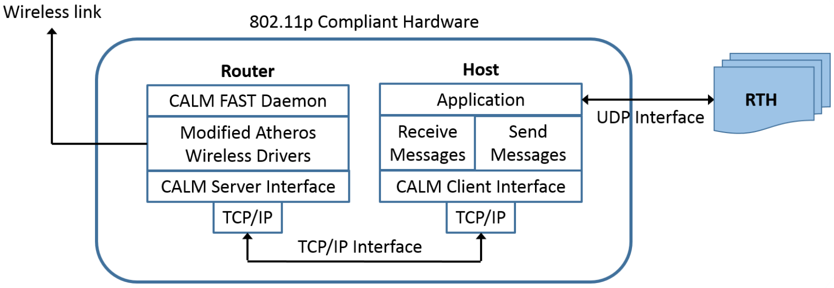
Wireless link
802.11p Compliant Hardware
Router
CALM FAST Daemon
Modified Atheros Wireless Drivers
CALM Server Interface
TCP/IP
Host
Application
Receive Messages
Send Messages
CALM Client Interface
TCP/IP
TCP/IP Interface
UDP Interface
RTH

Figure 6.10: V2V Communication Block diagram.

6.6 Clock Synchronization

We assume the communication boxes are installed on the three vehicles, configured both as WAVE (Wireless Access for Vehicular Environment) receivers and transmitters. According to [103], an on-board Global Positioning System (GPS) receiver guarantees knowledge of some variables, such as absolute position, velocity and UTC (i.e. timestamps). The clocks running on the experimental setup described in Section 6.2, Section 6.3 and Section 6.4 can be synchronized to external sources of highly accurate time. In our experimental setup we consider the GPS receivers the external source such to synchronize the clocks running on the experimental setup [63]. In so doing, we have to consider the *drift rate*, i.e. the change in the offset - difference in reading - between the clock and a nominal perfect reference clock per unit of time measured by the reference clock [25]. The most accurate physical clocks use atomic oscillators: their drift rate is about one part in 10^{13}. The output of these atomic clocks, known as *International*

Atomic Time, is the standard for elapsed real time.
The *Coordinated Universal Time-UTC* is an international standard for timekeeping [25]. It is based on atomic time, managed occasionally to keep it in step with astronautical time. UTC signals are synchronized and broadcast regularly from land-based radio stations and satellites (including *Global Positioning System - GPS*). The signals received from land-based stations have an accuracy on the order of of $0,1 - 10$ [ms], depending on the station used. Instead, signals received from GPS satellite are accurate to about 1 [μs].
In order to achieve a common notion of time, we use the *precision time protocol - PTP* [66]. Clocks are shared through the on-board local network such to synchronize the internal time of the on-board devices (i.e. the slave clocks; e.g. sensor-, communication- and control-nodes) to a master clock. According to [123], the synchronization quality in PTP could be affected by the stability of oscillators, the resolution of time-stamping the messages, the frequency of sending synchronization messages, and the propagation delay variation caused by the jitter in the intermediate elements. With the transparent clock implementation of PTP [58], the current state of the art guarantees a synchronization precision of 1 [μs] for topologies in the presence of no more than 30 consecutive slaves [123]. This assumption let us to neglect delay effects caused by synchronization in our experiments. Note that global clock synchronization achieved equipping each vehicle with a GPS is a common practice in the intelligent transportation field [132] , [64], [9], [40], [138].

Chapter 7

Experimental results

Contents

7.1 Experimental characterization of the inter-vehicular delays 69
7.1.1 Characterization of the delay on follower nr. 1 69
7.1.2 Characterization of the delay on follower nr. 2 78
7.2 Distributed coupling protocol validation 80
7.2.1 Consensus validation 80
7.2.2 Consensus in a joining maneuver 86
7.2.3 Tracking control 91

In this Chapter we show the experimental results achieved during the on the road tests. We consider a prototype of three vehicles such to validate the proposed distributed coupling protocol (4.6). There are two main activity performed: at first, the measurement and analysis of the *delay* $\tau_{ij}(t)$, typical in the Vehicle-to-Vehicle framework. We start analysing the delay $\tau_{ij}(t)$ due to received messages in Section 7.1, both on the follower nr.1, in Subsection 7.1.1, and follower nr. 2, in Subsection 7.1.2. The second activity focuses on the distributed coupling protocol validation in Section 7.2. In particular, consensus is discussed in Subsection 7.2.1; then, a *joining* maneuver is tested in Subsection 7.2.2. This action is typical in platooning when a driver wants to join a platoon on an highway. Finally, in Section 7.2.3 the proposed distributed coupling protocol is validated in the presence of a time-varying trajectory imposed by the leader vehicle.

7.1 Experimental characterization of the inter-vehicular delays

We start by describing the process to compute the communication *delay* $\tau_{ij}(t)$.

7.1.1 Characterization of the delay on follower nr. 1

We describe the experiments performed in the simplest platoon configuration, with the leader and the follower nr.1, as depicted in Fig. 7.1, top panel.

This experiment lets us to evaluate the *delay* $\tau_{ij}(t)$ due to both communication and processing delays in the leader-to-follower nr.1. The software module responsible

for computing the delay $\tau_{ij}(t)$ is inside the *additional communication* module (see Fig. 6.2): it compares the on-board clock (measurements available via RTK-GPS) with the timestamp of the data of interest inside the received packets from the neighboring vehicles, via Vehicle-to-Vehicle communication. Indeed, besides the *message timestamp*, defined as the time instant when the transmitter on the leader vehicle sends the message via V2V, all the on-board sensed measurements have a timestamp, i.e. the time instant when the information is measured, thanks to the synchronization of the network (for details, see Section 6.6). The latter is the information we use to compute the delay $\tau_{ij}(t)$. Note that this computation is done at least 1000 times each second. A detailed description of the *additional communication* module can be found in the Appendix E.1.
In order to perform our test such to compute the delay $\tau_{ij}(t)$, we consider a real leader vehicle, a Volvo $S80$, and a real follower nr.1, i.e. a Volvo $S60$, as depicted in Fig. 7.1, top panel. The leader and the follower nr.1 have been equipped with the experimental setup described in Section 6.3 and Section 6.4, respectively. In particular, the *communication* module used to perform Vehicle-to-Vehicle communication is described in Section 6.5.
The path followed by the message to be transmitted by the leader vehicle and received on the follower nr.1 is depicted in Fig. 7.1, down panel. The leader vehicle RTK-GPS has been set such to receive NMEA messages with a 4 [Hz] update rate(see details in Appendix D.1.1); instead, the follower nr.1 RTK-GPS has a 20 [Hz] update rate. Note that we select both GPS receiver with two different update rate in order to validate the controller in the presence of heterogeneous GPS behaviour. Moreover, the *transmitter* module in Fig. 7.1, down panel, is programmed such to send messages each $0,1[s]$.
According to this assumption, we suppose a *first scenario* with both leader and follower nr.1 *at standstill* with a distance of 5 [m] with each other. In Fig. 7.2, top and down panels, the *sequential number* of the received packet is shown and its enlarged version is in the down panel. In particular, in this experiment we have 450 packets sent by the leader and 449 packets received by the follower, obtaining the $0,22\%$ of *packet losses*.
In Fig. 7.3, top panel, we compare the timestamp measured on the follower nr.1 (measurements available via RTK-GPS) and the received data timestamp from the leader via Vehicle-to-Vehicle communication. In particular, in Fig. 7.3, down panel, we can see the piecewise continuous behaviour in the received data (i.e. a 4 [Hz] GPS update rate) and in the follower nr.1 GPS (i.e. a 20 [Hz] GPS update rate). In Fig. 7.4, we show the delay $\tau_{10}(t)$, as a difference of the red and blue lines in Fig. 7.3. We emphasize that the behaviour of $\tau_{10}(t)$ is influenced by the leader vehicle GPS update rate (4 [Hz]). Moreover, the effect of the follower nr.1 GPS update rate is hidden due to the *Unix Time*, i.e. a smoother version of the clock measurements than the GPS timestamp measurements. We emphasize that during testing it was found that sometimes CALM daemon running on the leader vehicle communication box crashed and the timing of the crash was random and unpredictable. In order to solve this problem, a delay of about 25-50 milliseconds between each read from CALM server interface on the transmitter side has been included: the effect of this phenomena is an offset on the delay $\tau_{10}(t)$. In Fig. 7.5, top panel, we show the delay $\tau_{10}(t)$ on a longer time interval than the ones described in Fig. 7.4. Moreover, in Fig. 7.5, down panel, there is a zoomed version of measurements in Fig. 7.5, top panel. In this experiment we have 4800 packets sent by the leader and 4756 packets received by the follower, obtaining the $0,92\%$ of *packet losses*.
We suppose the *second scenario* with both leader and follower nr.1 *moving* with a constant relative distance of 10 [m] with each other and a common velocity less than 15 [km/h]. If we compare Fig. 7.4 and Fig. 7.6, top panel, we emphasize the presence of

some spikes in Fig. 7.6, top panel, such to have the value of $\tau_{10}(t)$ greater than 300 [ms]. In this experiment we have 887 packets sent by the leader and 886 packets received by the follower, obtaining the $0,11\%$ of *packet losses*. As a consequence, the spikes in Fig. 7.6, top panel, mean the leader GPS receiver has not updated its position each 250 [ms], i.e. there are packet losses due to the GPS receiver on the leader vehicle. Instead, the packet losses are almost absent in Vehicle-to-Vehicle communication.

The *third scenario* is with both the leader and the follower nr.1, travelling at a common velocity, i.e. 20 [km/h] with a variable inter-vehicle distance from 5 to 15 [m]. Such as in Fig. 7.6, top panel, in Fig. 7.6, down panel, we show some spikes due to GPS receiver failure on the leader vehicle. In Vehicle-to-Vehicle communication we have 939 packets sent by the leader and 937 packets received by the follower, obtaining the $0,21\%$ of *packet losses*.

Although a delay $\tau_{10}(t)$ higher than $\tau^\star$ computed in Section 5.1, we underline that τ_{10} can be decreased by increasing both the update rate on the GPS receiver and the speed of the CALM FAST Daemon task.

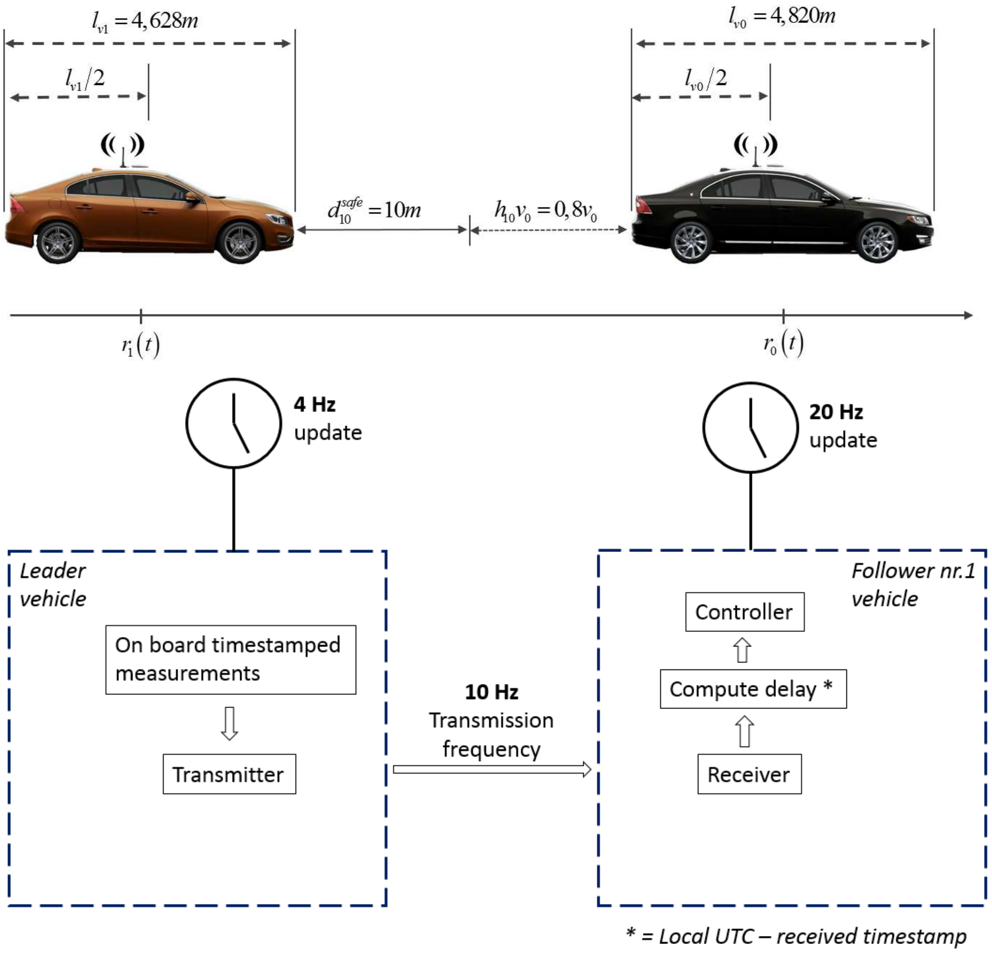
$l_{v1} = 4,628m$
$l_{v1}/2$
$l_{v0} = 4,820m$
$l_{v0}/2$
$d_{10}^{safe} = 10m$
$h_{10}v_0 = 0,8v_0$
$r_1(t)$
$r_0(t)$
4 Hz
update
20 Hz
update
Leader
vehicle
On board timestamped measurements
Transmitter
10 Hz
Transmission
frequency
Follower nr.1
vehicle
Controller
Compute delay *
Receiver
* = Local UTC – received timestamp

Figure 7.1: Leader-Follower nr.1 configuration. Top panel: vehicular parameters. Down panel: the path followed by the message to be transmitted by the leader to the follower nr.1.

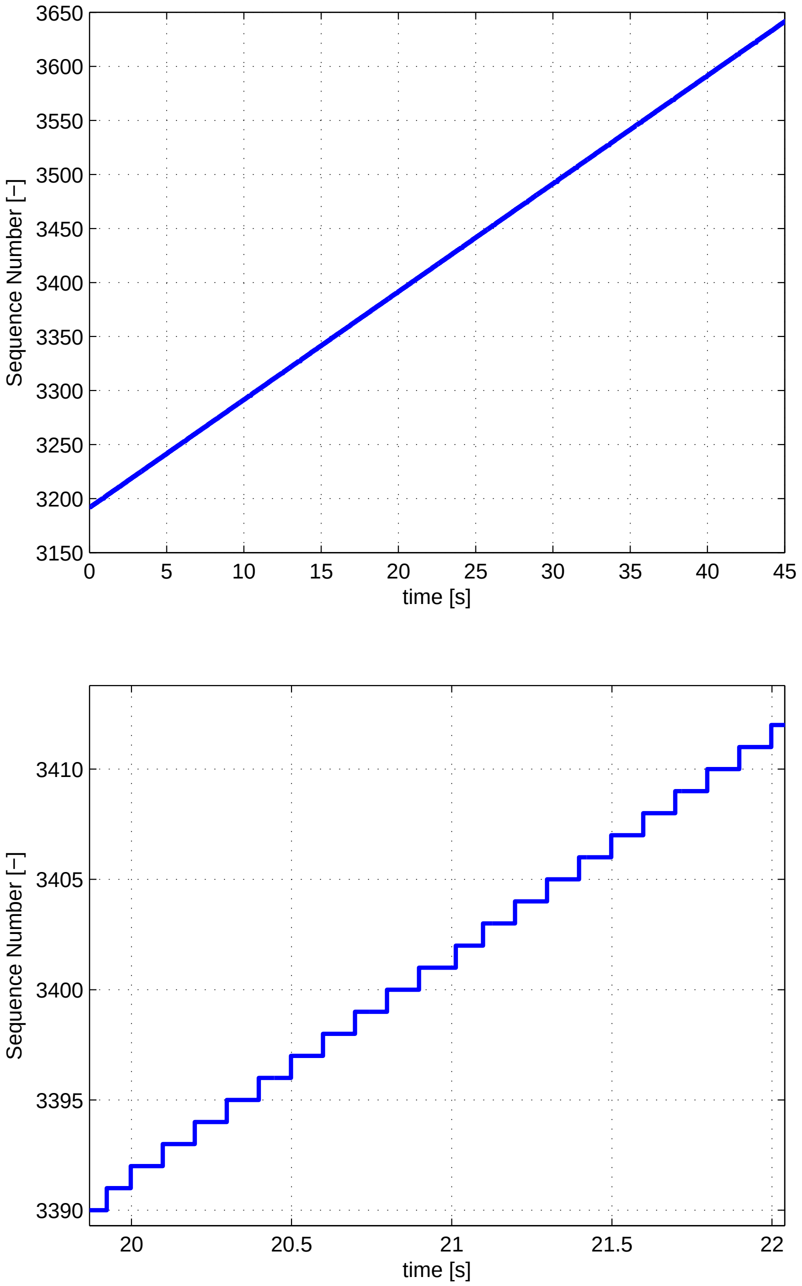

Figure 7.2: Leader-to-Follower nr.1 delay $\tau_{10}(t)$ at standstill. Top panel: received packet sequential number. Down panel: ZOOM - received packet sequential number.

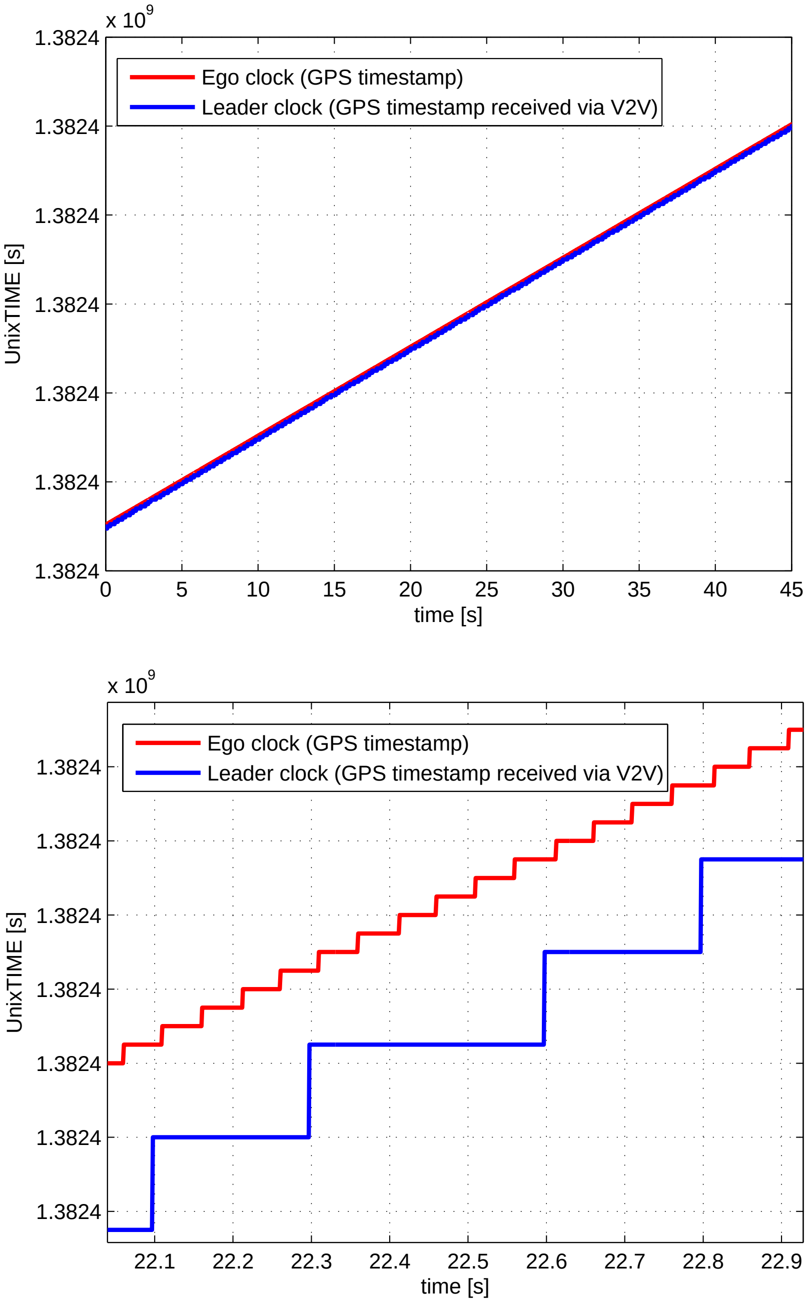

Figure 7.3: Leader-to-Follower nr.1 delay $\tau_{10}(t)$ at standstill. Top panel: GPS timestamp. Down panel: ZOOM - GPS timestamp.

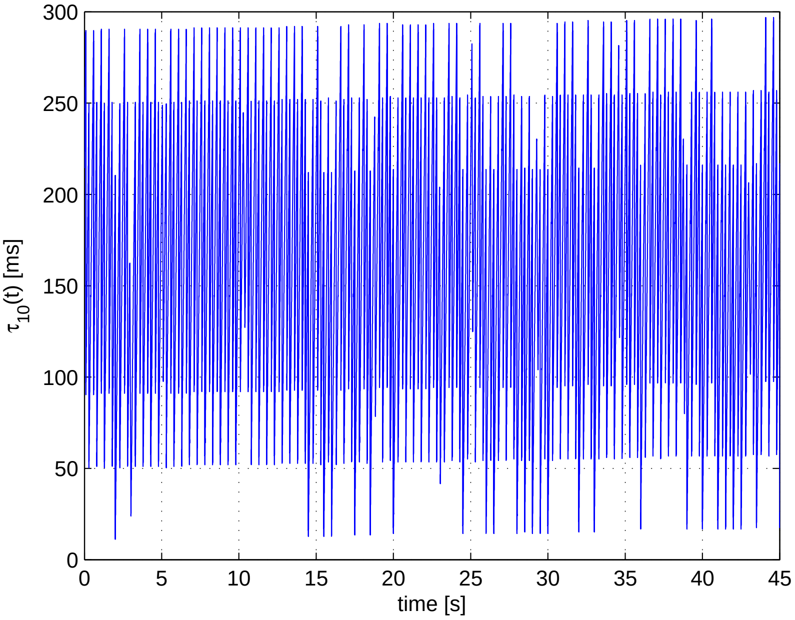

Figure 7.4: Leader-to-Follower nr.1 delay $\tau_{10}(t)$ at standstill.

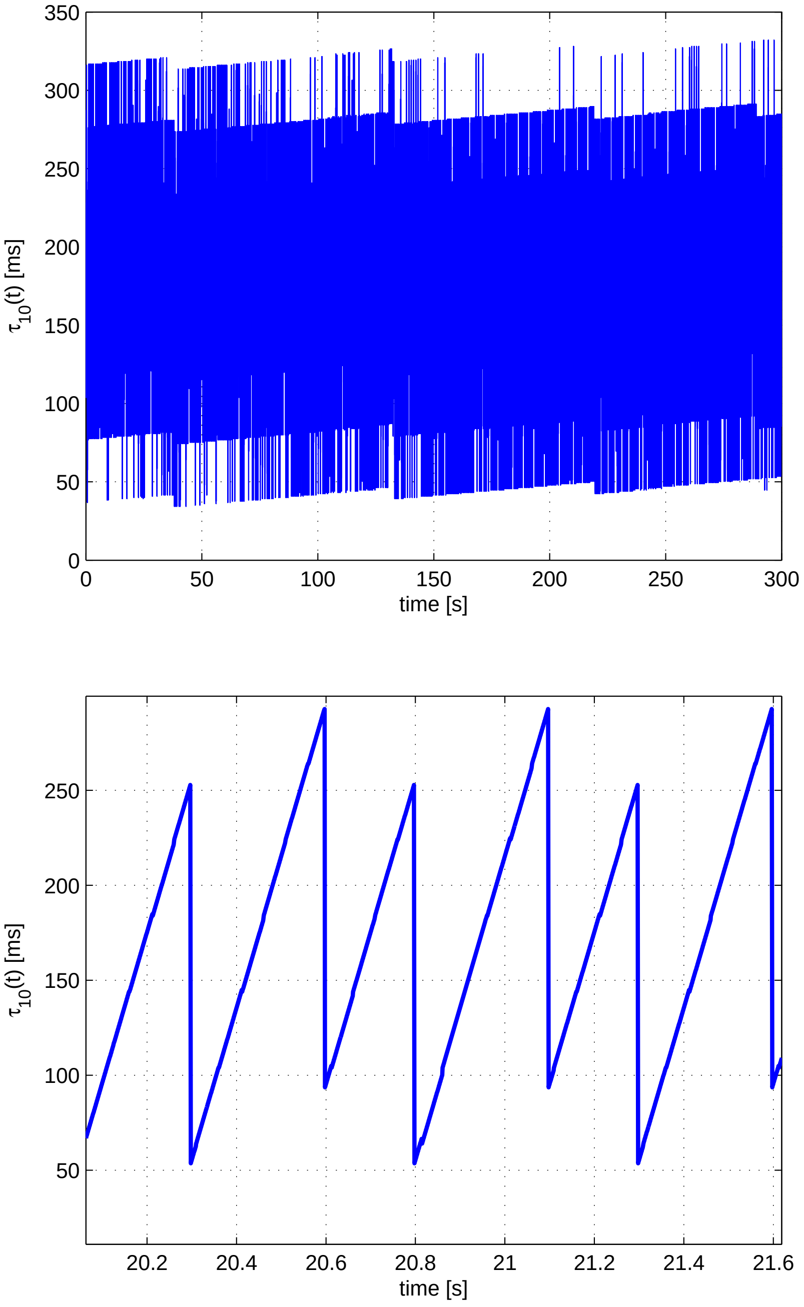

Figure 7.5: Leader-to-Follower nr.1 delay $\tau_{10}(t)$. Top panel: delay $\tau_{10}(t)$ for more than 1 minute. Down panel: ZOOM - delay $\tau_{10}(t)$.

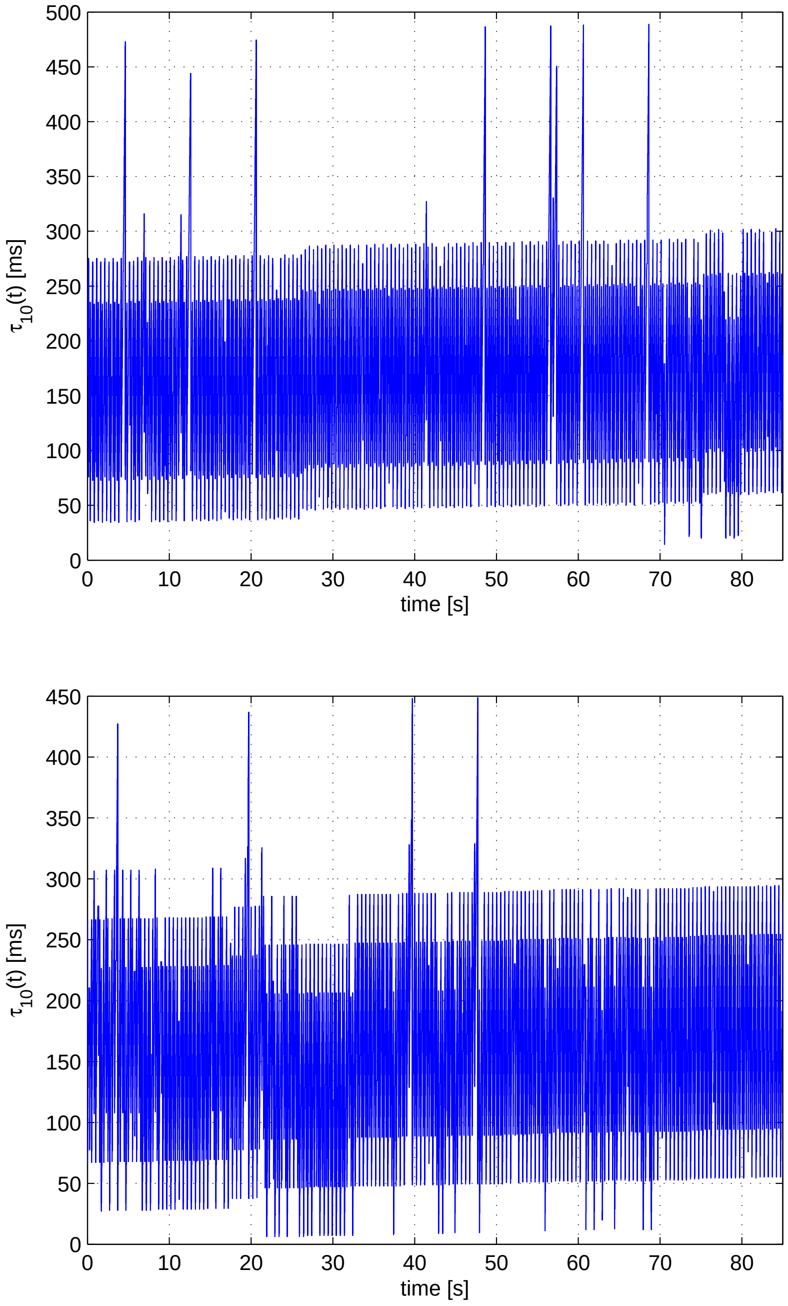

Figure 7.6: Leader-to-Follower nr.1 delay $\tau_{10}(t)$. Top panel: velocity less than 15 [km/h]. Down panel: velocity equal to 20 [km/h].

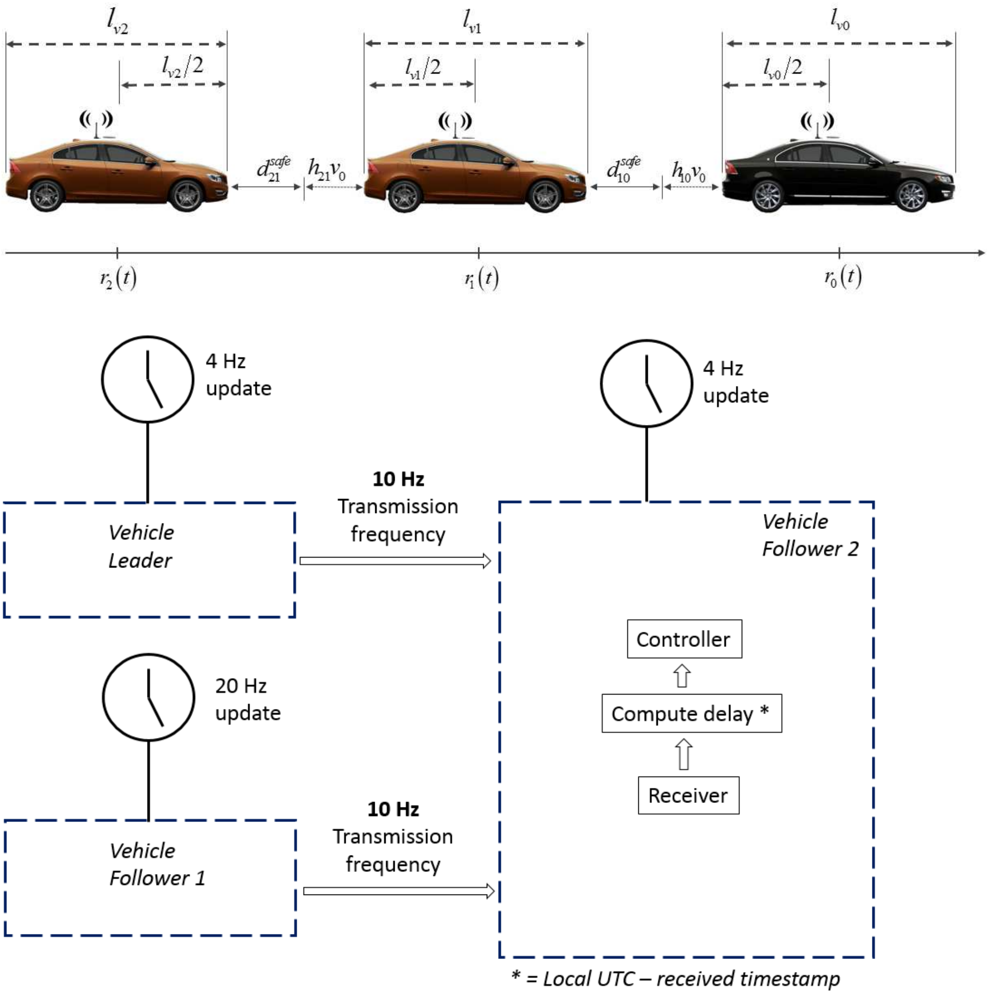
l_{v2}
$l_{v2}/2$
l_{v1}
$l_{v1}/2$
l_{v0}
$l_{v0}/2$
d_{21}^{safe}
$h_{21}v_0$
d_{10}^{safe}
$h_{10}v_0$
$r_2(t)$
$r_1(t)$
$r_0(t)$
4 Hz update
4 Hz update
Vehicle Leader
10 Hz Transmission frequency
Vehicle Follower 2
Controller
Compute delay *
Receiver
20 Hz update
Vehicle Follower 1
10 Hz Transmission frequency
* = Local UTC – received timestamp

Figure 7.7: Experimental setup: platoon of three vehicles. Top panel: vehicular parameters. Down panel: the path followed by the leader-to-follower nr.2 and by the follower nr.1-to-follower nr.2 data packets.

7.1.2 Characterization of the delay on follower nr. 2

Now we focus on the scenario depicted in Fig. 7.7, top panel. The path followed by the leader-to-follower nr.2 and by the follower nr.1-to-follower nr.2 data packets are depicted in Fig. 7.7, down panel. This experiment lets us to evaluate the delay $\tau_{ij}(t)$, i.e. the delays due to both communication and processing delays in the (i) leader-to-follower nr.1 communication $\tau_{10}(t)$, (ii) the leader-to-follower nr.2 communication $\tau_{20}(t)$ and (iii) the follower nr.1-to-follower nr.2 communication $\tau_{21}(t)$. We consider the experimental scenario depicted in Fig. 7.7, top panel in order to compute the delay $\tau_{ij}(t)$. We have three vehicles: a Volvo $S80$ (the leader), and two Volvo $S60$ (the followers nr.1 and nr.2). In Fig. 7.8 we have $\tau_{20}(t)$, i.e. the delay computed on the leader-to-follower nr.2 communication. Moreover, in Fig. 7.9 we show $\tau_{21}(t)$, i.e. the data delay in follower

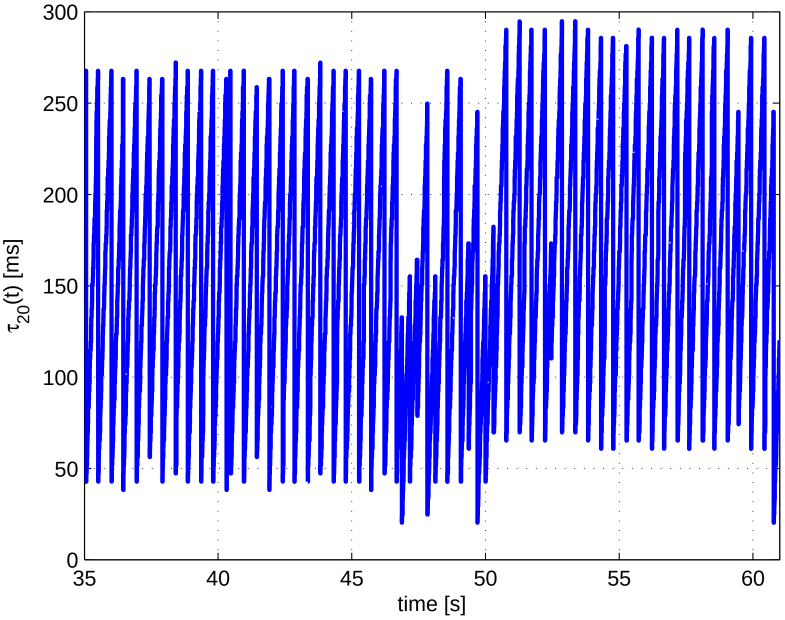

Figure 7.8: Leader-to-follower nr.2. $\tau_{20}(t)$.

nr.1-to-follower nr.2 communication. The measurements described in Fig. 7.8 and in Fig. 7.9 have been collected with the three vehicles travelling at about 40 [km/h], on a freeway in Göteborg, Sweden. We remark that the maximum amplitude of both the delay $\tau_{ij}(t)$ in Fig. 7.8 and in Fig. 7.9 differ due to the GPS update rate that are different on the leader, on the follower nr.1 and on the follower nr.2 (see Appendix D.1.2 for details on follower nr.2 GPS).

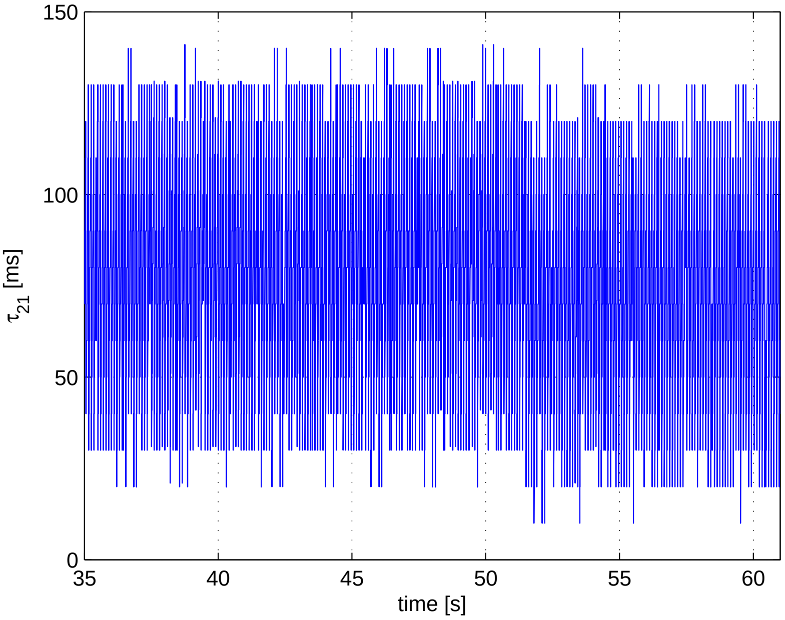

Figure 7.9: Follower nr.1-to-follower nr.2. $\tau_{21}(t)$.

7.2 Distributed coupling protocol validation

In this Section we show some of the experimental results achieved during the on the road tests with the prototype of three vehicles described in Chapter 6.

7.2.1 Consensus validation

Different experiments sets have been performed in order to validate the approach with the different topologies that can be originated by the communication network and the different active links. Control gains and spacing policy parameters have been set as in the numerical analysis, Section 5.1, and in Fig. 7.7 top panel, respectively.
The first experimental results refer to the single lane scenario where leader and followers share information via the wireless communication based on the IEEE 802.11p protocol as depicted in Fig. 7.11. The test track is a highway in the industrial area in Göteborg, Sweden. We suppose that both follower nr.1 and follower nr.2 start with different velocities, Fig. 7.10, left panel. In Fig. 7.12 are collected both the speeds of the three vehicles and the speed errors. Moreover, in Fig. 7.13 we have both the position errors and the control effort that determine the distributed coupling protocol action.
Experiments confirm the effectiveness of the consensus based strategy in creating and maintaining the platoon. Indeed, vehicles starting from different velocities and positions automatically converge to the desired common dynamic behavior (reaching and maintaining the constant leader velocity of 9.4 [m/s] and prefixed inter-vehicular distance of 17.5 [m]) as shown in Figs. 7.12 and 7.13. As evident from results, consensus is guaranteed and both speed and position errors go to zero (down panel in Fig. 7.12; top

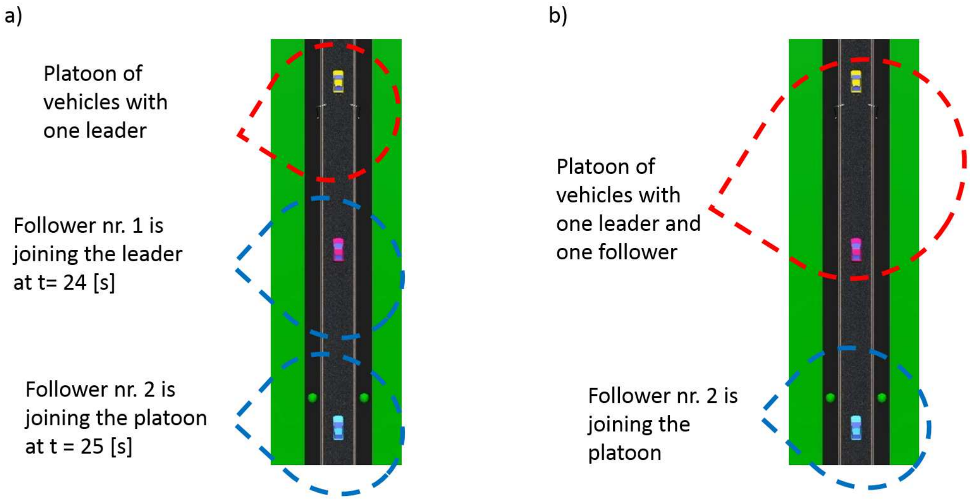
a)
Platoon of vehicles with one leader
Follower nr. 1 is joining the leader at t= 24 [s]
Follower nr. 2 is joining the platoon at t = 25 [s]
b)
Platoon of vehicles with one leader and one follower
Follower nr. 2 is joining the platoon

Figure 7.10: Platoon maneuver. Left panel: Consensus. Right panel: joining maneuver.

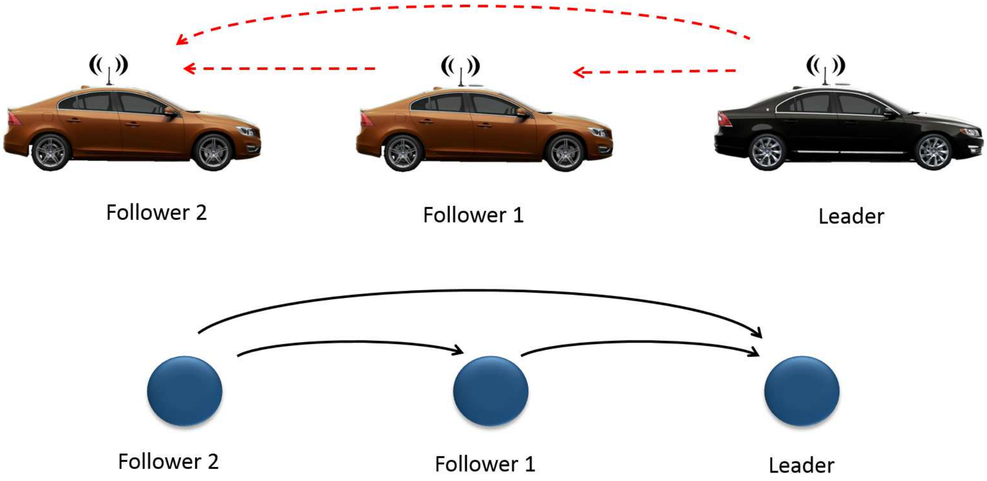
Follower 2
Follower 1
Leader
Follower 2
Follower 1
Leader

Figure 7.11: Leader-Follower nr.1-Follower nr.2 platoon configuration. Leader-predecessor topology.

panel in Fig. 7.13). Note that, as expected, the control effort reduces to zero once the consensus is achieved (see the down panel in Fig. 7.13).

Now, we emphasize each term of the distributed coupling protocol (4.6) computed on the follower nr.1: in particular, in Fig. 7.14, top panel, we show the effect due to the term $\tau_{10}(t)v_0$ in the relative distance between the leader and the follower nr.1 in the

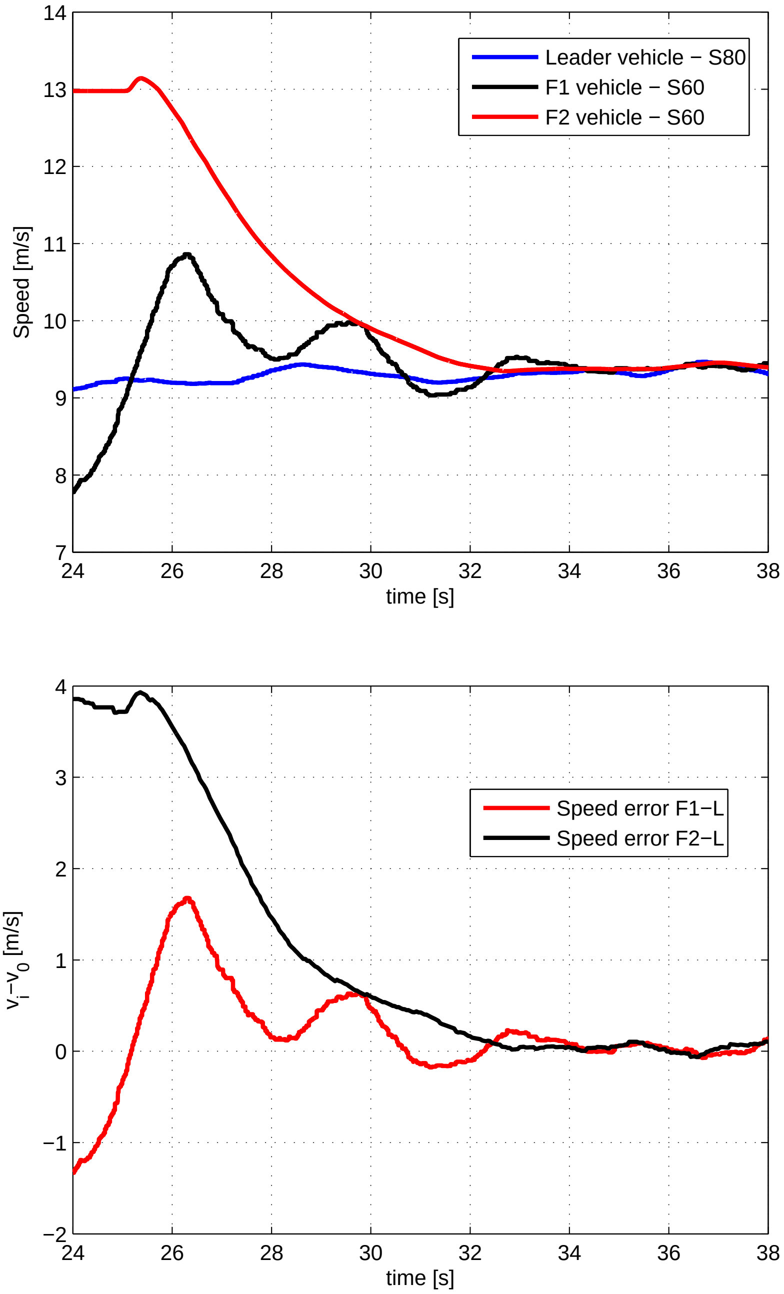

Figure 7.12: Leader-Follower nr.1-Follower nr.2 platoon configuration. Top panel: vehicles speed. Down panel: speed error.

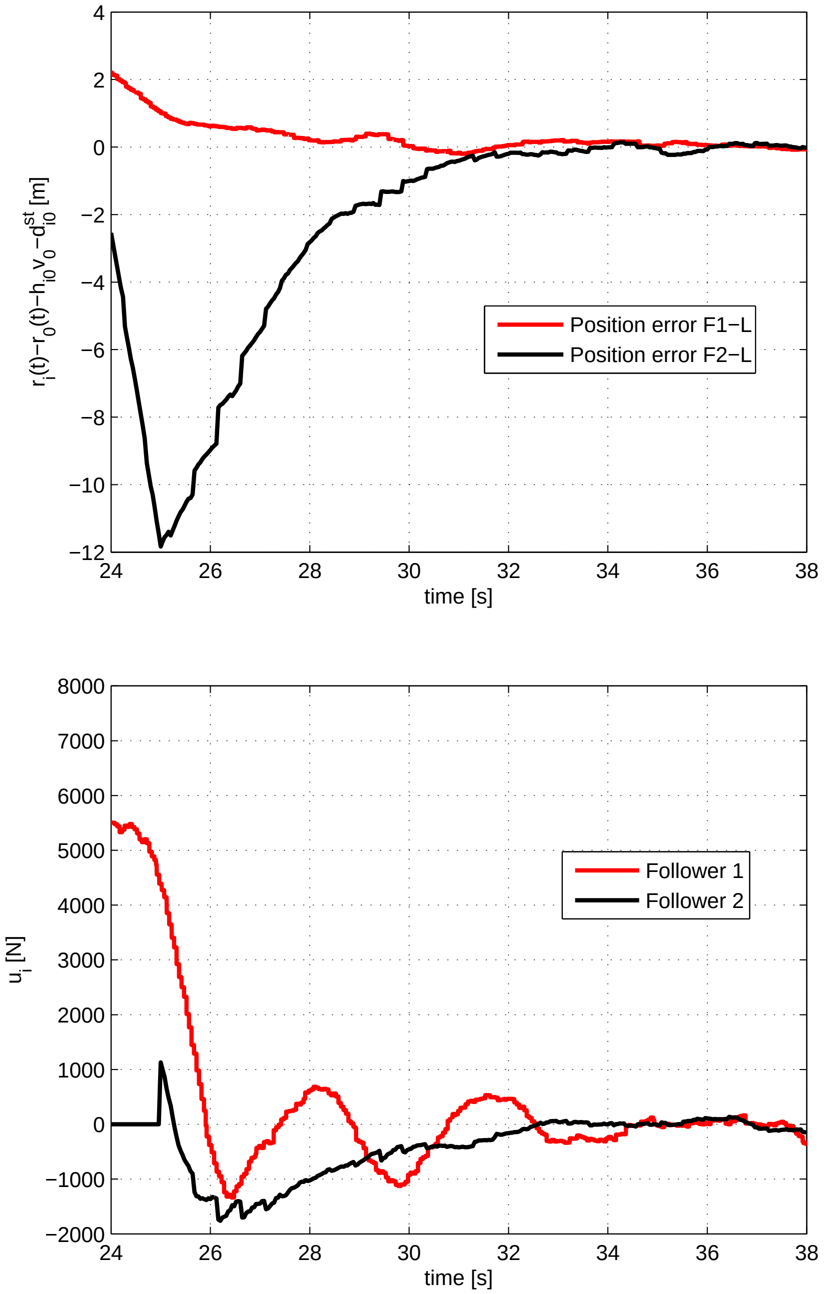

Figure 7.13: Leader-Follower nr.1-Follower nr.2 platoon configuration. Top panel: position error. Down panel: Control effort.

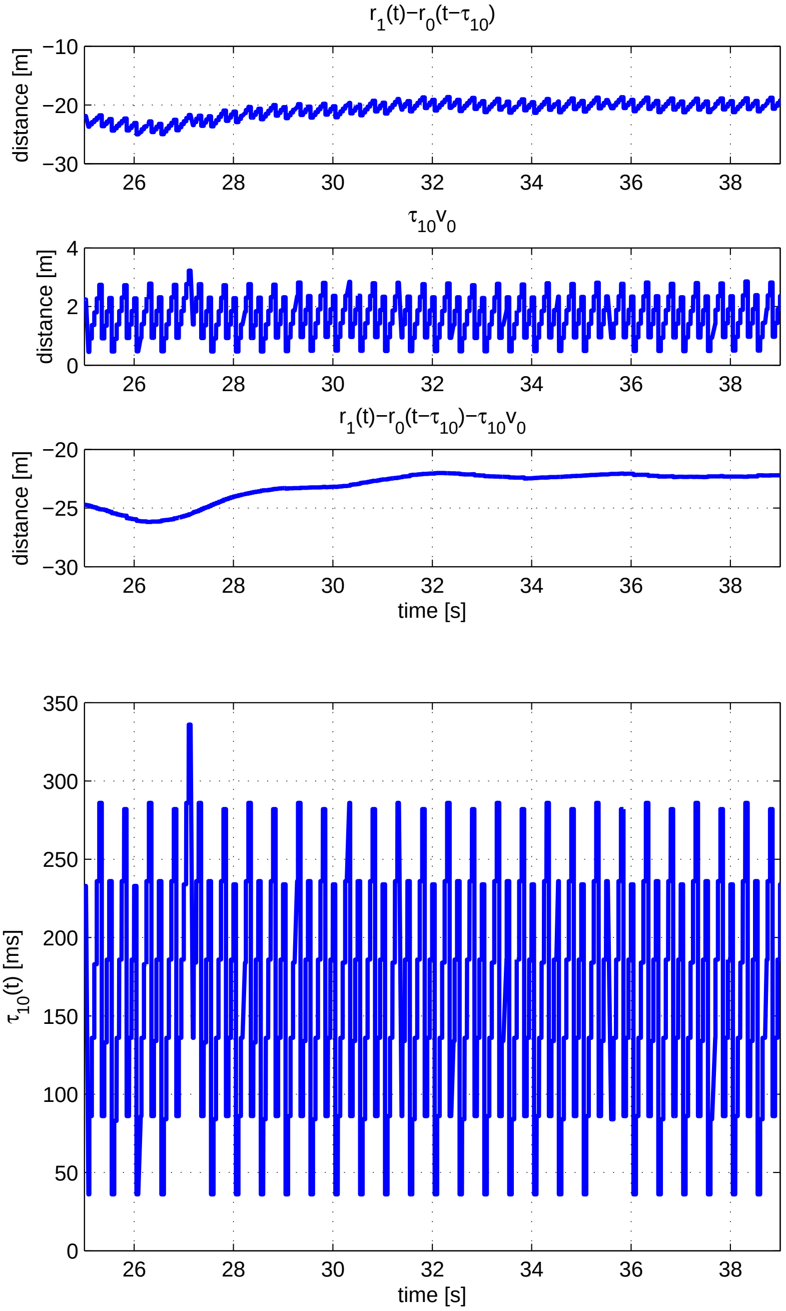

Figure 7.14: Leader-Follower nr.1-Follower nr.2 platoon configuration: Follower nr.1. Top panel: Relative distance. Down panel: delay $\tau_{10}(t)$.

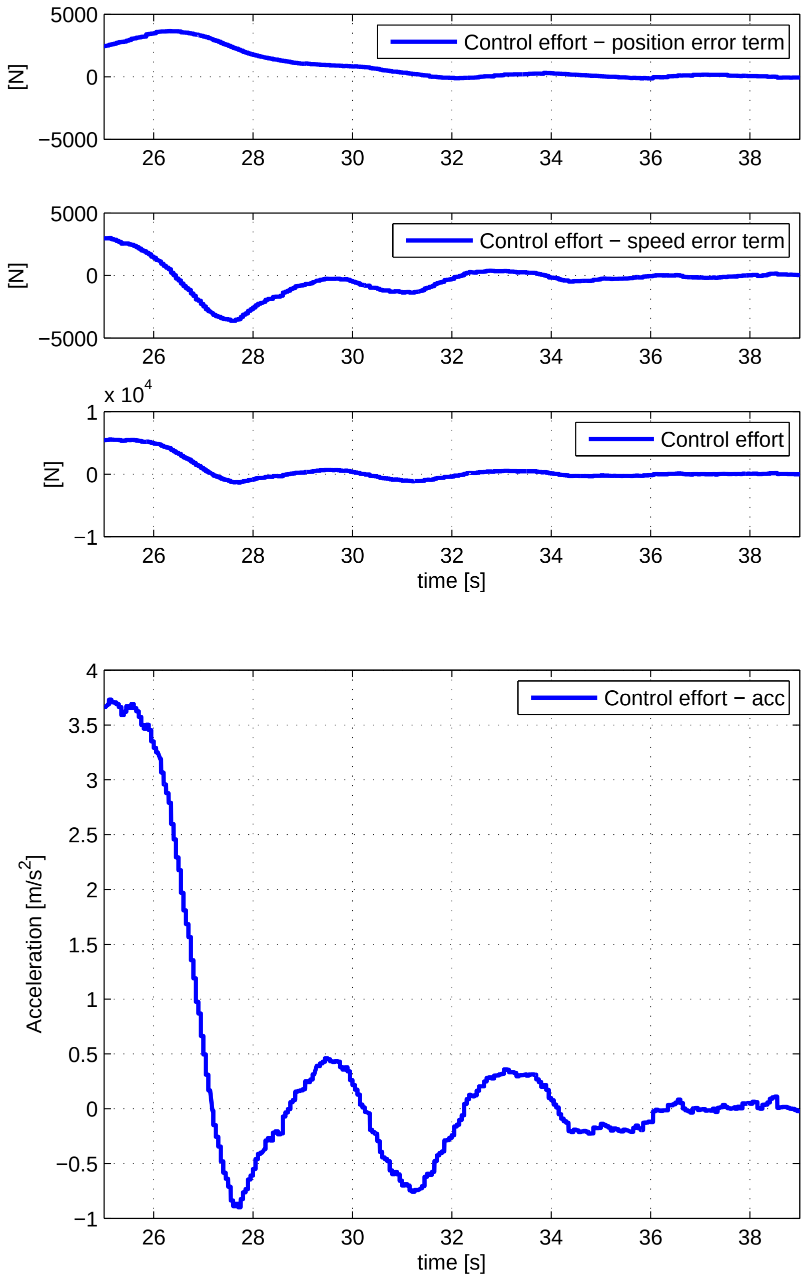

Figure 7.15: Leader-Follower nr.1-Follower nr.2 platoon configuration: Follower nr.1. Top panel: Control effort in consensus experiment. Down panel: desired vehicle acceleration.

leader-follower scenario; in Fig. 7.14 down panel, we show also the delay $\tau_{10}(t)$.
Each component in the control effort is described in Fig. 7.15 top panel. Moreover, the desired acceleration is shown in Fig. 7.15 down panel.

7.2.2 Consensus in a joining maneuver

Further experiments have been devoted to test the ability of the approach during the classical maneuver of joining a platoon. Namely, follower nr.2 has to automatically engage the platoon composed by the leader and the follower nr.1, travelling together with a common velocity of 9.2 [m/s] and a desired inter-vehicle distance of $17.3[m/s]$ (see Fig. 7.10, right panel). Experimental results are displayed in Fig. 7.16 and in Fig. 7.17. In particular, according to the network topology described in Fig. 7.11, we have that in Fig. 7.16 top panel, the measured speed of the leader vehicle, the measured speed of the follower nr.1 and the speed of the simulated follower nr.2 are displayed. Moreover, the speed errors between both the follower nr.1 and follower nr.2 respect to the leader vehicle are in Fig. 7.16, down panel. The position errors are shown in Fig. 7.17, top panel and the control effort acting on both the follower nr.1 and the follower nr.2 are in Fig. 7.17, down panel. Results shown in Figs. 7.16-7.17 show how the vehicle automatically performs the engaging maneuver and reaches the desired position and velocity. Again the control effort reduces to zero once the follower nr. 2 is in the platoon and travels with the others (down panel in Fig. 7.17). Now we show all the terms in the distributed coupling protocol (4.6) computed on the follower nr. 1. In particular, in Fig. 7.18, top panel, we emphasize the value due to the term $\tau_{10}(t)v_0$ in the relative distance between the leader and the follower. In Fig. 7.18 down panel, we show the delay $\tau_{10}(t)$ in Vehicle-to-Vehicle communication. About the control effort, it can be decoupled as described in Fig. 7.19 top panel. Moreover, the desired acceleration of the follower nr.1 is in Fig. 7.19 down panel.

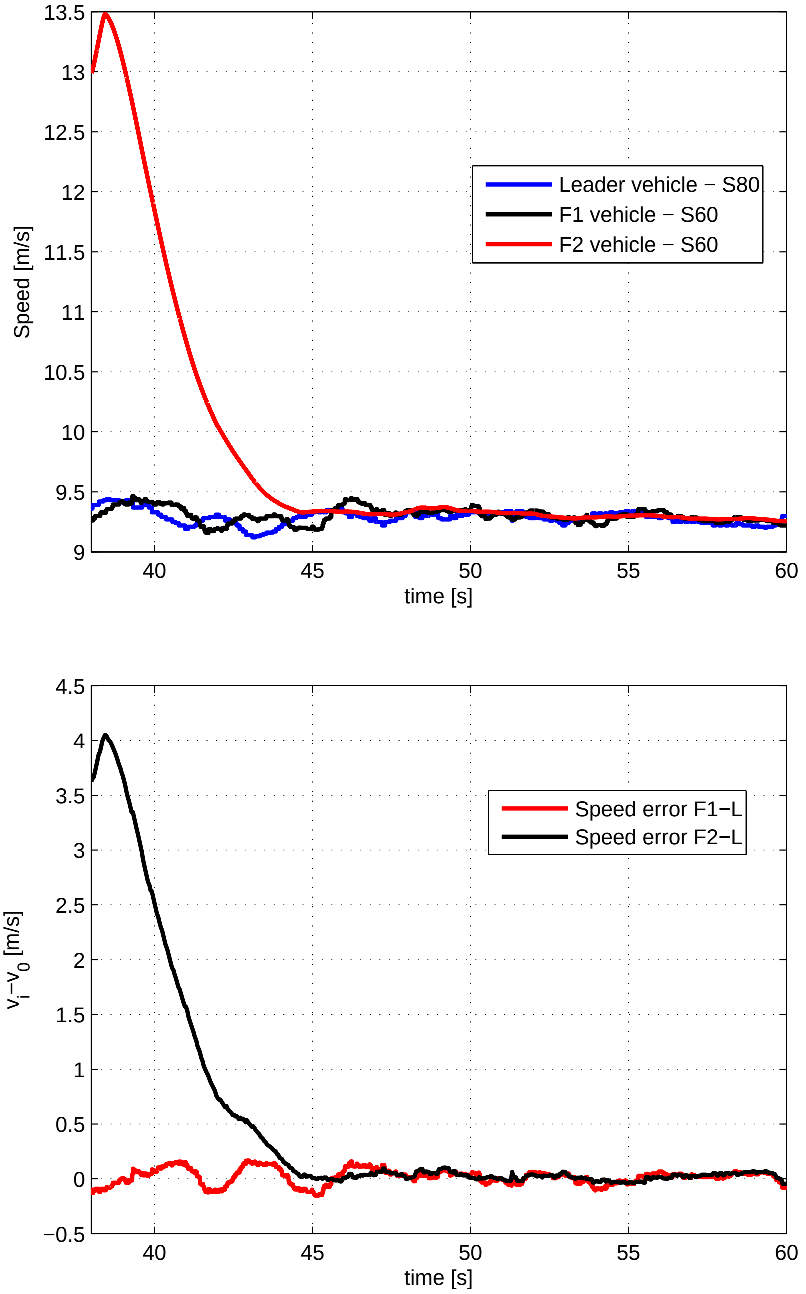

Figure 7.16: Leader-Follower nr.1-Follower nr.2 platoon configuration. Top panel: vehicles speed. Down panel: speed error.

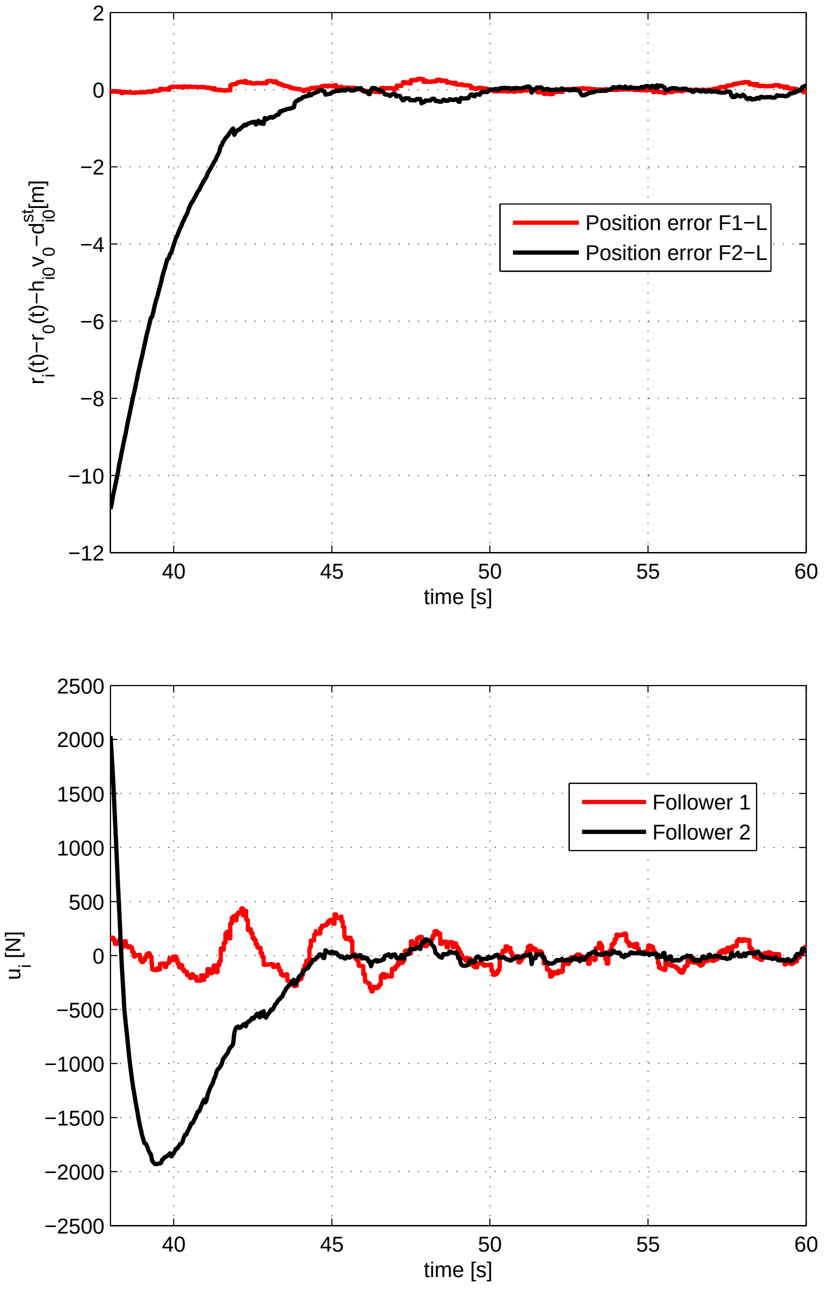

Figure 7.17: Leader-Follower nr.1-Follower nr.2 platoon configuration. Top panel: position error. Down panel: Control effort.

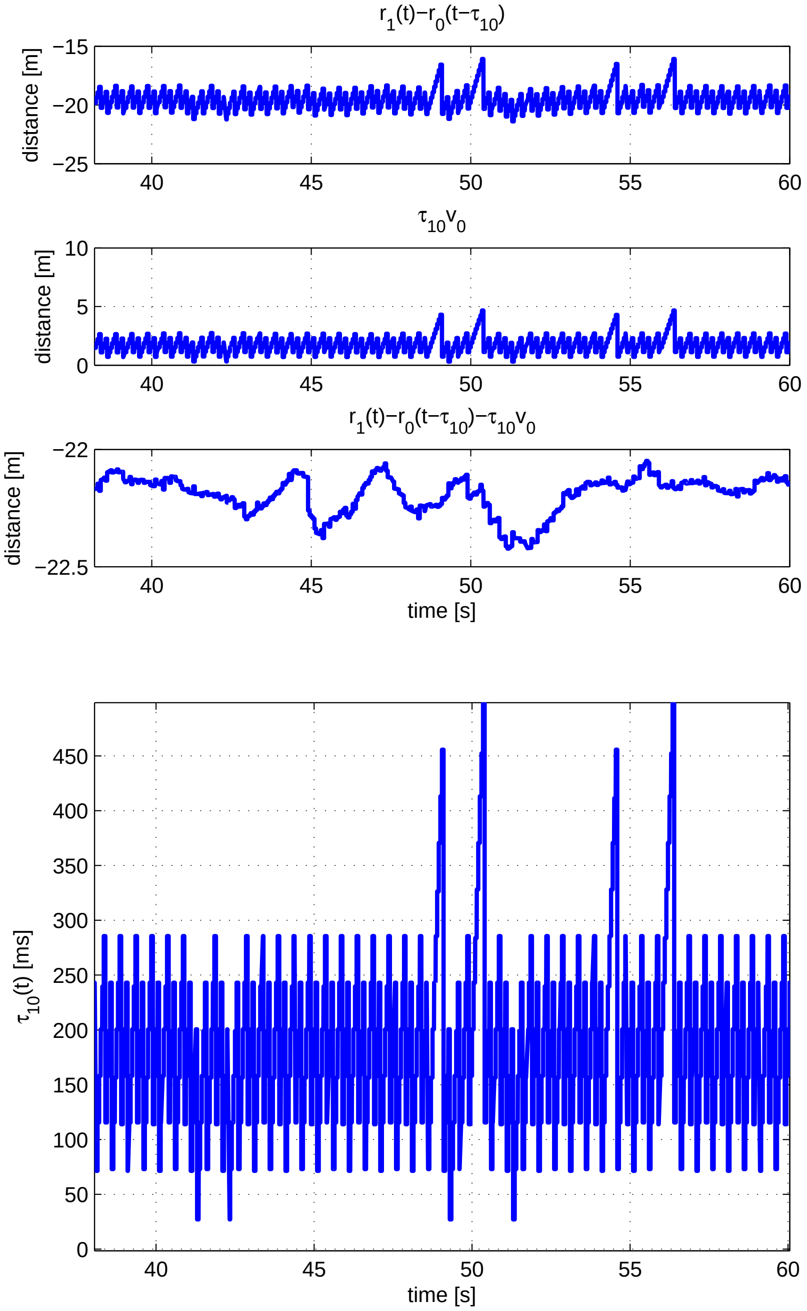

Figure 7.18: Leader-Follower nr.1-Follower nr.2 platoon configuration: Follower nr.1. Top panel: Relative distance. Down panel: delay $\tau_{10}(t)$.

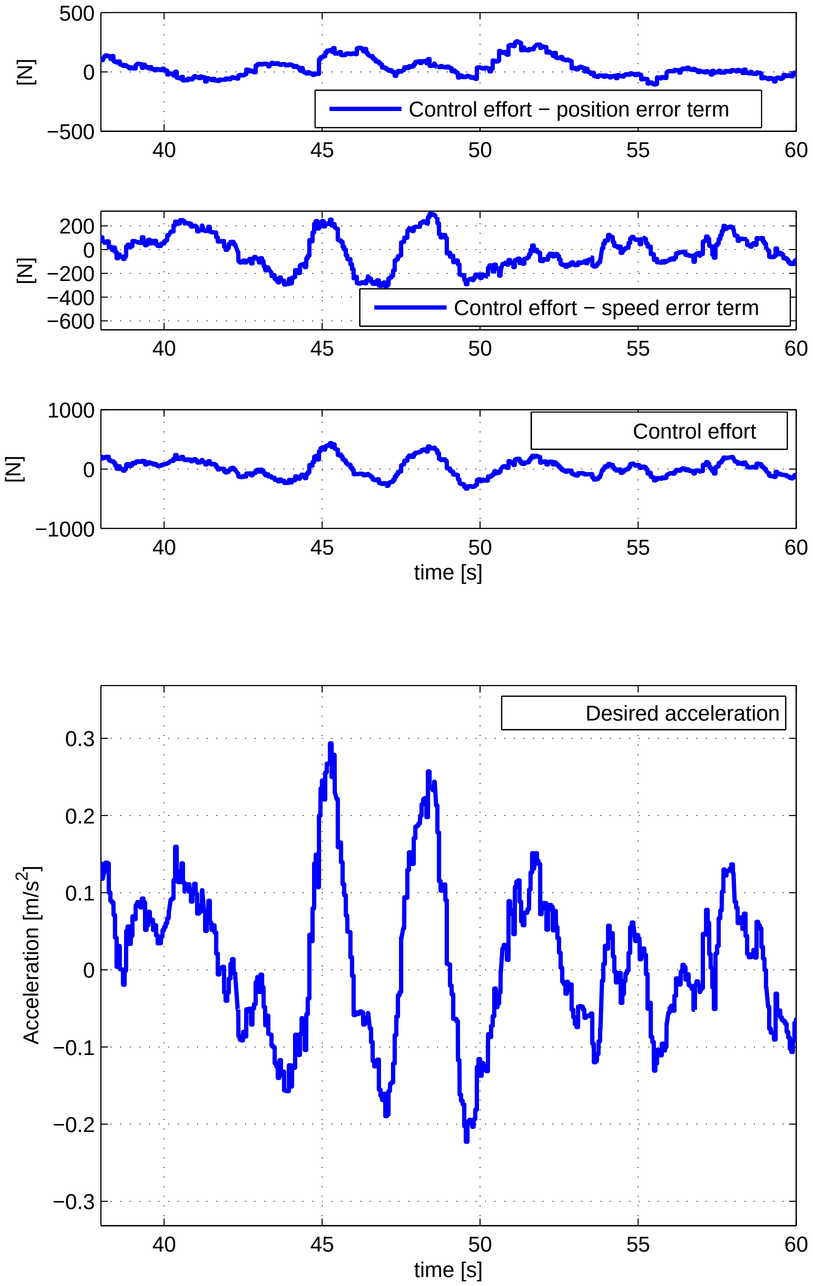

Figure 7.19: Leader-Follower nr.1-Follower nr.2 platoon configuration: Follower nr.1. Top panel: Control effort. Down panel: desired vehicle acceleration.

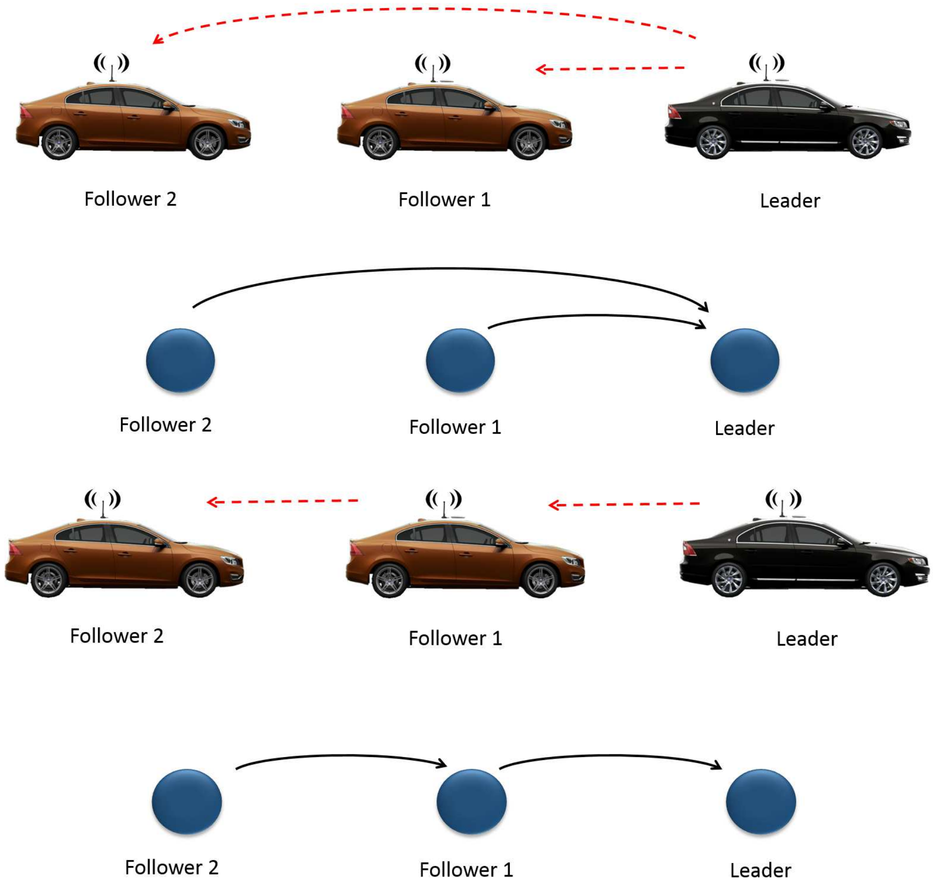

Figure 7.20: Leader-Follower nr.1-Follower nr.2 platoon configuration. Top panel: Leader topology. Down panel: Preceding vehicle topology.

7.2.3 Tracking control

Although the consensus is theoretically guaranteed in the case of constant leader velocity, further experiments have been devoted to test the ability of the strategy in tracking the leader when it is moving from rest to its final velocity v_0. To this aim the three vehicles are at rest at beginning of the experiments and they have initial inter-vehicle distances different from the one required by the spacing policy.

The first topology we assume is in Fig. 7.11 (leader-predecessor topology). In Fig. 7.21 top panel, we show the measured speed of the leader vehicle, the measured speed of the follower nr.1 and the speed of the simulated follower nr.2, respectively. The speed error between both the follower nr.1 and follower nr.2 respect to the leader vehicle are in Fig. 7.21, down panel. In Fig. 7.22, top panel, the position errors are displayed . Finally, in Fig. 7.22, down panel, we display the control effort acting on both the follower nr.1 and the follower nr.2. Results show that the approach is able to achieve tracking (see Fig. 7.21) bringing all vehicles to the desired mutual position (top panel in Fig. 7.22). As expected, again the control effort goes to zero when the platoon configuration is reached (down panel in Fig. 7.22).

Additional experiments have been dedicated to validate the strategy in different communication scenarios that can be of common use in ITS. Note that in all the considered scenarios node 0, i.e., the leader, is globally reachable as required in Theorem 4.3.1. Furthermore, the control gains have been not tuned again, and they are still the one selected during the numerical analysis.

The classical broadcast communication from leader to all followers has been investigated (see Fig. 7.20, top panel) under the action of the same reference maneuver depicted in Fig. 7.21, top panel - blue line. We show in Fig. 7.23, top panel, the position errors with respect to the leader vehicle. In Fig. 7.23, middle panel, we display the speed errors between both the follower nr.1 and follower nr.2 with respect to the leader vehicle. Experimental results related to a leader tracking maneuver (reported in Figs. 7.23) show how, also in this case, both speed and position errors go to zero, while the control action is inactive once the platoon is formed (see Fig. 7.23, down panel).

The other topology, which has been experimentally analyzed, refers to the classical predecessor-following architecture. This architecture is commonly used in CACC designing, where usually each vehicle is equipped with additional sensors (as radar, lidar and camera) for monitoring the state of its predecessor. Here we used the same architecture (and hence the topology depicted in Fig. 7.20, down panel) funding on wireless communication links (instead of on-board sensors), that do not suffer from the presence of sudden and unpredictable obstacles/obstructions between one vehicle and its ahead. Moreover, we have the same reference maneuver depicted in Fig. 7.21, top panel - blue line.

In Fig. 7.24 top panel, we display the position errors with respect to the predecessor. Moreover, the speed errors between both the follower nr.1 and follower nr.2 respect to the leader vehicle are in Fig. 7.24, middle panel. Finally, in Fig. 7.24, down panel, we show the control effort acting on both the follower nr.1 and the follower nr.2. Moreover, we have in Fig. 7.25 the position errors and the speed errors with respect to the leader. Also for this topology the consensus-based algorithm ensures good performance in achieving the desired collective platoon behavior as shown in Figs. 7.24. (Note that also for this topology the globally reachable hypothesis required by Theorem 4.3.1 is fulfilled. Again control gain are the one selected for achieving consensus for the all-to-all topology case.)

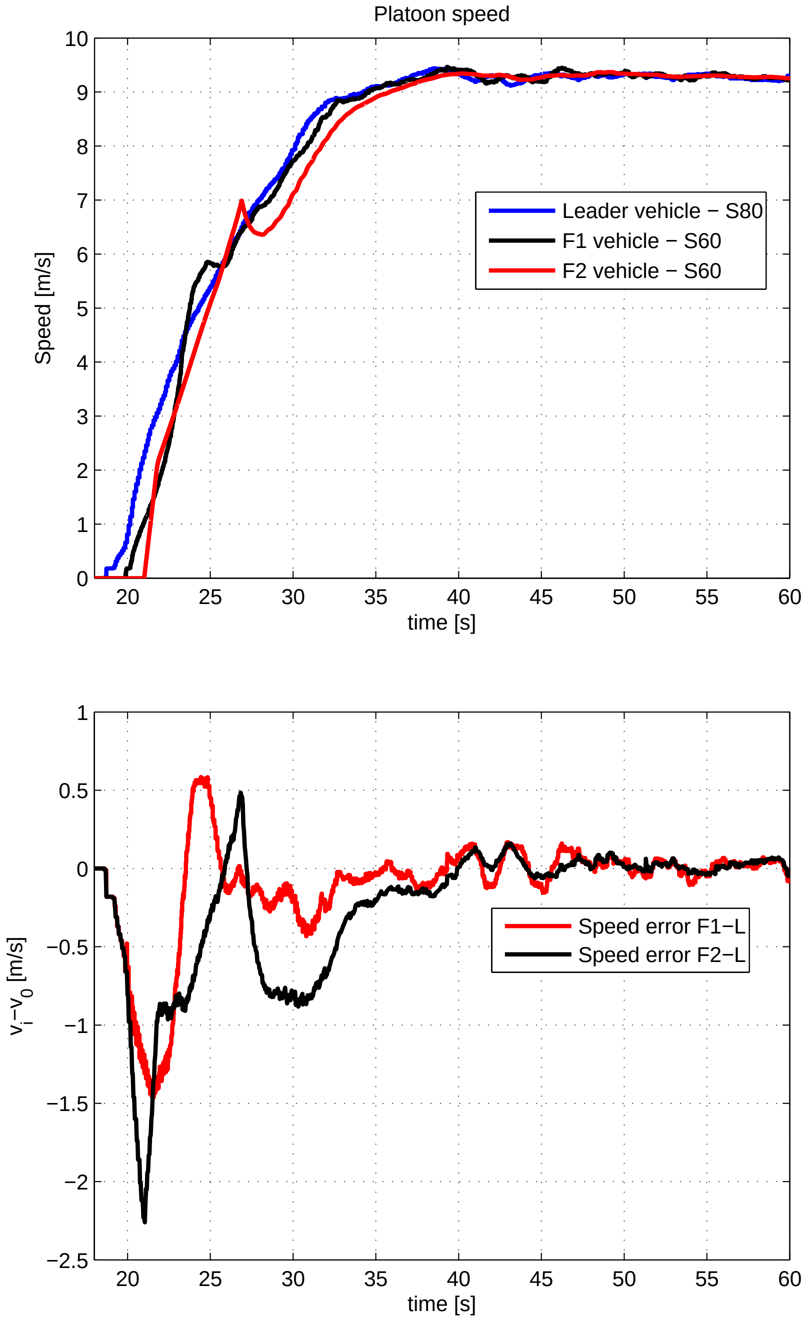

Figure 7.21: Leader-Follower nr.1-Follower nr.2 platoon configuration. Top panel: vehicle speed. Down panel: speed error.

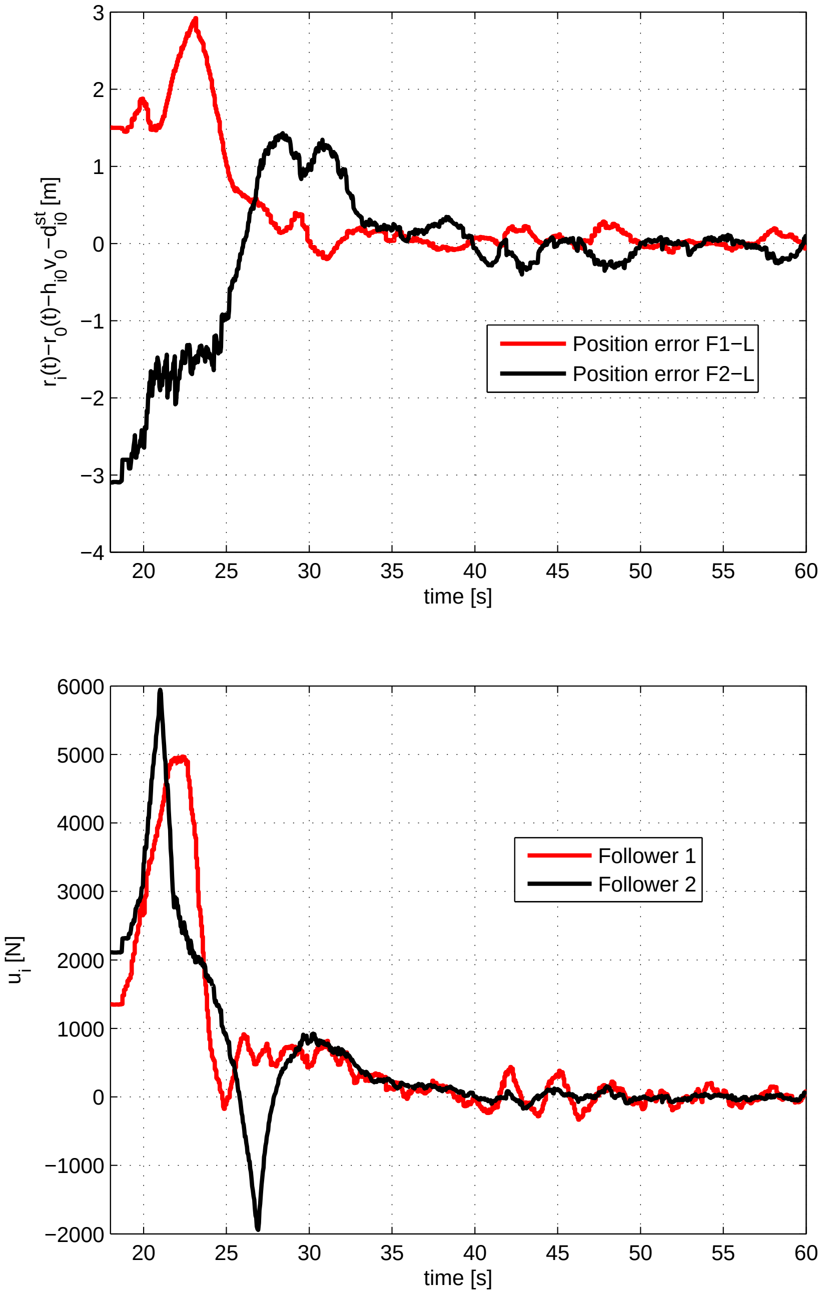

Figure 7.22: Leader-Follower nr.1-Follower nr.2 platoon configuration. Top panel: position error. Down panel: Control effort.

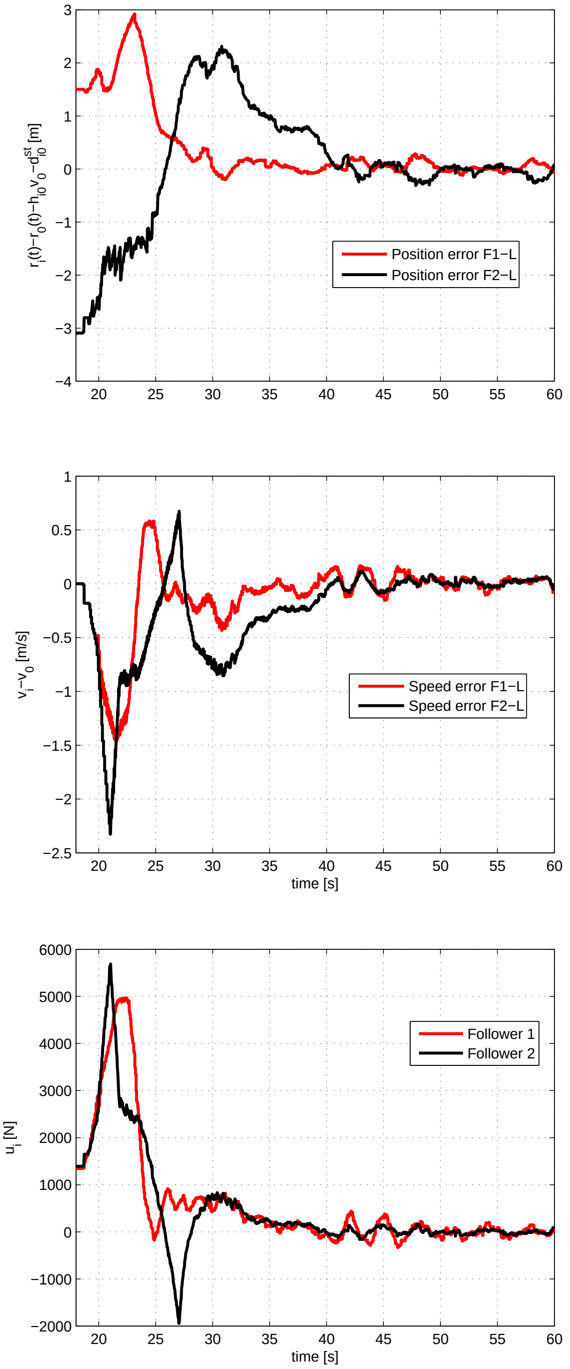

Figure 7.23: Leader-Follower nr.1-Follower nr.2 platoon configuration. Top panel: position error. Middle panel: speed error. Down panel: Control effort.

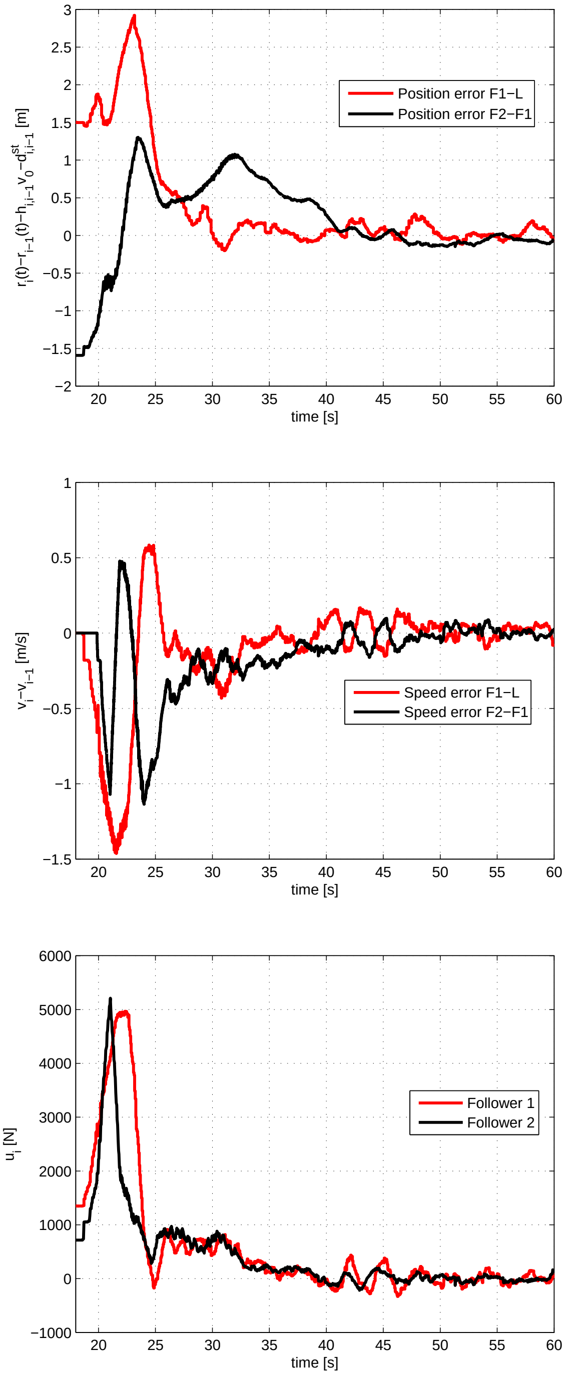

Figure 7.24: Leader-Follower nr.1-Follower nr.2 platoon configuration. Top panel: position error with respect to the predecessor. Middle panel: speed error with respect to the predecessor. Down panel: Control effort.

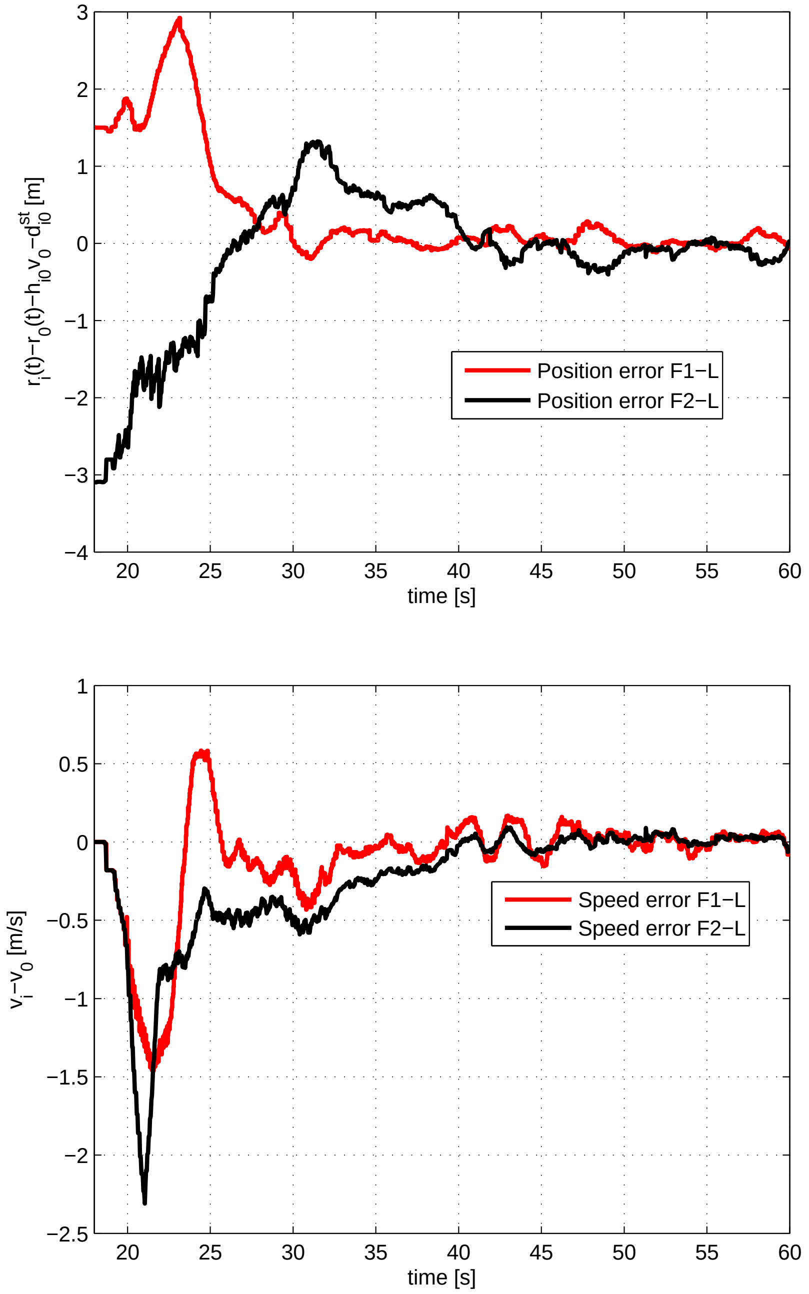

Figure 7.25: Leader-Follower nr.1-Follower nr.2 platoon configuration. Top panel: position error with respect to the leader. Down panel: speed error with respect to the leader.

Chapter 8

Conclusions

Contents

8.1 Contributions 99
8.2 Ideas for future research 100

In this thesis we describe a novel distributed control protocol to achieve platooning of vehicles in the presence of heterogeneous time-varying delays. By recasting the problem as that of achieving consensus in a closed-loop vehicular network, in Part I we prove local convergence and stability despite the presence of delays. We also investigate numerically the performance of the algorithm and its response to perturbations and communication failures. We found that the strategy is indeed effective in guaranteeing stability of the platoon even in the presence of disturbances. In Part II the physical implementation of the protocol is provided. In particular, a prototype of three vehicles, equipped with specific communication and control hardware, is used to validate the distributed coupling protocol. Experimental results confirm the achievement of consensus during the on the road tests in the presence of communication delays.

We wish to emphasize that the network paradigm proposed in this thesis can be particularly suitable for exploring communication strategies alternative to pairwise interactions. For example, the possibility can be investigated of vehicles communicating in clusters because of conditions due to their proximity and practical communication constraints.

8.1 Contributions

The contributions of the thesis can be summarized as follows:

- modeling of a platoon of vehicles communicating via V2V as a network of dynamical agents in Chapter 4: for the first time, tools from the networks of dynamical systems theory have been used to describe the coordination of a fleet of vehicles typical in a platooning scenario, in the presence of V2V communication.

- Definition of a distributed coupling protocol to achieve consensus of the entire network, such to solve the longitudinal control of a platoon of vehicles in the presence of heterogeneous and time-varying communication delays is provided in Chapter 4. A necessary and sufficient condition is shown under which the asymptotic controlled consensus is achieved, such as an upper bound for the maximum allowable communication delay is defined.

- Stability and robustness analysis of the consensus protocol with respect to both perturbation on the leader dynamics and communication failures are provided; numerical results to validate the proposed control strategy are in Chapter 5.
- A novel modular experimental set-up is provided to validate the platooning control strategy in Chapter 6. In particular, the proposed distributed coupling protocol has been validated on a prototype of three vehicles in Chapter 7, in the presence of maneuvers for both the platoon creation and joining. Moreover, also tracking has been tested, such to demonstrate the effectiveness of the proposed control strategy in the presence of a time-varying reference due to the leader.

8.2 Ideas for future research

As immediate extensions of the thesis work, we can consider the following points:

- robustness analysis of the distributed coupling protocol has been investigated in Section 5.2 with respect to any sudden perturbation on the leading vehicle dynamics with a leader-predecessor topology, in the presence of time-varying delays setted to the maximum admissible value $\tau_{ij}(t) = \tau \leq \tau^{\star}$. However, further study is needed to extend all the results presented in Section 5.2 to the case of both (i) switching topologies and (ii) time-varying delays. Moreover, an interesting topic under investigation is the analysis of disturbances acting on each vehicle of the platoon.
- Numerical analysis in Subsection 5.2.1 confirms that string stability is guaranteed with sudden variation on the leader dynamics. The experimental validation of this property, such as the use of a RTK-GPS equipping the follower vehicle nr.2, is an ongoing work with the collaboration of the Mechatronic group, Chalmers University of Technology, Göteborg, Sweden.
- Since numerical analysis in Subsection 5.2.2 shows that the distributed coupling protocol guarantees the controlled consensus of the delayed vehicular network in the presence of time-varying topologies if the leader is globally reachable, tools to demonstrate asymptotic stability in the presence of switching topologies are under investigation.

Bibliography

[1] GCDC, commstackv3-openwrtgcdc, Netherland 2011, http://www.gcdc.net.

[2] GCDC, interaction protocol 2.4, Netherland 2011, http://www.gcdc.net.

[3] *XSens MTi datasheet. www.xsens.com.*

[4] Circular Error Probable (CEP). *Air Force Operational Test and Evaluation Center Technical Paper*, page 1, 1987.

[5] A. Al Alam, A. Gattami, and K. H. Johansson. An experimental study on the fuel reduction potential of heavy duty vehicle platoooning. In *IEEE Conference on Intelligent Transportation Systems*, 2010.

[6] W. Alasmary and W. Zhuang. Mobility impact in ieee 802.11p infrastructureless vehicular networks. *Ad Hoc Networks*, 10(2):222 – 230, 2012.

[7] B. Anderson and J. B. Moore. *Optimal control: linear quadratic methods*. Prentice-Hall, Inc., 1990.

[8] P. Barooah and J.P. Hespanha. Error amplification and disturbance propagation in vehicle strings with decentralized linear control. In *Proceedings of the IEEE Conference on Decision and Control and European Control Conference (CDC-ECC)*, pages 4964 – 4969, 2005.

[9] R. Ben-El-Kezadri and G. Pau. Timeremap: stable and accurate time in vehicular networks. *IEEE Communications Magazine*, 48(12):52 –57, december 2010.

[10] C. Bergenhem, E. Hedin, and D. Skarin. Vehicle-to-Vehicle communication for a platooning system. *Procedia - Social and Behavioral Sciences*, 48(0):1222 – 1233, 2012.

[11] T. Bıyıkoglu, J. Leydold, and P. F. Stadler. Laplacian eigenvectors of graphs. *Lecture notes in mathematics*, 1915, 2007.

[12] S. Boccaletti, V. Latora, Y. Moreno, M. Chavez, and D. U. Hwang. Complex networks: structure and dynamics. *Physics Reports*, 424:175–308, 2006.

[13] F. Borrelli and T. Keviczky. Distributed lqr design for identical dynamically decoupled systems. *IEEE Transactions on Automatic Control*, 53(8):1901–1912, 2008.

[14] A. Botta, A. Pescapé, and G. Ventre. Quality of service statistics over heterogeneous networks: Analysis and applications. *European Journal of Operational Research*, 191(3):1075 – 1088, 2008.

[15] Y. Cao, W. Ren, and Y. Li. Distributed discrete-time coordinated tracking with a time-varying reference state and limited communication. *Automatica*, 45(5):1299–1305, 2009.

[16] J. Carbaugh, D. N. Godbole, and R. Sengupta. Safety and capacity analysis of automated and manual highway systems. *Transportation Research Part C: Emerging Technologies*, 6(1):69 – 99, 1998.

[17] B. Catino, S. Santini, and M. di Bernardo. MCS adaptive control of vehicle dynamics: an application of bifurcation techniques to control system design. In *Proceedings of the IEEE Conference on Decision and Control (CDC)*, pages 2252 – 2257, 2003.

[18] R. Cepeda-Gomez and N. Olgac. Exact stability analysis of second-order leaderless and leader–follower consensus protocols with rationally-independent multiple time delays. *Systems & Control Letters*, 62(6):482 – 495, 2013.

[19] G. Chen and F. L. Lewis. Leader-following control for multiple inertial agents. *International Journal of Robust and Nonlinear Control*, 21(8):925 – 942, 2011.

[20] L. Chen, J. Lu, and J. Lu. Synchronization of the time-varying discrete biological networks. In *IEEE International Symposium on Circuits and Systems, ISCAS 2007*, pages 2650–2653, 2007.

[21] K. C. Chu. Decentralized control of high-speed vehicular strings. *Transportation Science*, 8(4):361–384, 1974.

[22] E. Coelingh and S. Solyom. All aboard the robotic road train. *IEEE Spectrum*, 49(11):34 – 39, 2012.

[23] D. Corona and B. De Schutter. Adaptive cruise control for a smart car: A comparison benchmark for mpc-pwa control methods. *IEEE Transactions on Control Systems Technology*, 16(2):365 –372, march 2008.

[24] J. Corts, S. Martinez, and F. Bullo. Robust rendezvous for mobile autonomous agents via proximity graphs in arbitrary dimensions. *IEEE Trans. Autom. Control*, 51(8):1289–1298, August 2004.

[25] G. F. Coulouris, J. Dollimore, and T. Kindberg. *Distributed systems: concepts and design.* pearson education, 2005.

[26] S. Darbha. String stability of interconnected systems: An application to platooning in automated highway systems. Technical report, UC Berkeley: California Partners for Advanced Transit and Highways (PATH), 1997.

[27] S. Darbha and J.K. Hedrick. String stability of interconnected systems. *IEEE Transactions on Automatic Control*, 41(3):349 – 357, 1996.

[28] S. Darbha, J.K. Hedrick, C.C. Chien, and P. Ioannou. A comparision of spacing and headway control laws for automatically controlled vehicles. *Vehicle System Dynamics*, 23(1):597–625, 1994.

[29] S. Darbha and K.R. Rajagopal. Intelligent cruise control systems and traffic flow stability. *Transportation Research Part C: Emerging Technologies*, 7(6):329 – 352, 1999.

[30] L. B. de Oliveira and E. Camponogara. Multi-agent model predictive control of signaling split in urban traffic networks. *Transportation Research Part C: Emerging Technologies*, 18(1):120 – 139, 2010.

[31] P. DeLellis, M. di Bernardo, T. E. Gorochowski, and G. Russo. Synchronization and control of complex networks via contraction, adaptation and evolution. *IEEE Circuits and System Magazine*, 3:64–82, 2010.

[32] P. DeLellis, M. di Bernardo, and G. Russo. On quad, lipschitz, and contracting vector fields for consensus and synchronization of networks. *IEEE Transactions on Circuits and Systems I: Regular Papers*, 58(3):576 – 583, 2011.

[33] J.P. Desai, J. Ostrowski, and V. Kumar. Controlling formations of multiple mobile robots. In *in Proceedings of the IEEE International Conference on Robotics and Automation*, volume 4, pages 2864–2869 vol.4, 1998.

[34] C. A. Desoer and M .Vidyasagar. *Feedback systems: input-output properties*, volume 55. SIAM, 2009.

[35] D. V. Dimarogonas and K. J. Kyriakopoulos. On the rendezvous problem for multiple nonholonomic agents. *IEEE Transactions on Automatic Control*, 52(5):916–922, 2007.

[36] T. Dolff, J. Eklöv, R. Hult, and A. Raza. *CoAct 2012 - Technical Manual*, 2013.

[37] F. Dörfler and F. Bullo. Synchronization and transient stability in power networks and non-uniform kuramoto oscillators. In *Proceedings of the 2010 American Control Conference*, 2010.

[38] J. C. Doyle, B. A. Francis, and A. Tannenbaum. *Feedback control theory*. Macmillan, 1992.

[39] S. Eichler. Performance evaluation of the ieee 802.11p WAVE communication standard. In *Proceedings of the IEEE Vehicular Technology Conference (VTC)*, pages 2199 – 2203, 2007.

[40] J. Elson and K. Römer. Wireless sensor networks: A new regime for time synchronization. *ACM SIGCOMM Computer Communication Review*, 33(1):149–154, 2003.

[41] J. A. Fax and R. M. Murray. Information flow and cooperative control of vehicle formations. *IEEE Transactions on Automatic Control*, 49(9):1465–1476, 2004.

[42] M. Frasca, A. Buscarino, A. Rizzo, and L. Fortuna. Spatial pinning control. *Phys. Rev. Lett.*, 108:204102, May 2012.

[43] G. Guo and W. Yue. Autonomous platoon control allowing range-limited sensors. *IEEE Transactions on Vehicular Technology*, 61(7):2901 – 2912, 2012.

[44] J. K. Hale and S. M. Verduyn Lunel. *Introduction to functional differential equations*. Applied mathematical science. Springer-Verlag New York Inc., 1993.

[45] H. Hao and P. Barooah. Stability and robustness of large platoons of vehicles with double-integrator models and nearest neighbor interaction. *International Journal of Robust and Nonlinear Control*, pages 1099 – 1125, 2012.

[46] J. K. Hedrick, M. Tomizuka, and P. Varaiya. Control issues in automated highway systems. *IEEE Control Systems*, 14(6):21–32, 1994.

[47] W. P. M. Heemels, A. R. Teel, N. van de Wouw, and D. Nesic. Networked control systems with communication constraints: Tradeoffs between transmission intervals, delays and performance. *IEEE Transactions on Automatic Control*, 55(8):1781–1796, 2010.

[48] D. Hershkowitz. Recent directions in matrix stability. *Linear Algebra and its Applications*, 171(0):161 – 186, 1992.

[49] J.P. Hespanha, P. Naghshtabrizi, and Y. Xu. A survey of recent results in networked control systems. *Proceedings of the IEEE*, 95(1):138 – 162, 2007.

[50] J. B. Heywood. *Internal combustion engine fundamentals*, volume 930. McGraw-Hill New York, 1988.

[51] D. J. Hill and G. Chen. Power systems as dynamic networks. In *Proceedings of the IEEE International Symposium on Circuits and Systems*, 2006.

[52] R. A. Horn and C. R. Johnson. *Matrix Analisis*. University Press, Cambridge, 1987.

[53] https://www.trimble.com/. *Trimble SPS852 GNSS modular receiver.*

[54] http://www.nmea.org/. *National Marine Electronics Association (NMEA) Standard.*

[55] J. Hu and Y. Hong. Leader-following coordination of multi-agent systems with coupling time delays. *Physica A: Statistical Mechanics and its Applications*, 374(2):853 – 863, 2007.

[56] C. Huang, Y.P. Fallah, R. Sengupta, and H. Krishnan. Adaptive intervehicle communication control for cooperative safety systems. *IEEE Network*, 24(1):6–13, Jan 2010.

[57] A. Jadbabaie, J. Lin, and A. S. Morse. Coordination of groups of mobile autonomous agents using nearest neighbor rules. *IEEE Transactions on Automatic Control*, 48(6):988–1001, 2003.

[58] J. Jasperneite, K. Shehab, and K. Weber. Enhancements to the time synchronization standard ieee-1588 for a system of cascaded bridges. In *IEEE International Workshop on Factory Communication Systems, 2004. Proceedings. 2004*, pages 239–244, Sept 2004.

[59] Q. Jia and W.K.S. Tang. Consensus of nonlinear agents in directed network with switching topology and communication delay. *IEEE Transactions on Circuits and Systems I: Regular Papers*, 59(12):3015–3023, 2012.

[60] Q. Jia, W.K.S. Tang, and W.A. Halang. Leader following of nonlinear agents with switching connective network and coupling delay. *IEEE Transactions on Circuits and Systems I: Regular Papers*, 58(10):2508–2519, 2011.

[61] R. K. Jurgen. Adaptive cruise control. *Training*, 2012:11–19, 2006.

[62] H. K. Khalil. *Nonlinear Systems*. Prentice Hall, 2002.

[63] R. Kianfar, B. Augusto, A. Ebadighajari, U. Hakeem, J. Nilsson, A. Raza, R. S. Tabar, NV Irukulapati, C. Englund, P. Falcone, et al. Design and experimental validation of a cooperative driving system in the grand cooperative driving challenge. *IEEE Transactions on Intelligent Transportation Systems*, 13(3):994–1007, 2012.

[64] H. Kim and X. Ma. Clock synchronization without exchanging timestamps. In *the 45th Annual Conference on Information Sciences and Systems (CISS)*, pages 1 –6, march 2011.

[65] H. Lee and M. Tomizuka. Adaptive vehicle traction force control for intelligent vehicle highway systems (IVHSs). *IEEE Transactions on Industrial Electronics*, 50(1):37 – 47, 2003.

[66] K. Lee, J. C. Eidson, H. Weibel, and D. Mohl. IEEE 1588-standard for a precision clock synchronization protocol for networked measurement and control systems. In *Conference on IEEE*, volume 1588, 2005.

[67] C. Lei, E.M. van Eenennaam, W. Klein Wolterink, G. Karagiannis, G. Heijenk, and J. Ploeg. Impact of packet loss on cacc string stability performance. In *ITS Telecommunications (ITST), 2011 11th International Conference on*, pages 381–386. IEEE, 2011.

[68] T. Li and J. F. Zhang. Mean square average-consensus under measurement noises and fixed topologies: Necessary and sufficient conditions. *Automatica*, 45(8):1929 – 1936, 2009.

[69] T. Li and J. F. Zhang. Consensus conditions of multi-agent systems with time-varying topologies and stochastic communication noises. *IEEE Transactions on Automatic Control*, 55(9):2043–2057, 2010.

[70] K. Lidström, K. Sjöberg, U. Holmberg, J. Andersson, F. Bergh, M. Bjäde, and S. Mak. A modular CACC system integration and design. *IEEE Transactions on Intelligent Transportation Systems*, 13(3):1050 – 1061, 2012.

[71] J. Lin, A. S. Morse, and B. D. Anderson. The multi-agent rendezvous problem. part 1: The synchronous case. *SIAM Journal on Control and Optimization*, 46(6):2096–2119, 2007.

[72] J. Lin, A. S. Morse, and B. D. Anderson. The multi-agent rendezvous problem. part 2: The asynchronous case. *SIAM Journal on Control and Optimization*, 46(6):2120–2147, 2007.

[73] Z. Lin, M. Broucke, and B. Francis. Local control strategies for groups of mobile autonomous agents. *IEEE Transactions on Automatic Control*, 49(4):622–629, 2004.

[74] Z. Lin, B. Francis, and M. Maggiore. Necessary and sufficient graphical conditions for formation control of unicycles. *IEEE Transactions on Automatic Control*, 50(1):121 – 127, 2005.

[75] B. Liu, W. Lu, and T. Chen. Consensus in networks of multiagents with switching topologies modeled as adapted stochastic processes. *SIAM Journal on Control and Optimization*, 49:1:227–253, 2011.

[76] C. Liu and F. Liu. Consensus problem of second-order dynamic agents with heterogeneous input and communication delays. *International Journal of Computers, Communication & Control*, 5(3):325–335, 2010.

[77] C. Liu and F. Liu. Consensus problem of second-order multi-agent systems with time-varying communication delay and switching topology. *Journal of Systems Engineering and Electronics,*, 22(4):672–678, 2011.

[78] X. Liu, A. Goldsmith, S. S. Mahal, and J. K. Hedrick. Effects of communication delay on string stability in vehicle platoons. In *Proceedings on IEEE Intelligent Transportation Systems*, pages 625 –630, 2001.

[79] W. Lu, F. M. Atay, and J. Jost. Synchronization of discrete-time dynamical networks with time-varying couplings. *SIAM Journal on Mathematical Analysis*, 39(4):1231–1259, 2007.

[80] W. Lu, M. A. Fatihcan, and J. Jost. Consensus and synchronization in discrete-time networks of multi-agents with stochastically switching topologies and time delays. *arXiv preprint arXiv:0912.2425*, 2009.

[81] J. Lunze. An internal-model principle for the synchronisation of autonomous agents with individual dynamics. In *Proceedings of the IEEE Conference on Decision and Control and European Control Conference (CDC-ECC)*, pages 2106 – 2111, 2011.

[82] G. Marsden, M. McDonald, and M. Brackstone. Towards an understanding of adaptive cruise control. *Transportation Research Part C: Emerging Technologies*, 9(1):33–51, 2001.

[83] Z. Meng, W. Ren, Y. Cao, and Z. You. Leaderless and leader-following consensus with communication and input delays under a directed network topology. *IEEE Transactions on Systems, Man, and Cybernetics, Part B: Cybernetics*, 41(1):75 – 88, feb. 2011.

[84] N . Michael, D. Mellinger, Q. Lindsey, and V. Kumar. The GRASP multiple micro-UAV testbed. *IEEE Robotics Automation Magazine*, 17(3):56–65, 2010.

[85] R. H. Middleton and J. H. Braslavsky. String instability in classes of linear time invariant formation control with limited communication range. *IEEE Transactions on Automatic Control*, 55(7):1519 – 1530, 2010.

[86] L. Moreau. Stability of multiagent systems with time-dependent communication links. *IEEE Transactions on Automatic Control*, 50(2):169–182, 2005.

[87] U. Münz, A. Papachristodoulou, and F. Allgöwer. Nonlinear multi-agent system consensus with time-varying delays. In *Proc. the 17th IFAC World Congress, Seoul, Korea*, pages 1522–1527, 2008.

[88] T. Murray, M. Cojocari, and H. Fu. Measuring the performance of IEEE 802.11p using NS-2 simulator for vehicular networks. In *Proceedings of the IEEE International Conference on Electro/Information Technology (EIT)*, pages 498 –503, may 2008.

[89] G.J.L. Naus, R.P.A. Vugts, J. Ploeg, M.J.G. van de Molengraft, and M. Steinbuch. String-stable cacc design and experimental validation: A frequency-domain approach. *IEEE Transactions on Vehicular Technology*, 59(9):4268 – 4279, 2010.

[90] M. E. J. Newman. The structure and function of complex networks. *Siam review*, 45(2):167–256, 2003.

[91] M. E. J. Newman, A. L. Barabàsi, and D. J. Watts. *The structure and dynamics of complex networks.* Princeton University Press, 2006.

[92] Mark Newman, Albert-Laszlo Barabasi, and Duncan J Watts. *The structure and dynamics of networks.* Princeton University Press, 2006.

[93] W. Ni and D. Cheng. Leader-following consensus of multi-agent systems under fixed and switching topologies. *Systems & Control Letters*, 59(3):209 – 217, 2010.

[94] A. Noureldin, A. El-Shafie, and M. Bayoumi. Gps/ins integration utilizing dynamic neural networks for vehicular navigation. *Information Fusion*, 12(1):48–57, 2011.

[95] K. Oh, B. Kim, and J. Choi. Novel integrated gps/rkes/pcs antenna for vehicular application. *IEEE Microwave and Wireless Components Letters*, 15(4):244–246, April 2005.

[96] R. Olfati-Saber. Flocking for multi-agent dynamic systems: algorithms and theory. *IEEE Transactions on Automatic Control*, 51(3):401 – 420, 2006.

[97] R. Olfati-Saber, J. A. Fax, and R. M. Murray. Consensus and cooperation in networked multi-agent systems. *Proceedings of the IEEE*, 95(1):215 – 233, 2007.

[98] R. Olfati-Saber and R. Murray. Consensus problems in networks of agents with switching topology and time-delays. *IEEE Transactions on Automatic Control*, 49(9):1521 – 1533, 2004.

[99] Reza Olfati-Saber, J. Alex Fax, and Richard Murray. Consensus and cooperation in networked multi-agent system. In *Proceedings of the IEEE*, volume 95, pages 215–233, January 2007.

[100] S. Oncü, N. van de Wouw, W.P.M. Heemels, and H. Nijmeijer. String stability of interconnected vehicles under communication constraints. In *Proceedings of the IEEE Conference on Decision and Control (CDC)*, pages 2459 – 2464, 2012.

[101] S. Oncü, N. van de Wouw, and H. Nijmeijer. Cooperative adaptive cruise control: Tradeoffs between control and network specifications. In *Proceedings of the IEEE Conference on Intelligent Transportation Systems (ITSC)*, pages 2051 – 2056, 2011.

[102] G. V. Osipov, J. Kurths, and C. Zhou. *Synchronization in Oscillatory Networks.* Springer-Verlag, 2007.

[103] A. Paier, R. Tresch, A. Alonso, D. Smely, P. Meckel, Y. Zhou, and N. Czink. Average downstream performance of measured ieee 802.11p infrastructure-to-vehicle links. In *Proceedings of the IEEE International Conference on Communications Workshops (ICC)*, pages 1 – 5, 2010.

[104] L. Pallottino, V. G. Scordio, A. Bicchi, and E. Frazzoli. Decentralized cooperative policy for conflict resolution in multivehicle systems. *IEEE Transactions on Robotics*, 23(6):1170–1183, 2007.

[105] P. Papadimitratos, A. La Fortelle, K. Evenssen, R. Brignolo, and S. Cosenza. Vehicular communication systems: Enabling technologies, applications, and future outlook on intelligent transportation. *IEEE Communications Magazine*, 47(11):84–95, November 2009.

[106] P. C. Parks and V. Hahn. *Stability theory*. Prentice Hall New York, 1993.

[107] A. Partovi, H. Lin, and J. Zhijian. Structural controllability of high order dynamic multi-agent systems. In *IEEE conference on robotics automation and mechatronics*, pages 327–332, 2010.

[108] L. Peppard. String stability of relative-motion pid vehicle control systems. *IEEE Transactions on Automatic Control*, 19(5):579–581, Oct 1974.

[109] A. Pikovsky, M. Rosenblum, and J. Kurths. *Synchronization: a Universal Concept in Nonlinear Science*. Cambrige University Press, 2001.

[110] J. Ploeg, N. van de Wouw, and H. Nijmeijer. Lp string stability of cascaded systems: Application to vehicle platooning. *IEEE Transactions on Control Systems Technology*, 22(2):786–793, March 2014.

[111] R. Rajamani. *Vehicle dynamics and control*. Springer-Verlag, New York, 2006.

[112] H. Raza and P. Ioannou. Vehicle following control design for automated highway systems. *IEEE Control Systems*, 16(6):43–60, Dec 1996.

[113] A. Réka and A. L. Barabási. Statistical mechanics of complex networks. *Rev. Mod. Phys.*, 74:47–97, Jan 2002.

[114] W. Ren, R. W. Beard, and E. M. Atkins. Information consensus in multivehicle cooperative control. *IEEE Control Systems*, 27(2):71 – 82, 2007.

[115] W. Ren, R. W. Beard, and E.M. Atkins. A survey of consensus problems in multi-agent coordination. *Proc. American Control Conference*, 3:1859–1864, June 2005.

[116] W. Ren, R. W. Beard, and T. W. McLain. Coordination variables and consensus building in multiple vehicle systems. In *Cooperative Control*, pages 171–188. Springer, 2005.

[117] W. Ren and R.W. Beard. Formation feedback control for multiple spacecraft via virtual structures. *IEE Proceedings of Control Theory and Applications*, 151(3):357–368, 2004.

[118] G. Russo and M. di Bernardo. Solving the rendezvous problem for multi-agent systems using contraction theory. In *Proceedings of the IEEE Conference on Decision and Control and Chinese Control Conference (CDC/CCC)*, pages 5821 – 5826, 2009.

[119] G. Russo, M. di Bernardo, and JE Slotine. A graphical approach to prove contraction of nonlinear circuits and systems. *IEEE Transactions on Circuits and Systems I: Regular Papers*, 58(2):336 – 348, 2011.

[120] G. Russo, M. di Bernardo, and E.D. Sontag. A contraction approach to the hierarchical analysis and design of networked systems. *IEEE Transactions on Automatic Control*, 58(5):1328 – 1331, 2013.

[121] J. Ryu and J. C. Gerdes. Integrating inertial sensors with gps for vehicle dynamics control. *Journal of Dynamic Systems, Measurement, and Control*, 126(2):243 – 254, 2004.

[122] K. Santhanakrishnan and R. Rajamani. On spacing policies for highway vehicle automation. *IEEE Transactions on Intelligent Transportation Systems*, 4(4):198–204, Dec 2003.

[123] R. L. Scheiterer, C. Na, D. Obradovic, and G. Steindl. Synchronization performance of the precision time protocol in industrial automation networks. *IEEE Transactions on Instrumentation and Measurement*, 58(6):1849–1857, 2009.

[124] M. Segata, F. Dressler, R. Lo Cigno, and M. Gerla. A simulation tool for automated platooning in mixed highway scenarios. *ACM SIGMOBILE Mobile Computing and Communications Review*, 16(4):46–49, 2013.

[125] P. Seiler, A. Pant, and J. K. Hedrick. Disturbance propagation in vehicle strings. *IEEE Transactions on Automatic Control*, 49(10):1835 – 1842, 2004.

[126] E. Shaw and J.K. Hedrick. String stability analysis for heterogeneous vehicle strings. In *American Control Conference, 2007. ACC '07*, pages 3118–3125, July 2007.

[127] S. E. Shladover. Path at 20-history and major milestones. *IEEE Transactions on intelligent transportation systems*, 8(4):584–592, 2007.

[128] S. E. Shladover, C. A. Desoer, J. K. Hedrick, M. Tomizuka, J. Walrand, W. Zhang, D. H. McMahon, H. Peng, S. Sheikholeslam, and N. McKeown. Automated vehicle control developments in the path program. *IEEE Transactions on Vehicular Technology*, 40(1):114–130, 1991.

[129] M.L. Sichitiu and M. Kihl. Inter-vehicle communication systems: a survey. *IEEE Communications Surveys Tutorials*, 10(2):88 – 105, 2008.

[130] G. Silberg, R. Wallace, G. Matuszak, J. Plessers, C. Brower, and D. Subramanian. Self-driving cars: The next revolution. *KPMG and Center for Automotive Research*, pages 10–15, 2012.

[131] C. Sommer, S. Joerer, M. Segata, O. Tonguz, R. Lo Cigno, and F. Dressler. How shadowing hurts vehicular communications and how dynamic beaconing can help. In *Proceedings IEEE INFOCOM*, pages 110–114. IEEE, 2013.

[132] P. Sommer and R. Wattenhofer. Gradient clock synchronization in wireless sensor networks. In *Information Processing in Sensor Networks, 2009. IPSN 2009. International Conference on*, pages 37 –48, april 2009.

[133] B. E. Stilwell, D. J. Bishop. Platoons of underwater vehicles. *IEEE Control Systems Magazine*, 20(6):45–52, 2000.

[134] S. H. Strogatz. Exploring complex networks. *Nature*, 410:268–276, March 2001.

[135] K. R. Stromberg. *An introduction to classical real analysis*. Wadsworth International, Belmont, 1981.

[136] D. Sun, C. Wang, W. Shang, and G. Feng. A synchronization approach to trajectory tracking of multiple mobile robots while maintaining time-varying formations. *IEEE Transactions on Robotics*, 25(5):1074–1086, 2009.

[137] Y. G. Sun and L. Wang. Consensus of multi-agent systems in directed networks with nonuniform time-varying delays. *IEEE Transactions on Automatic Control*, 54(7):1607 – 1613, 2009.

[138] B. Sundararaman, U. Buy, and A. D. Kshemkalyani. Clock synchronization for wireless sensor networks: a survey. *Ad Hoc Networks*, 3(3):281 – 323, 2005.

[139] R. Szalai and G. Orosz. Decomposing the dynamics of heterogeneous delayed networks with applications to connected vehicle systems. *Physical Review E*, 88(4):040902, 2013.

[140] H. G. Tanner, A. Jadbabaie, and G. J. Pappas. Stable flocking of mobile agents, part I. In *IEEE Conference of Decision and Control*, 2003.

[141] H. G. Tanner, A. Jadbabaie, and G. J. Pappas. Stable flocking of mobile agents, part II. In *IEEE Conference of Decision and Control*, 2003.

[142] H. G. Tanner, A. Jadbabaie, and G. J. Pappas. Flocking in fixed and switching networks. APRIL 2005.

[143] H.G. Tanner, G.J. Pappas, and V. Kumar. Leader-to-formation stability. *IEEE Transactions on Robotics and Automation*, 20(3):443–455, 2004.

[144] S. Tsugawa, S. Kato, and K. Aoki. An automated truck platoon for energy saving. In *IEEE/RSJ International Conference on Intelligent Robots and Systems (IROS), 2011*, pages 4109–4114, Sept 2011.

[145] M. Turpin, N. Michael, and V. Kumar. Trajectory design and control for aggressive formation flight with quadrotors. *Autonomous Robots*, 33(1-2):143–156, 2012.

[146] E. van Nunen, R. J. A. E. Kwakkernaat, J. Ploeg, and B. D. Netten. Cooperative competition for future mobility. *Intelligent Transportation Systems, IEEE Transactions on*, 13(3):1018–1025, 2012.

[147] L. Wang, G. Yin, H. Zhang, L. Xu, A. Syed, G. Yin, A. Pandya, and H. Zhang. Control of vehicle platoons for highway safety and efficient utility: Consensus with communications and vehicle dynamics. *to appear in Journal of Systems Science and Complexity.*

[148] L. Y. Wang, A. Syed, G. Yin, A. Pandya, and H. Zhang. Coordinated vehicle platoon control: Weighted and constrained consensus and communication network topologies. In *Proceedings of IEEE Conference on Decision and Control (CDC)*, pages 4057–4062, December 2012.

[149] Y. Wang, A. Ahmed, B. Krishnamachari, and K. Psounis. IEEE 802.11p performance evaluation and protocol enhancement. In *IEEE International Conference on Vehicular Electronics and Safety, ICVES*, pages 317–322, 2008.

[150] R. Wei and R. W. Beard. *Distributed Consensus in Multi-vehicle Cooperative Control: Theory and Applications*. Springer-Verlag, 2008.

[151] E. Xargay, V. Dobrokhodov, I. Kaminer, A.M. Pascoal, N. Hovakimyan, and Chengyu Cao. Time-critical cooperative control of multiple autonomous vehicles: Robust distributed strategies for path-following control and time-coordination over dynamic communications networks. *IEEE Control Systems*, 32(5):49–73, 2012.

[152] L. Xiao and F. Gao. Practical string stability of platoon of adaptive cruise control vehicles. *IEEE Transactions on Intelligent Transportation Systems*, 12(4):1184 – 1194, 2011.

[153] G. Xie and L. Wang. Consensus control for a class of networks of dynamic agents. *International Journal of Robust and Nonlinear Control*, 17(10-11):941–959, 2007.

[154] L. Xu, L. Wang, G. Yin, and H. Zhang. Coordinated control and communication for enhanced safety of highway vehicle platoons. *in Proceedings of the IEEE International Conference on Connected Vehicles and Expo (ICVVE)*, 2013.

[155] W. Yang, A. L. Bertozzi, and X. Wang. Stability of a second order consensus algorithm with time delay. In *47th IEEE Conference on Decision and Control, CDC*, pages 2926–2931, 2008.

[156] S. Yousefi, E. Altman, R. El-Azouzi, and M. Fathy. Analytical model for connectivity in vehicular ad hoc networks. *IEEE Transactions on Vehicular Technology*, 57(6):3341 – 3356, 2008.

[157] W. Yu, G. Chen, and M. Cao. Distributed leader follower flocking control for multi-agent dynamical systems with time-varying velocities. *Systems & Control Letters*, 59(9):543 – 552, 2010.

[158] W. Yu, G. Chen, and M. Cao. Some necessary and sufficient conditions for second-order consensus in multi-agent dynamical systems. *Automatica*, 46(6):1089–1095, 2010.

[159] W. Yu, P. DeLellis, G. Chen, M. di Bernardo, and J. Kurths. Distributed adaptive control of synchronization in complex networks. *IEEE Transactions on Automatic Control*, 57(8):2153–2158, 2012.

[160] W. Zhu and D. Cheng. Leader-following consensus of second-order agents with multiple time-varying delays. *Automatica*, 46(12):1994 – 1999, 2010.

Appendix A

Auxiliary results for Chapter 4

A.1 Discussion on the spacing policy

Consider the parameters relative to any couple of vehicles in the platoon according to the schematic in Fig 4.1. The distance between the two adjacent vehicles, the i-th vehicle and its preceding, at standstill can be expressed easily expressed in terms of both the vehicle lengths and the safety distance required as [122]:

$$d_{ii-1}^{st} = l_{vi}/2 + l_{vi-1}/2 + d_{ii-1}^{safe} \tag{A.1}$$

where d_{ii-1}^{safe} is the safety distance (i.e. the minimum distance to be guaranteed between two adjacent vehicles) from vehicle $i-1$ to vehicle i and l_{vi}, l_{vi-1} are the vehicles lengths (we assume the vehicle reference is located half the length of each vehicle; note that different choices can be also made as for example in [122] where the vehicle reference is located on the front of each vehicle).

Generalizing expression (A.1), the distance at standstill between the i-th vehicle and anyone of its proceeding vehicles (not necessarily the adjacent) along the string ($i > j$), is:

$$d_{ij}^{st} = \sum_{p=j+1}^{i} d_{pp-1}^{st}. \tag{A.2}$$

Analogously, the distance between a vehicle i and one of its followers j (not necessarily the adjacent) at standstill ($j > i$) can be expressed as:

$$d_{ji}^{st} = \sum_{p=i+1}^{j} d_{pp-1}^{st}. \tag{A.3}$$

Note that exploiting the above expressions the distance between vehicles i and j can be recast in terms of standstill distances with respect to the leading vehicle as $\hat{d}_{ij}^{st} = \hat{d}_{i0}^{st} - \hat{d}_{j0}^{st}$. Moreover, we underline that $d_{ij}^{st} = -d_{ji}^{st}$. Furthermore, according to [29] in this paper we assume that desired following distance is linearly proportional to the leader velocity, $d_{ij} = h_{ij}v_0 + d_{ij}^{st}$, and that the constant headway time of vehicle i with respect to vehicle j can be computed from the headway time with respect to the leading vehicle as $h_{ij} = h_{i0} - h_{j0}$ (for example, with vehicles moving at the same constant velocity).

A.2 Algebraic manipulation on the distributed protocol

We start writing (4.6) as:

$$\begin{aligned} u_i\left(t\right) = \quad & -b\bar{v}_i - \tfrac{1}{d_i}\sum_{j=1}^{N} k_{ij}a_{ij}\left[r_i\left(t\right) - r_j\left(t-\tau_{ij}\left(t\right)\right) - \tau_{ij}\left(t\right)v_0 - h_{ij}v_0 - d_{ij}^{st}\right] \\ & -\tfrac{1}{d_i}k_{i0}a_{i0}\left[r_i\left(t\right) - r_0\left(t-\tau_{i0}\left(t\right)\right) - \tau_{i0}\left(t\right)v_0 - h_{i0}v_0 - d_{i0}^{st}\right] \end{aligned} \tag{A.4}$$

Manipulating (A.4) yelds:

$$\begin{aligned} u_i\left(t\right) = \quad & -b\bar{v}_i - \tfrac{1}{d_i}\sum_{j=1}^{N} k_{ij}a_{ij}\left[r_i\left(t\right) - r_0\left(t\right) - h_{i0}v_0 - d_{i0}^{st}\right] \\ & -\tfrac{1}{d_i}\sum_{j=1}^{N} k_{ij}a_{ij}\left[-r_j\left(t-\tau_{ij}\left(t\right)\right) + r_0\left(t-\tau_{ij}\left(t\right)\right) + h_{j0}v_0 + d_{0j}^{st}\right] \\ & -\tfrac{1}{d_i}k_{i0}a_{i0}\left[r_i\left(t\right) - r_0\left(t-\tau_{i0}\left(t\right)\right) - \tau_{i0}\left(t\right)v_0 - h_{i0}v_0 - d_{i0}^{st}\right] \\ & -\tfrac{1}{d_i}\sum_{j=1}^{N} k_{ij}a_{ij}\left[r_0\left(t\right) - r_0\left(t-\tau_{ij}\left(t\right)\right) - \tau_{ij}\left(t\right)v_0\right] \end{aligned} \tag{A.5}$$

being $h_{ij} = h_{i0} - h_{j0}$ and $d_{ij}^{st} = d_{i0}^{st} - d_{j0}^{st}$.
Now expression (A.5) can be recast as:

$$\begin{aligned} u_i\left(t\right) = \quad & -b\bar{v}_i - \tfrac{1}{d_i}\sum_{j=1}^{N} k_{ij}a_{ij}\left[\bar{r}_i\left(t\right) - \bar{r}_j\left(t-\tau_{ij}\left(t\right)\right)\right] \\ & -\tfrac{1}{d_i}k_{i0}a_{i0}\left[r_i\left(t\right) - r_0\left(t-\tau_{i0}\left(t\right)\right) - \tau_{i0}\left(t\right)v_0 - h_{i0}v_0 - d_{i0}^{st}\right] \\ & -\tfrac{1}{d_i}\sum_{j=1}^{N} k_{ij}a_{ij}\left[r_0\left(t\right) - r_0\left(t\right)\right] \end{aligned} \tag{A.6}$$

being $r_0(t) = r_0\left(t-\tau_{ij}\left(t\right)\right) + \tau_{ij}(t)v_0$. It follows that:

$$\begin{aligned} u_i\left(t\right) = \quad & -b\bar{v}_i - \tfrac{1}{d_i}\sum_{j=1}^{N} k_{ij}a_{ij}\left[\bar{r}_i\left(t\right) - \bar{r}_j\left(t-\tau_{ij}\left(t\right)\right)\right] \\ & -\tfrac{1}{d_i}k_{i0}a_{i0}\left[r_i\left(t\right) - r_0\left(t\right) - h_{i0}v_0 - d_{i0}^{st}\right] \end{aligned} \tag{A.7}$$

being $r_0(t) = r_0\left(t-\tau_{i0}\left(t\right)\right) + \tau_{i0}(t)v_0$. In so doing, expression (4.8) can be obtained.

Appendix B

Auxiliary results for Chapter 5

B.1 String Stability analysis

B.1.1 Spacing error dynamics on follower nr.1

Considering formula (5.4) in (5.3), we have that:

$$X_1 + bHX_1s = k_{10}HE_1 + bHX_0s + \frac{x_1(0)}{s} \tag{B.1}$$

$$(1 + bHs)X_1 = k_{10}HE_1 + bHX_0s + \frac{x_1(0)}{s} \tag{B.2}$$

in order to have:

$$X_1 = k_{10}\bar{H}E_1 + b\bar{H}X_0s + \frac{1}{1 + bHs}\frac{x_1(0)}{s} \tag{B.3}$$

with:

$$\bar{H} = \frac{H}{1 + bHs} \tag{B.4}$$

According to (5.5), equation (B.3) becomes:

$$\frac{d_{10}}{s} + \left(e^{-\tau s} + \tau s + h_{10}s\right) X_0 - E_1 = k_{10}\bar{H}E_1 + b\bar{H}X_0s + \frac{1}{1 + bHs}\frac{x_1(0)}{s} \tag{B.5}$$

$$\frac{d_{10}}{s} + \left(e^{-\tau s} + \tau s + h_{10}s\right) X_0 - b\bar{H}X_0s = \left(k_{10}\bar{H} + 1\right) E_1 + \frac{1}{1 + bHs}\frac{x_1(0)}{s} \tag{B.6}$$

$$E_1 = \frac{e^{-\tau s}}{1 + k_{10}\bar{H}}X_0 + \frac{\tau + h_{10} - b\bar{H}}{1 + k_{10}\bar{H}}X_0s + \frac{1}{1 + k_{10}\bar{H}}\left(\frac{d_{10}}{s} - \frac{1}{1 + bHs}\frac{x_1(0)}{s}\right). \tag{B.7}$$

Moreover, we analyze string stability when the platoon achieves consensus: this let us to assume $x_1(0) = d_{10}$.
In so doing, we have:

$$E_1(s) = W_1(s)X_0(s) + S_1(s)\frac{d_{10}}{s} \tag{B.8}$$

with:

$$W_1\left(s\right) = \frac{e^{-\tau s} + \tau s + h_{10}s - b\bar{H}s}{k_{10}\bar{H} + 1} \tag{B.9}$$

$$S_1(s) = \frac{1}{1 + k_{10}\bar{H}}\left(1 - \frac{1}{1 + bHs}\right) \tag{B.10}$$

B.1.2 Spacing error dynamics on follower nr.2

Considering equation (5.13), with $i = 2$ and a leader-predecessor topology, we have that:

$$\begin{aligned} X_2 \quad &= \quad \tfrac{k_{20}H}{d_2}\left(X_0 e^{-\tau s} - X_2 + \tau X_0 s + h_{20}X_0 s + \tfrac{d_{20}}{s}\right) \\ &\quad + \tfrac{k_{21}H}{d_2}E_2 + bH(X_0 - X_2)s + \tfrac{x_2(0)}{s} \end{aligned} \tag{B.11}$$

Assuming consensus as initial condition, we consider $h_{20} = h_{10} + h_{21}$; moreover, with $d_{20} = d_{10} + d_{21}$, we obtain:

$$\begin{aligned} X_2 \quad &= \quad \tfrac{k_{20}H}{d_2}\left(X_0 e^{-\tau s} - X_2 + \tau X_0 s + h_{21}X_0 s + h_{10}X_0 s + \tfrac{d_{21}}{s} + \tfrac{d_{10}}{s} + \right) \\ &\quad + \tfrac{k_{21}H}{d_2}E_2 + bH(X_0 - X_2)s + \tfrac{x_2(0)}{s} + \tfrac{k_{20}H}{d_2}(-X_1 + X_1) \end{aligned} \tag{B.12}$$

$$X_2 \quad = \quad \tfrac{k_{20}H}{d_2}\left(E_1 - X_2 + X_1 + h_{21}X_0 s + \tfrac{d_{21}}{s}\right) + \tfrac{k_{21}H}{d_2}E_2 \tag{B.13}$$

$$\begin{aligned} X_2 + \tfrac{k_{20}H}{d_2}X_2 + bHX_2 s \quad &= \quad \tfrac{k_{20}H}{d_2}\left(E_1 + X_1 + h_{21}X_0 s + \tfrac{d_{21}}{s}\right) \\ &\quad + \tfrac{k_{21}H}{d_2}E_2 + bHX_0 s + \tfrac{x_2(0)}{s} \end{aligned} \tag{B.14}$$

Then

$$\left(B_2\right)X_2 = \frac{k_{21}H}{d_2}E_2 + \frac{k_{20}H}{d_2}\left(E_1 + X_1 + h_{21}X_0 s + \frac{d_{21}}{s}\right) + bHX_0 s + \frac{x_2(0)}{s} \tag{B.15}$$

with:

$$B_2 = 1 + \frac{k_{20}H}{d_2} + bHs \tag{B.16}$$

We obtain that:

$$X_2 = D_2E_2 + C_2\left(E_1 + X_1 + h_{21}X_0 s + \frac{d_{21}}{s}\right) + \frac{bH}{B_2}X_0 s + \frac{1}{B_2}\frac{x_2(0)}{s} \tag{B.17}$$

with

$$C_2 = \frac{k_{20}H}{d_2B_2} \tag{B.18}$$

$$D_2 = \frac{k_{21}H}{d_2B_2} \tag{B.19}$$

$$X_2 = D_2E_2 + C_2E_1 + C_2X_1 + C_2h_{21}X_0 s + \frac{bH}{B_2}X_0 s + C_2\frac{d_{21}}{s} + \frac{1}{B_2}\frac{x_2(0)}{s} \tag{B.20}$$

$$\begin{aligned} X_2 - X_1 e^{-\tau s} + X_1 e^{-\tau s} &= D_2 E_2 + C_2 E_1 + C_2 X_1 + C_2 h_{21} X_0 s \\ &\quad + \tfrac{bH}{B_2} X_0 s + C_2 \tfrac{d_{21}}{s} + \tfrac{1}{B_2} \tfrac{x_2(0)}{s} \end{aligned} \tag{B.21}$$

$$\begin{aligned} X_2 - X_1 e^{-\tau s} &= D_2 E_2 + C_2 E_1 + \left(C_2 - e^{-\tau s}\right) X_1 + C_2 h_{21} X_0 s \\ &\quad + \tfrac{bH}{B_2} X_0 s + C_2 \tfrac{d_{21}}{s} + \tfrac{1}{B_2} \tfrac{x_2(0)}{s} \end{aligned} \tag{B.22}$$

According to (5.7), equation (B.22) becomes:

$$\begin{aligned} \tfrac{d_{21}}{s} - E_2 + \tau X_0 s + h_{21} X_0 s &= C_2 E_1 + \left(C_2 - e^{-\tau s}\right) X_1 + C_2 h_{21} X_0 s \\ &\quad + D_2 E_2 + \tfrac{bH}{B_2} X_0 s + C_2 \tfrac{d_{21}}{s} + \tfrac{1}{B_2} \tfrac{x_2(0)}{s} \end{aligned} \tag{B.23}$$

$$\begin{aligned} \left(-1 - D_2\right) E_2 &= C_2 E_1 + \left(-\tau - h_{21} + C_2 h_{21} + \tfrac{bH}{B_2}\right) X_0 s \\ &\quad + \left(C_2 - e^{-\tau s}\right) X_1 - \tfrac{d_{21}}{s} + C_2 \tfrac{d_{21}}{s} + \tfrac{1}{B_2} \tfrac{x_2(0)}{s} \end{aligned} \tag{B.24}$$

We define:

$$F_2 = -\tau - h_{21} + C_2 h_{21} + \frac{bH}{B_2} \tag{B.25}$$

such that (B.24) becomes:

$$\left(-1 - D_2\right) E_2 = C_2 E_1 + F_2 X_0 s + \left(C_2 - e^{-\tau s}\right) X_1 - \frac{d_{21}}{s} + C_2 \frac{d_{21}}{s} + \frac{1}{B_2} \frac{x_2(0)}{s} \tag{B.26}$$

We substitute X_1 in (B.26) according to (B.3); we have that (B.26) becomes

$$\begin{aligned} \left(-1 - D_2\right) E_2 &= \left(C_2 - e^{-\tau s}\right) \left(k_{10} \bar{H} E_1 + b\bar{H} X_0 s + \tfrac{1}{1+bHs} \tfrac{x_1(0)}{s}\right) \\ &\quad + C_2 E_1 + F_2 X_0 s - \tfrac{d_{21}}{s} + C_2 \tfrac{d_{21}}{s} + \tfrac{1}{B_2} \tfrac{x_2(0)}{s} \end{aligned} \tag{B.27}$$

$$\begin{aligned} \left(-1 - D_2\right) E_2 &= \left[C_2 + \left(C_2 - e^{-\tau s}\right) k_{10} \bar{H}\right] E_1 + \left[F_2 + \left(C_2 - e^{-\tau s}\right) b\bar{H}\right] X_0 s \\ &\quad + \tfrac{\left(C_2 - e^{-\tau s}\right)}{1+bHs} \tfrac{x_1(0)}{s} - \tfrac{d_{21}}{s} + C_2 \tfrac{d_{21}}{s} + \tfrac{1}{B_2} \tfrac{x_2(0)}{s} \end{aligned} \tag{B.28}$$

and considering $X_0(s)$ according to (B.8)

$$\begin{aligned} \left(-1 - D_2\right) E_2 &= \left[C_2 + \left(C_2 - e^{-\tau s}\right) k_{10} \bar{H}\right] E_1 \\ &\quad + \left[F_2 + \left(C_2 - e^{-\tau s}\right) b\bar{H}\right] W^{-1} E_1 s \\ &\quad - \left[F_2 + \left(C_2 - e^{-\tau s}\right) b\bar{H}\right] W^{-1} S_1 \tfrac{d_{10}}{s} s \\ &\quad + \tfrac{\left(C_2 - e^{-\tau s}\right)}{1+bHs} \tfrac{x_1(0)}{s} - \tfrac{d_{21}}{s} + C_2 \tfrac{d_{21}}{s} + \tfrac{1}{B_2} \tfrac{x_2(0)}{s} \end{aligned} \tag{B.29}$$

$$\begin{aligned}
E_2 \quad = \quad & \tfrac{1}{(-1-D_2)}\left[C_2+\left(C_2-e^{-\tau s}\right)k_{10}\bar{H}\right]E_1 \\
& +\tfrac{1}{(-1-D_2)}\left[W^{-1}F_2 s+W^{-1}\left(C_2-e^{-\tau s}\right)b\bar{H}s\right]E_1 \\
& +\tfrac{1}{(-1-D_2)}\left[\tfrac{\left(C_2-e^{-\tau s}\right)}{1+bHs}\tfrac{x_1(0)}{s}-\tfrac{d_{21}}{s}+C_2\tfrac{d_{21}}{s}\right] \\
& +\tfrac{1}{(-1-D_2)}\left[\tfrac{1}{B_2}\tfrac{x_2(0)}{s}-\left(W^{-1}F_2 s+W^{-1}\left(C_2-e^{-\tau s}\right)b\bar{H}s\right)S_1\tfrac{d_{10}}{s}\right]
\end{aligned} \tag{B.30}$$

So, we have that:

$$E_2\left(s\right)=T_2\left(s\right)E_1\left(s\right)+S_2\left(s\right)\frac{d_{21}}{s} \tag{B.31}$$

with:

$$\begin{aligned}
T_2\left(s\right) \quad = \quad & \tfrac{1}{(-1-D_2)}\left[C_2+\left(C_2-e^{-\tau s}\right)k_{1,0}\bar{H}\right] \\
& +\tfrac{1}{(-1-D_2)}\left[W_1^{-1}F_2 s+W_1^{-1}\left(C_2-e^{-\tau s}\right)b\bar{H}s\right]
\end{aligned} \tag{B.32}$$

$$\begin{aligned}
S_2\left(s\right) \quad = \quad & \tfrac{1}{(-1-D_2)}\left[\tfrac{\left(C_2-e^{-\tau s}\right)}{1+bHs}-1+C_2+\tfrac{2}{B_2}\right] \\
& +\tfrac{1}{(-1-D_2)}\left[-W^{-1}\left(F_2 s+\left(C_2-e^{-\tau s}\right)b\bar{H}s\right)S_1\right]
\end{aligned} \tag{B.33}$$

with $x_1(0)=d_{10}$, $x_2(0)=d_{20}=2d_{21}=2d_{10}$.

Remark B.1.1. Note that expression (B.31) can be generalized to the case of a platoon of N vehicles (i.e. $i=2,...,N$).

B.1.3 Numerical results on string stability

In what follows some numerical results aimed to show string stability are reported.

Specifically, $T_2(s)$ and $S_2(s)$ are depicted in Fig. B.1 , for increasing values of parameter k, when $\tau = 0$ and $b = 1800$. Note that b is selected as in Section 5.1. We underline that $T_2(s)$ in Fig. B.1 satisfies the string stability definition (see Subsection 2.2.1), such to attenuate the position error upstream the platoon. Moreover, Fig. B.2 describes $T_2(s)$ and $S_2(s)$ for increasing values of b, when $\tau = 0$ and $k = 800$. Finally, in Fig. B.3 we display both $T_2(s)$ and $S_2(s)$, with $k = 800$, $b = 1800$ and increasing the value of τ. Note that the string stability condition is affected by the maximum value of τ. According to results in Fig. B.3, for values of $\tau > 60$ [ms] string stability cannot be guaranteed numerically in the presence of disturbances limited to a specific range of frequencies. However, we underline that, in practice, the spacing errors have most of their energy at low frequencies (i.e. lower than 1]Hz]) and hence it may be sufficient to require $|T_i(j\omega)| < 1$ at these frequencies [125].

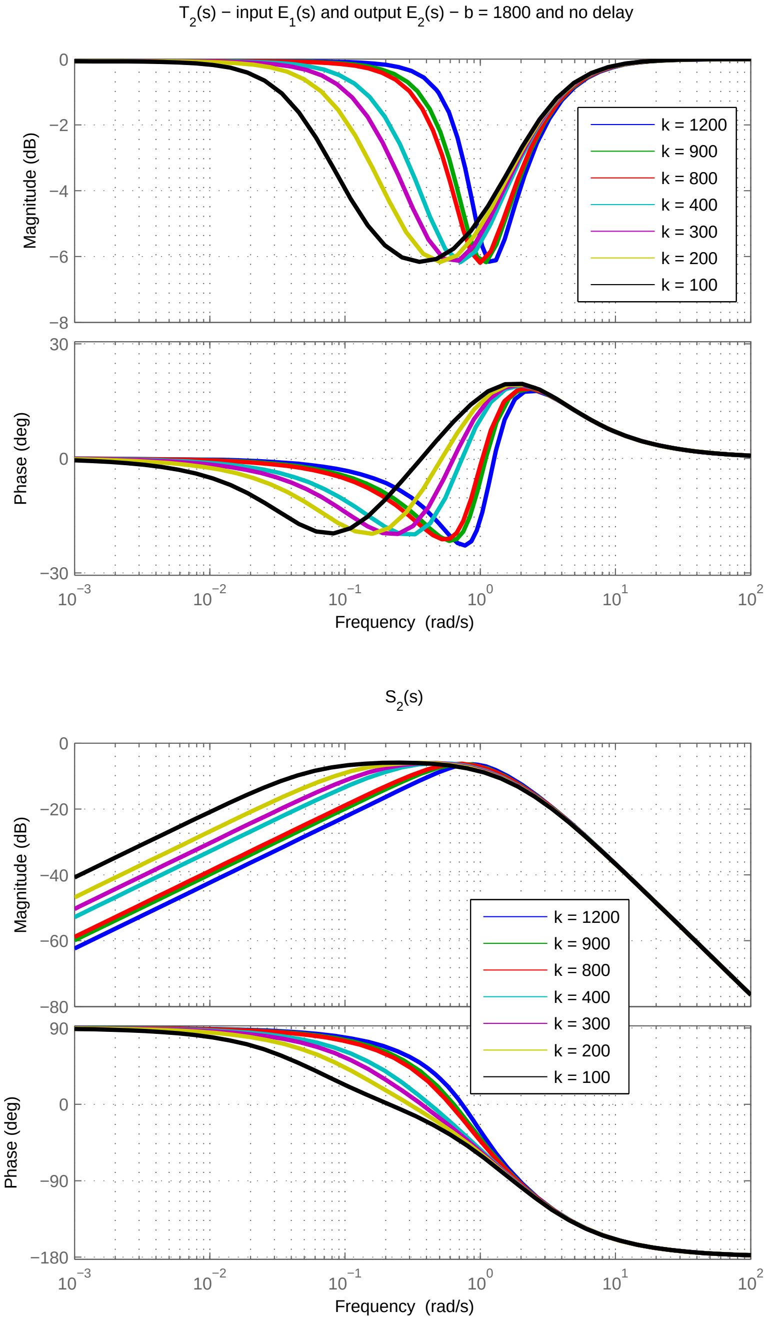

Figure B.1: Bode diagram for $T_2(s)$ and $S_2(s)$ in (B.32) and (B.33), respectively; $\tau = 0$ and $b = 1800$ for increasing values of parameter k.

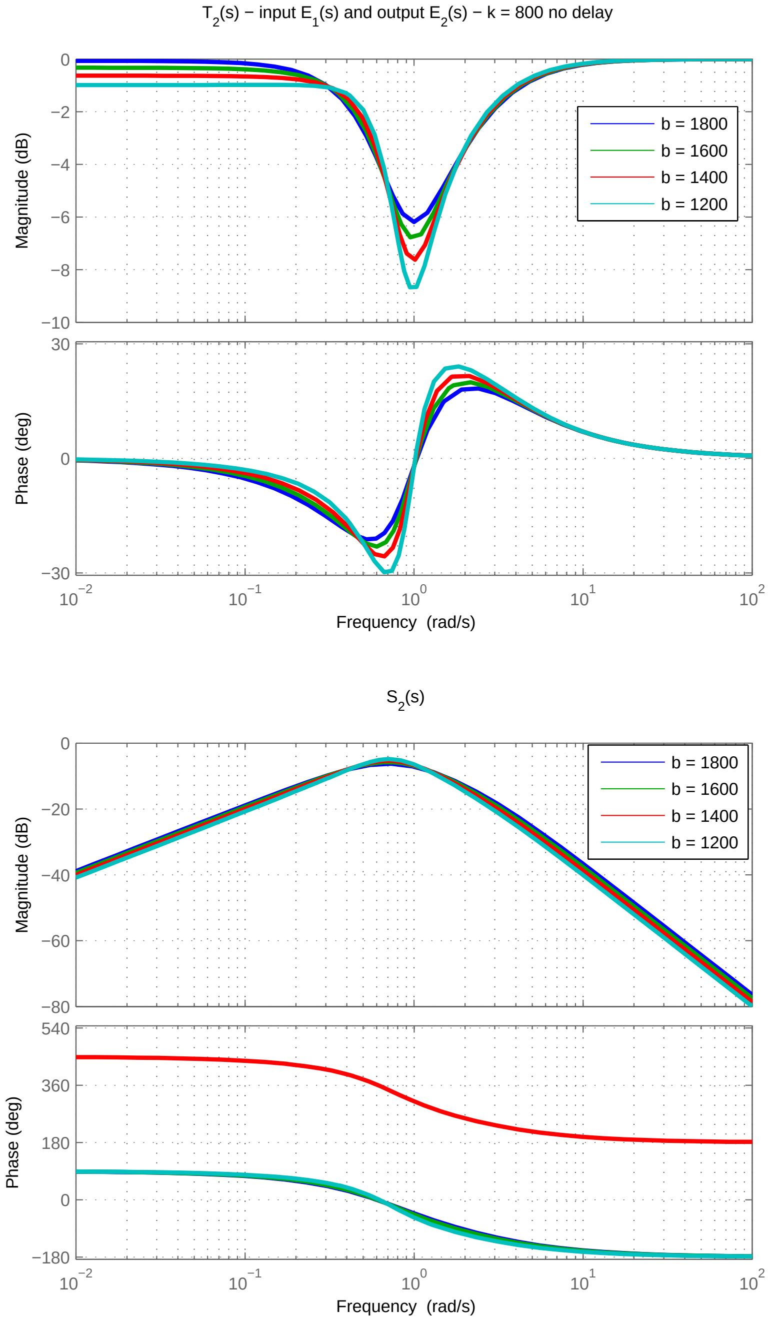

Figure B.2: Bode diagram for $T_2(s)$ and $S_2(s)$ in (B.32) and (B.33), respectively; $\tau = 0$ and $k = 800$ for increasing values of parameter b.

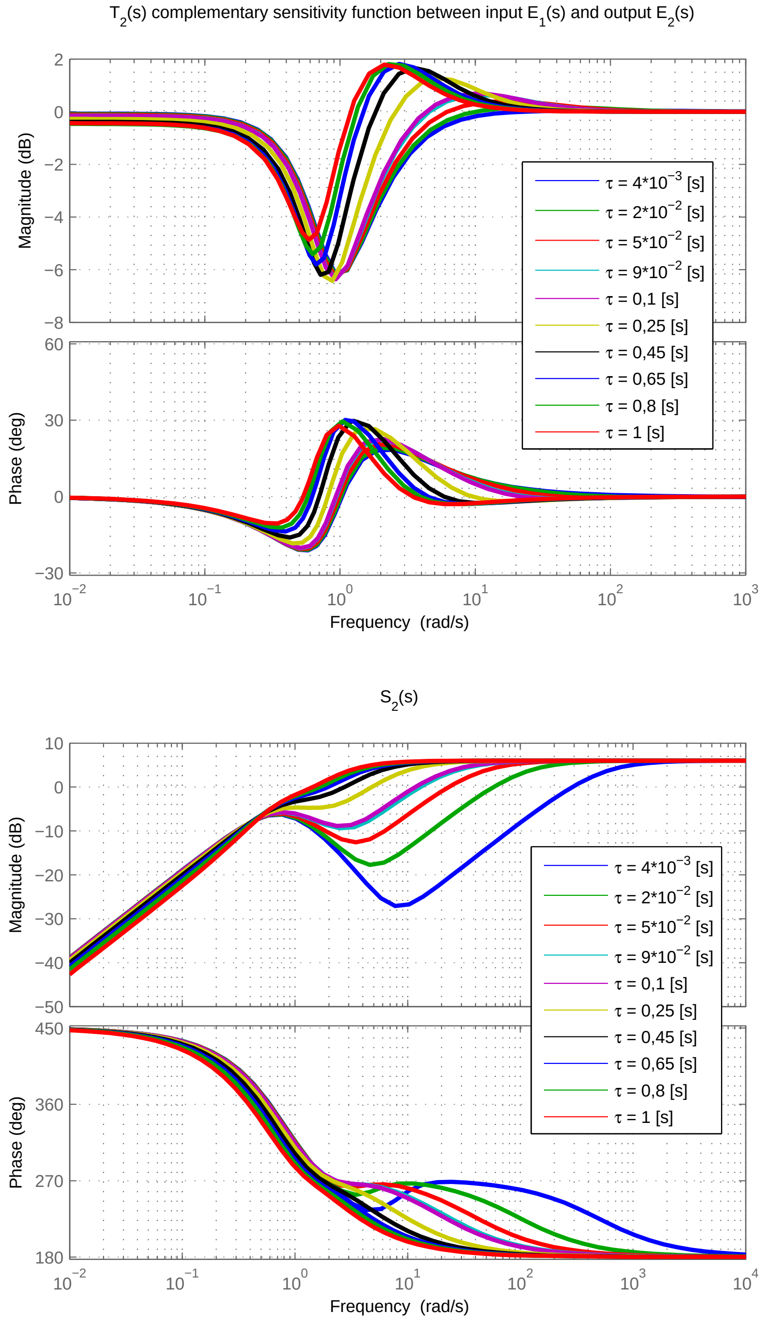

Figure B.3: Bode diagram for $T_2(s)$ and $S_2(s)$ in (B.32) and (B.33), respectively; $b = 1800$ and $k = 800$ for increasing values of parameter τ.

B.1.4 Error propagation

Under the assumption of neglecting the communication delay (i.e. $\tau = 0$) and considering a classical proportional controller on the position error (i.e. $b = 0$), our analysis on string stability is similar to that described in [125] and [126]; indeed, we have that expression (5.10) becomes:

$$W_1(s) = \frac{1}{1 + k_{10}H} \tag{B.34}$$

and (5.11) is:

$$S_1(s) = 0 \tag{B.35}$$

Moreover, (5.15) is:

$$T_2(s) = \frac{1}{(-1 - D_2)}\left[C_2 + (C_2 - 1)\, k_{10}H\right] \tag{B.36}$$

where B_2,C_2 and D_2 are defined in (B.16), (B.18) and (B.19), respectively. In particular we rewrite:

$$\begin{aligned}
T_2(s) &= \frac{1}{-1-\frac{Hk_{21}}{2+Hk_{20}}}\left[\frac{Hk_{20}}{2+Hk_{20}} + \frac{H^2k_{20}k_{10}}{2+Hk_{20}} - Hk_{10}\right] \\
&= -\frac{2+Hk_{20}}{2+Hk_{20}+Hk_{21}}\left[\frac{Hk_{20}+H^2k_{20}k_{10}-2Hk_{10}-H^2k_{20}k_{10}}{2+Hk_{20}}\right] \\
&= -\frac{Hk_{20}-2Hk_{10}}{2+Hk_{20}+Hk_{21}} \\
&= -\frac{-Hk}{2+2Hk}
\end{aligned} \tag{B.37}$$

such that (B.36) becomes:

$$T_2(s) = \frac{k}{2} \cdot \frac{H}{1 + Hk} \tag{B.38}$$

with the assumption of $k_{10} = k_{20} = k$. Finally, (5.16) is:

$$S_2(s) = \frac{1}{(-1 - D_2)}\left[C_2 - 1 - 1 + C_2 + \frac{2}{B_2}\right] \tag{B.39}$$

such to have

$$\begin{aligned}
S_2(s) &= -\frac{2+Hk_{20}}{2+Hk_{20}+Hk_{21}}\left[\frac{Hk_{20}}{2+Hk_{20}} - 1 - 1 + \frac{Hk_{20}}{2+Hk_{20}} + \frac{2}{1+\frac{Hk_{20}}{2}}\right] \\
&= -\frac{2+Hk_{20}}{2+Hk_{20}+Hk_{21}}\left[\frac{Hk_{20}}{2+Hk_{20}} - 1 - 1 + \frac{Hk_{20}}{2+Hk_{20}} + \frac{4}{2+Hk_{20}}\right] \\
&= \frac{2+Hk_{20}}{2+Hk_{20}+Hk_{21}}\left[\frac{Hk_{20}-2-Hk_{20}-2-Hk_{20}+Hk_{20}+4}{2+Hk_{20}}\right] \\
&= 0
\end{aligned} \tag{B.40}$$

Appendix C

Auxiliary results for Chapter 6 - part 1

C.1 Vehicle dynamics: a simulation model for the Real-Time Hardware

According to the experimental setup described in Subsection 6.4.2, the on-board GPS receiver cannot be used in RTK mode: in so doing, it's not possible to guarantee a good accuracy in measuring the vehicle position. For that reason, a model of vehicle dynamics has been developed such to run in real-time on the RTH, in order to validate the distributed coupling protocol (4.6), i.e. the closed loop stability of the vehicular network.

The first dynamic we consider is to describe the intake manifold behaviour; with the assumption that ideal gas law holds in the intake manifold, we have the following equations:

$$\dot{m}_{man} = \dot{m}_{th} - \dot{m}_a \tag{C.1}$$

with m_{man} the mass of air in the intake manifold, $\dot{m}_{th}$ the mass flow rate through the throttle body and $\dot{m}_a$ the mass flow through the intake valve. Then, we have:

$$p_{man} V = m_{man} R T_{man} \tag{C.2}$$

with T_{man} the constant temperature, p_{man} the intake manifold pressure, R the gas constant for air and V the intake manifold volume (see Fig. C.1, top panel). According to [50], the *mass flow rate* $\dot{m}_{th}$ is:

$$\dot{m}_{th} = \frac{C_D A_T p_{bth}}{\sqrt{R T_{bth}}} \gamma^{1/2} \left(\frac{2}{\gamma + 1} \right)^{(\gamma+1)/2(\gamma-1)} \tag{C.3}$$

when the flow is choked, i.e. $\frac{p_{man}}{p_{bth}} \leq \left(\frac{2}{\gamma+1} \right)^{\frac{\gamma}{\gamma-1}}$. In particular C_D is the discharge coefficient, p_{bth} and T_{bth} are the air pressure and temperature before throttle, respectively, $A_T = A_T(\alpha)$ is the reference area, with α the throttle body angle. γ is the ratio of the specific heats if air is both at constant pressure and constant volume. Instead, $\dot{m}_{th}$ is:

$$\dot{m}_{th} = \frac{C_D A_T p_{bth}}{\sqrt{R T_{bth}}} \left(\frac{p_{man}}{p_{bth}} \right)^{1/\gamma} \left\{ \frac{2\gamma}{\gamma - 1} \left[1 - \left(\frac{p_{man}}{p_{bth}} \right)^{(\gamma-1)/\gamma} \right] \right\}^{1/2} \tag{C.4}$$

when the flow is not choked, i.e. $\frac{p_{man}}{p_{bth}} > \left(\frac{2}{\gamma+1}\right)^{\frac{\gamma}{\gamma-1}}$. Note that the product $C_D A_T$ is the effective flow area of the valve assembly, and depends on the throttle angle. Then, according to expressions (C.3) and (C.4), $\dot{m}_{th}$ can be computed both controlling the throttle body angle and measuring the other states.
The second equation we have is to determine the engine dynamics:

$$\frac{d\omega_e}{dt} = \frac{1}{J_e^{'}}\left(T_{net} - T_t^{'}\right) \tag{C.5}$$

where ω_e is the engine speed, T_{net} is the net combustion engine (i.e. the indicated - friction torque), $J_e^{'}$ is the combined engine/wheel rotational inertia (i.e. the vehicle mass and the wheel inertias are referred to the engine side), $T_t^{'} = \frac{1}{\bar{\tau}}\left(T_{sl} + T_{br} + T_{fr}\right)$, where T_{sl} is the torque due to the street slope, T_{br} is the torque due to the brake action and T_{fr} is the torque due to friction (see Fig. C.1), down panel; $\bar{\tau}$ is the total drive-line gear ratio ($\bar{\tau} > 1$; we assume the drive axle is rigid). Note that T_{net} depends on the engine speed ω_e and intake manifold pressure p_{man}, through non-linear functions: we use look-up tables of T_{net} in our model to manage T_{net}. We assume that:

$$v = \frac{r_t \omega_e}{\bar{\tau}} \tag{C.6}$$

i.e. we neglect slip phenomena on wheels. This assumption is common in control practice, as done in [26]. Then, we assume the following vehicle dynamics:

$$\begin{cases} \dot{r}_i = v_i = \frac{r_t \omega_e}{\bar{\tau}} \\ \dot{v}_i = \frac{r_t}{\bar{\tau} J_e^{'}}\left(T_{net} - T_t^{'}\right) \end{cases} \tag{C.7}$$

with r_t the tire radius. The vehicular parameter used in our model have been tuned on real parameters.
In order to guarantee $e_{vel}(t) \rightarrow 0$ when $t \rightarrow +\infty$, with $e_{vel}(t) = v_i(t) - v_{targ}(t)$, with $v_{targ}(t)$ the target speed we have to follow, we consider a low level control action inspired to adaptive control theory [7], [13]. The analytical investigation of this low level controller is beyond the scope of this Subsection and, for the sake of simplicity, we show the controller validation results. The closed loop response with respect to a constant real vehicle speed measurement and $e_{vel}(t)$ are displayed in Fig. C.3, top and down panels, respectively. Moreover, the response with respect to a variable real vehicle speed measurement and $e_{vel}(t)$ are displayed in Fig. C.4, top and down panels, respectively. Note that the importance of using a vehicle dynamics model during the on the road validation increases thanks the application of this model on the Real-Time Hardware (see Fig. C.2): indeed, the latter let us to consider on testing the unmodeled dynamics overlooked in the controller synthesis.

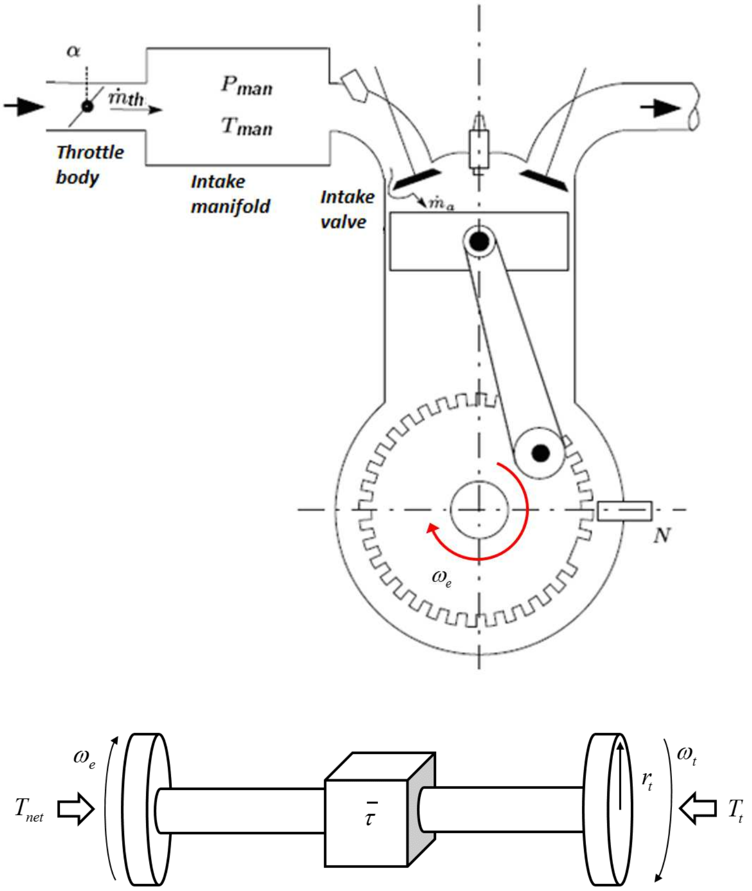
α
$\dot{m}_{th}$
P_{man}
T_{man}
Throttle body
Intake manifold
Intake valve
$\dot{m}_a$
N
ω_e
T_{net}
ω_e
$\bar{\tau}$
r_t
ω_t
T_t

Figure C.1: Vehicle dynamics. Top panel: air path model. Down panel: driveline on RTH.

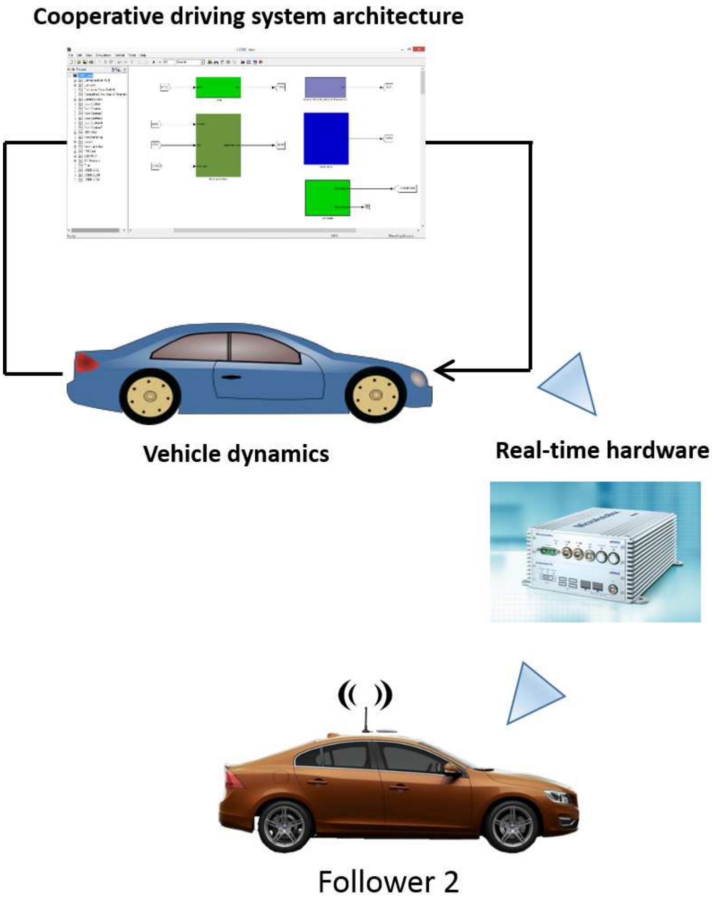
Cooperative driving system architecture
Vehicle dynamics
Real-time hardware
Follower 2

Figure C.2: Vehicle dynamics on RTH.

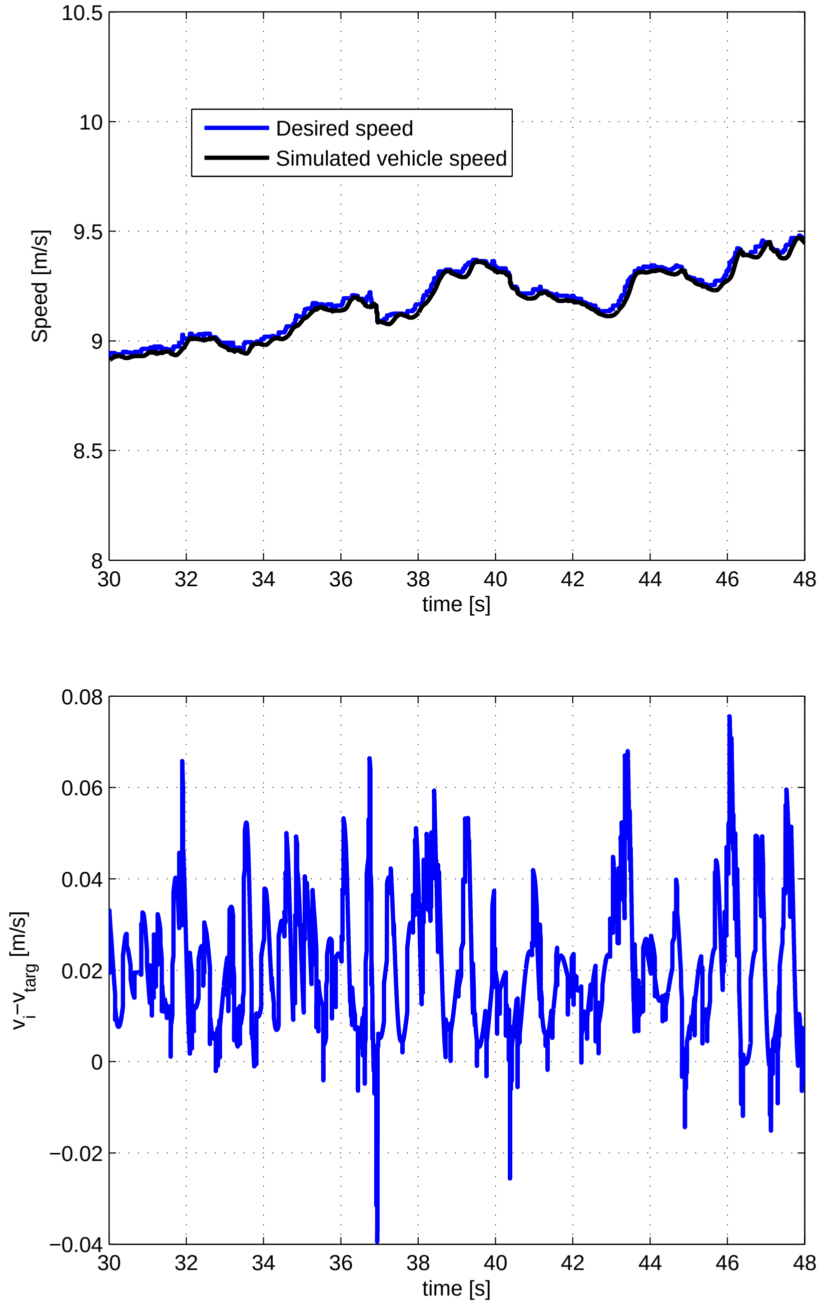

Figure C.3: Low level controller validation. Top panel: constant vehicle speed. Down panel: vehicle speed error with respect to constant vehicle speed.

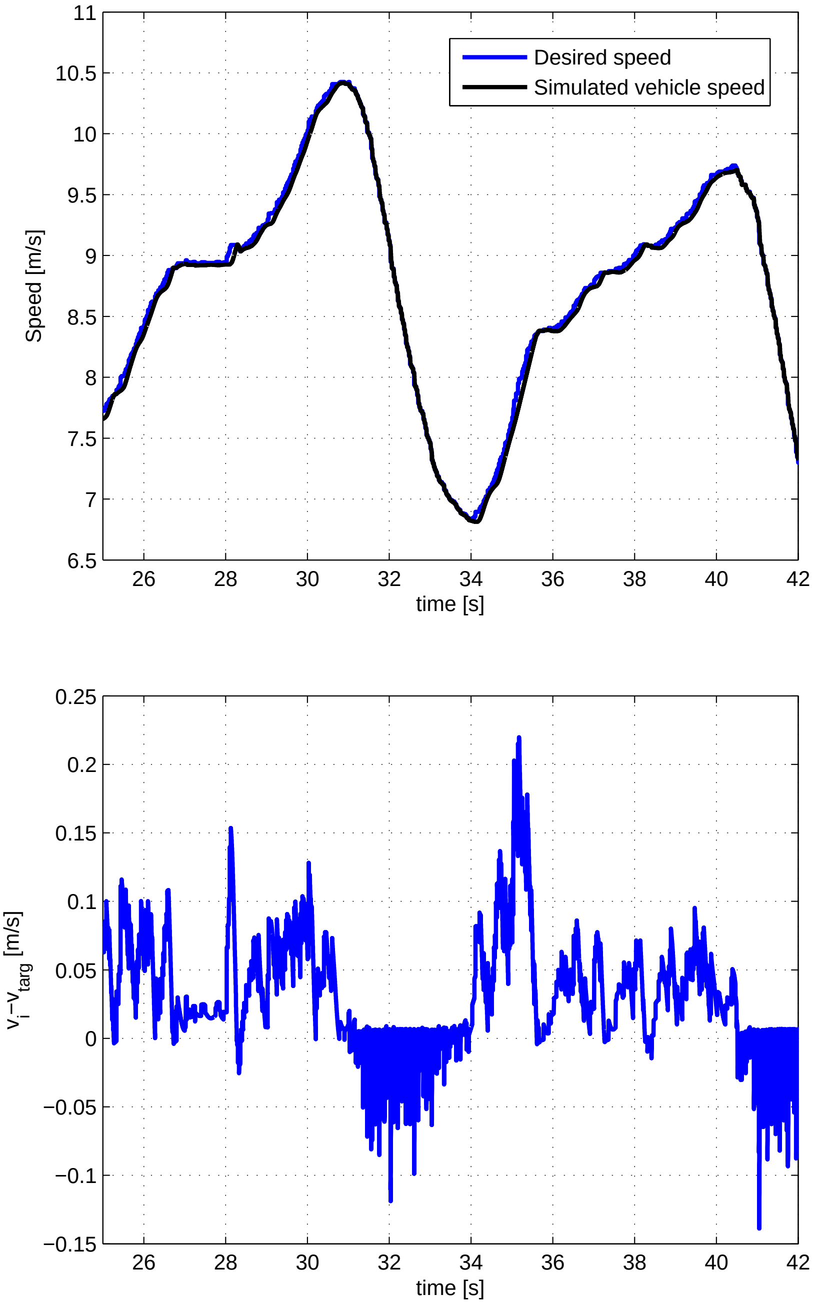

Figure C.4: Low level controller validation. Top panel: variable vehicle speed. Down panel: vehicle speed error with respect to variable vehicle speed.

Appendix D

Auxiliary results for Chapter 6 - part 2

D.1 Global Positioning System: Devices and software solutions

In this appendix we describe more in detail both the devices and the software used to develop the experimental setup. We start describing in Subsection D.1.1 the RTK-GPS used both on the leader and the follower nr.1; then, in Subsection D.1.2 the GPS on-board the follower nr.2 is explained.

D.1.1 RTK-GPS module receiver: Trimble SPS852

GNSS are the principle enabling technology to be used in cooperative driving applications: for example, GPS receivers are essential to provide both the Earth Coordinate Frame and the common global clock in order to perform the best platooning strategy. In order to know the leader and the follower nr.1 position, the experimental setup developed to enable platooning has been equipped with a high precision RTK-GPS (Real-Time Kinematic Global Positioning System) receiver: model Trimble $SPS852$ GNSS Modular Receiver (see Fig.D.1). The module has been used as Real-Time Kinematic GPS (see Chapter 6.6) such to measure:

- accurate longitude and latitude measurement (**horizontal accuracy**: 8 [mm] + 1 ppm RMS; **vertical accuracy**:15 [mm] + 1 ppm RMS; see [53] for details;
- longitudinal acceleration and heading;
- UTC.

In order to modify GPS receiver settings, we can manage either the device or the web interface. Among all the parameters, the *update rate* of the receiver position measurements is one of the most important to be tuned (i.e. 1 [Hz], 2 [Hz], 5 [Hz], 10 [Hz], and 20 [Hz] positioning update rate can be set; see [53] for details). A lot of settings can be managed through the web interface; see Fig.D.3 for a web interface screen-shot. In particular, output signals can be set in a group of several options: the most common data used to provide real time position information is in NMEA format [54] and the

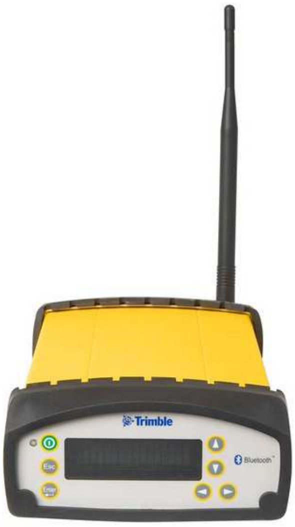
Trimble
Esc
Enter
Bluetooth

Figure D.1: Trimble $SPS852$ GNSS Modular Receiver - Overview.

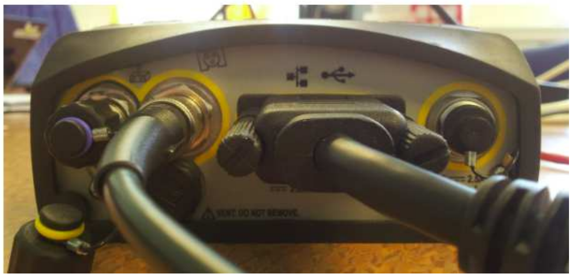

Figure D.2: Trimble $SPS852$ GNSS Modular Receiver - Wiring.

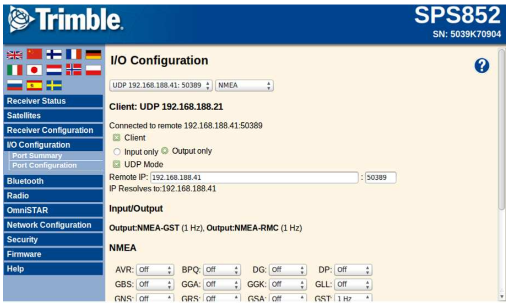
Trimble
SPS852
SN: 5039K70904
Receiver Status
Satellites
Receiver Configuration
I/O Configuration
Port Summary
Port Configuration
Bluetooth
Radio
OmniSTAR
Network Configuration
Security
Firmware
Help

I/O Configuration

UDP 192.168.188.41: 50389 | NMEA

Client: UDP 192.168.188.21

Connected to remote 192.168.188.41:50389

☑ Client

○ Input only ● Output only

☑ UDP Mode

Remote IP: 192.168.188.41 : 50389

IP Resolves to:192.168.188.41

Input/Output

Output:NMEA-GST (1 Hz), **Output:NMEA-RMC** (1 Hz)

NMEA

AVR: Off BPQ: Off DG: Off DP: Off

GBS: Off GGA: Off GGK: Off GLL: Off

GNS: Off GRS: Off GSA: Off GST: 1 Hz

Figure D.3: Trimble $SPS852$ GNSS Modular Receiver - Web interface.

GPS receiver communication applies this specification. In order to measure position, velocity, time etc., NMEA specification includes independent sentences: one sentence differs from the other according to the device class. To have a full detailed description of NMEA sentences see [54]. In our scenario, the RTK-GPS receiver has been set to send the following correctly formatted NMEA sentences:

- GST: GPS Pseudorange Noise Statistics; an example is
  $GPGST,035613.00,2.6,5.8,4.8,36.8,6.2,5.4,20.0*48
  where:
    a) 035613.00 fix taken at $03:56:13.00$ UTC
    b) 2.6 total RMS standard deviation of ranges inputs to the navigation solution
    c) 5.8 standard deviation (meters) of semi-major axis of error ellipse
    d) 4.8 standard deviation (meters) of semi-minor axis of error ellipse
    e) 36.8 orientation of semi-major axis of error ellipse (true north degrees)
    f) 6.2 standard deviation (meters) of latitude error
    g) 5.4 standard deviation (meters) of longitude error
    h) 20.0 standard deviation (meters) of altitude error
    i) *48 checksum
- RMC: recommended minimum data for gps; an example is
  $GPRMC,111526.00,A,5105.024,N,01041.000,E,014.4,076.6,160709,003.5,W*6A
  where:
    a) 111526.00 Fix taken at $11:15:26.00$ UTC
    b) A Status A=active or V=Void
    c) 5105.024,N Latitude 51 deg $05.024'$ N=Nord
    d) 01041.000,E Longitude 10 deg $41.000'$ E=Est
    e) 014.4 Speed over the ground in knots
    f) 076.6 Track angle in degrees True
    g) 160709 Date - $16th$ of July 2009
    h) 003.5,W Magnetic Variation
    i) *6A checksum

The two latter prefix defines the device that uses that sentence type, i.e. GP for GPS. In order to read GPS information via Serial-to-USB connector on the leader vehicle we use the Labview code, as depicted in Fig. D.4. The Virtual Instrument Software Architecture (VISA) is a I/O API used to configure the Serial Interface; the main module is the $GPS\_NMEA.vi$, depicted in detail in Fig. D.5 and Fig. D.6. In Fig. D.5 the Labview code is such to (i) configure the serial port (baud rate, data bits, parity, stop bits and flow control), set the termination character and time-out period for the reading operation; (ii) read the bytes in the buffer to filter $\$GPRMC$ messages. Then, in Fig. D.6 the code unzips the received $\$GPRMC$ message in order to read each field of information in the message.

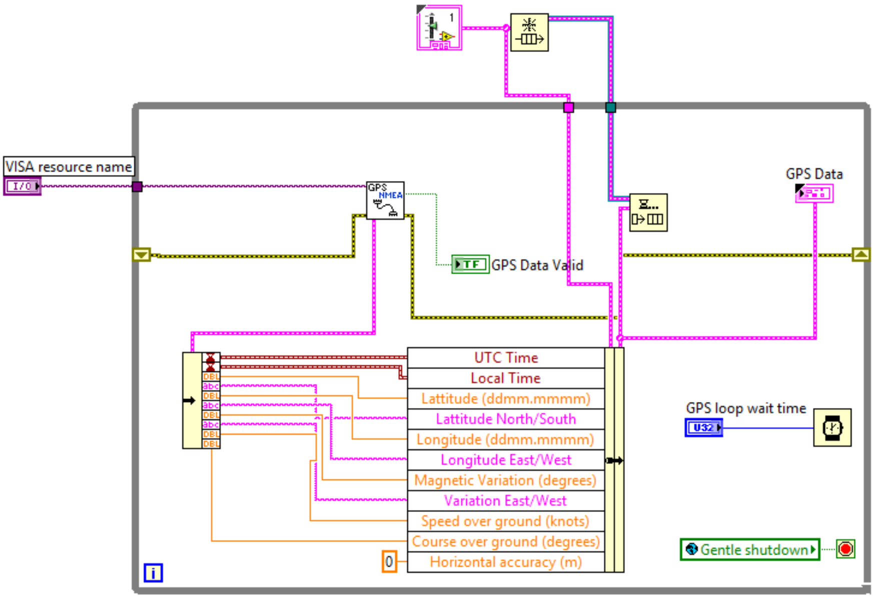
1
VISA resource name
I/O
GPS
NMEA
GPS Data Valid
TF
GPS Data
UTC Time
Local Time
Lattitude (ddmm.mmmm)
Lattitude North/South
Longitude (ddmm.mmmm)
Longitude East/West
Magnetic Variation (degrees)
Variation East/West
Speed over ground (knots)
Course over ground (degrees)
Horizontal accuracy (m)
DBL
abc
0
GPS loop wait time
U32
Gentle shutdown
i

Figure D.4: GPS acquisition module.

D.1.2 GPS module receiver: XSens MTi-G

The XSens MTi-G is a miniature inertial measurement unit (IMU), gyro-enhanced Attitude and Heading Reference System (AHRS), equipped with a low-power signal processor that succeeds to collect lots of information (i.e $3D$ orientation, earth magnetic field and acceleration data) [3]. The MTi-G is used both to estimate (with inertial sensors) and to calculate (gyroscopes) orientation, with the gravity and the earth magnetic field used as reference vectors to compensate the integration drift. The XSens MTi-G model is equipped with an integrated GPS receiver used to collect GPS information, i.e. latitude, longitude, heading, timestamps and so on.
In the experimental setup described in Section 6.4, we use GPS and timestamps in order to compute the follower nr.2 absolute position. In particular, accuracy position (SPS - Standard Positioning Service) is 2.5 [m] CEP (Circular Error Probable).

Definition D.1.1. *Circular Error Probable (CEP) is the radius of a circle containing* 50% *of the individual measurements [4].*

A receiver with an accuracy of 100 meters CEP means that 50% of the time the solution will be correct within a radius of 100 meters and 50% of the time the error will be greater than 100 meters. CEP usually refers to accuracy in the horizontal plane only without regard to vertical (altitude) accuracy.
In order to integrate GPS in the experimental setup on the follower nr.2, a Labview application has been developed. In particular, GPS is connected via Serial-to-USB to a laptop. The latter reads GPS information with the GPS.vi Labview file and, after decoding, forwards data through the Ethernet UDP protocol interface and addressed to the Real-Time Hardware. In order to program the GPS.vi, we modified a previous application file in Labview, provided by National Instrument, such to enable Ethernet

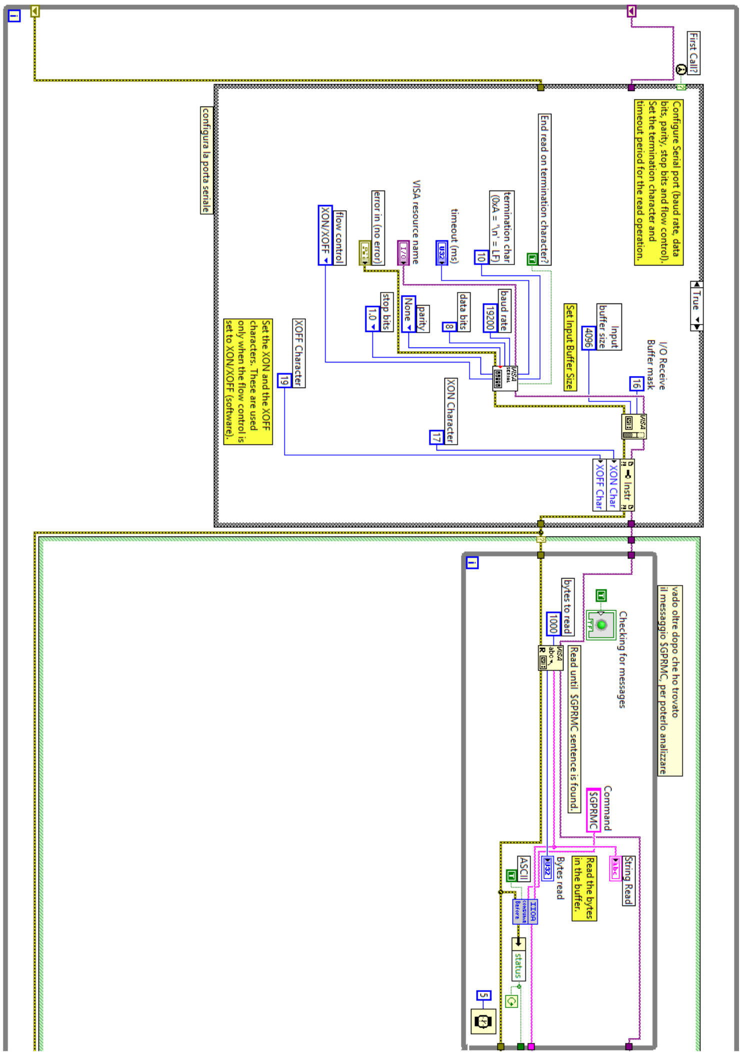
First Call?
True
Configure Serial port (baud rate, data bits, parity, stop bits and flow control). Set the termination character and timeout period for the read operation.
End read on termination character?
termination char (0xA = '\n' = LF)
10
timeout (ms)
VISA resource name
error in (no error)
flow control
XON/XOFF
configura la porta seriale
baud rate
19200
data bits
8
parity
None
stop bits
1.0
Set Input Buffer Size
Input buffer size
4096
I/O Receive Buffer mask
16
XON Character
17
XOFF Character
19
XON Char
XOFF Char
Set the XON and the XOFF characters. These are used only when the flow control is set to XON/XOFF (software).
vado oltre dopo che ho trovato il messaggio $GPRMC, per poterlo analizzare
Checking for messages
bytes to read
1000
Read until $GPRMC sentence is found.
Command
$GPRMC
String Read
Read the bytes in the buffer.
Bytes read
ASCII
status
5

Figure D.5: GPS NMEA module - part 1.

UDP protocol communication. In Fig. D.7 the GPS.vi file front panel is depicted; moreover, in Fig D.8 we can find the GPS.vi block diagram.

D.2 Real-Time Environment

A general overview of the Labview file is described in Subsection D.2.1: this application is running on a laptop such to manage all the devices equipping the experimental setup on the leader vehicle described in Chapter 6.

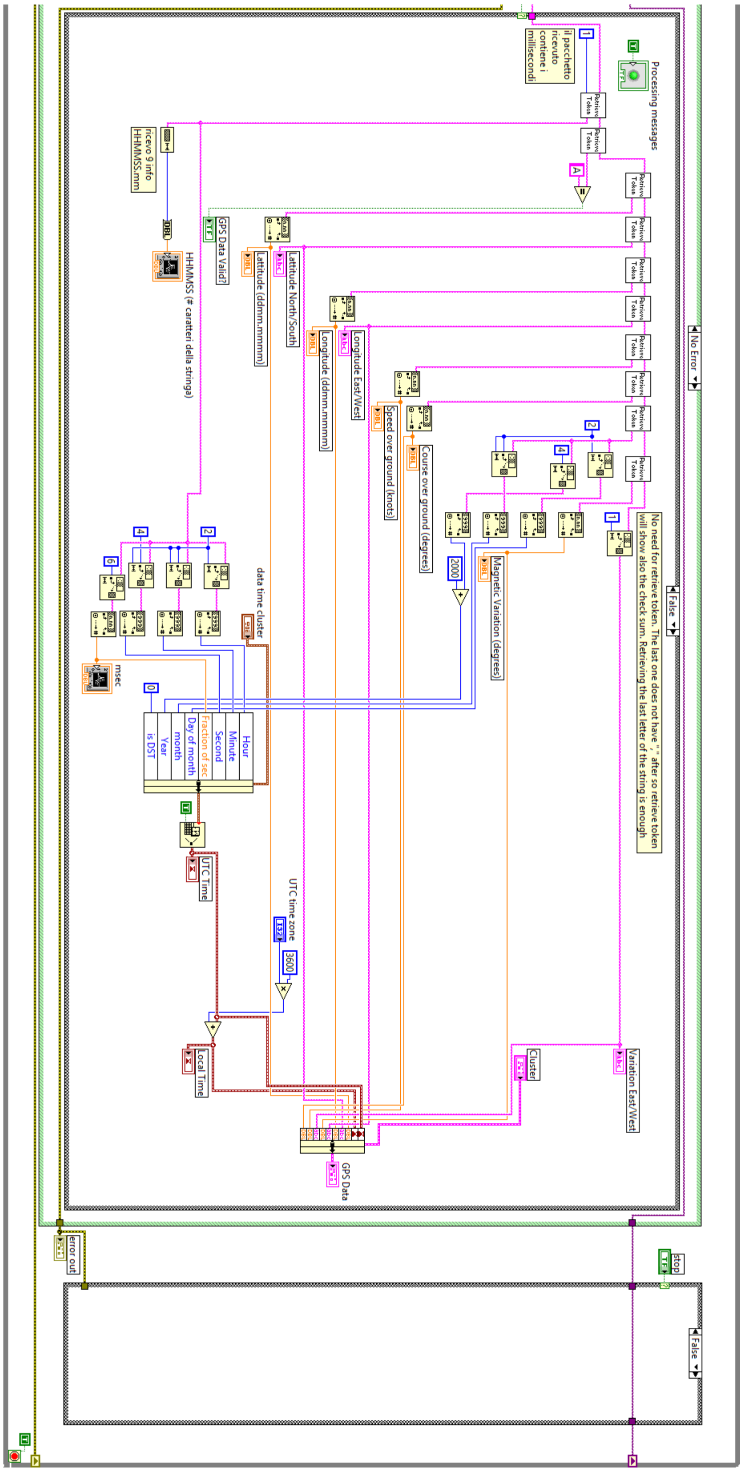
Processing messages
No Error
False
il pacchetto ricevuto contiene i millisecondi
1
A
ricevo 9 info HHMMSS.mm
DBL
HHMMSS (# caratteri della stringa)
GPS Data Valid?
Latitude (ddmm.mmmm)
Latitude North/South
Longitude (dddmm.mmmm)
Longitude East/West
Speed over ground (knots)
Course over ground (degrees)
2
4
2000
Magnetic Variation (degrees)
No need for retrieve token. The last one does not have "," after so retrieve token will show also the check sum. Retrieving the last letter of the string is enough
data time cluster
6
msec
0
Hour
Minute
Second
Fraction of sec
Day of month
month
Year
is DST
UTC Time
UTC time zone
3600
Local Time
Cluster
Variation East/West
GPS Data
error out
stop
False

Figure D.6: GPS NMEA module - part 2.

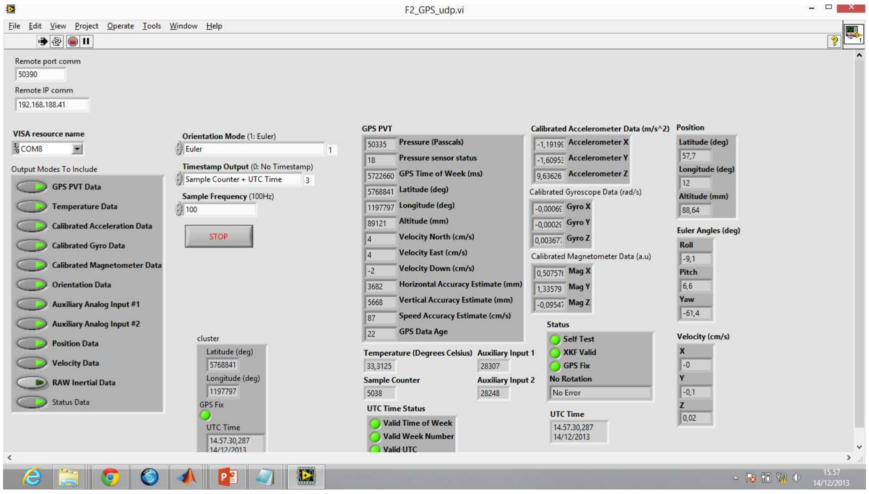

Remote port comm	50390
Remote IP comm	192.168.188.41
VISA resource name	COM8
Orientation Mode (1: Euler)	Euler 1
Timestamp Output (0: No Timestamp)	Sample Counter + UTC Time 3
Sample Frequency (100Hz)	100

Output Modes To Include
- GPS PVT Data
- Temperature Data
- Calibrated Acceleration Data
- Calibrated Gyro Data
- Calibrated Magnetometer Data
- Orientation Data
- Auxiliary Analog Input #1
- Auxiliary Analog Input #2
- Position Data
- Velocity Data
- RAW Inertial Data
- Status Data

cluster

Latitude (deg)	5768841
Longitude (deg)	1197797
GPS Fix	●
UTC Time	14.57.30,287 14/12/2013

GPS PVT

50335	Pressure (Passcals)
18	Pressure sensor status
5722660	GPS Time of Week (ms)
5768841	Latitude (deg)
1197797	Longitude (deg)
89121	Altitude (mm)
4	Velocity North (cm/s)
4	Velocity East (cm/s)
-2	Velocity Down (cm/s)
3682	Horizontal Accuracy Estimate (mm)
5668	Vertical Accuracy Estimate (mm)
87	Speed Accuracy Estimate (cm/s)
22	GPS Data Age

Temperature (Degrees Celsius)	33,3125
Sample Counter	5038
Auxiliary Input 1	28307
Auxiliary Input 2	28248

UTC Time Status
- ● Valid Time of Week
- ● Valid Week Number
- ● Valid UTC

Calibrated Accelerometer Data (m/s^2)

-1,1919	Accelerometer X
-1,6095	Accelerometer Y
9,63626	Accelerometer Z

Calibrated Gyroscope Data (rad/s)

-0,0006	Gyro X
-0,0002	Gyro Y
0,00367	Gyro Z

Calibrated Magnetometer Data (a.u)

0,50757	Mag X
1,33579	Mag Y
-0,09547	Mag Z

Status
- ● Self Test
- ● XKF Valid
- ● GPS Fix

No Rotation
No Error

UTC Time
14.57.30,287
14/12/2013

Position

Latitude (deg)	57,7
Longitude (deg)	12
Altitude (mm)	88,64

Euler Angles (deg)

Roll	-9,1
Pitch	6,6
Yaw	-61,4

Velocity (cm/s)

X	-0
Y	-0,1
Z	0,02

Figure D.7: Front panel of the GPS.vi file.

D.2.1 Labview application on the leader vehicle

The laptop used on the leader vehicle is equipped with a main application that collects on-board information and forwards them to the communication box [36]. In Fig. D.9 the application Front Panel is depicted, while a schematic of the Block Diagram can be found in Fig. 6.5. The front panel is divided in:

- *hardware* section: verifies that the connections with the other devices (GPS, TWG and Communication Box) work as expected;
- *controls* section: useful to manage IP-addresses and ports for communication and for setting the platoon parameters (i.e., Ego vehicle ID, Ego platoon ID);
- *platooning* section: monitors requests for joining from the vehicles in the platoon;
- *communication* section: displays all the vehicle ID in the communication range that are sending out information;
- *maneuver requests* section: used to share requests with the followers.

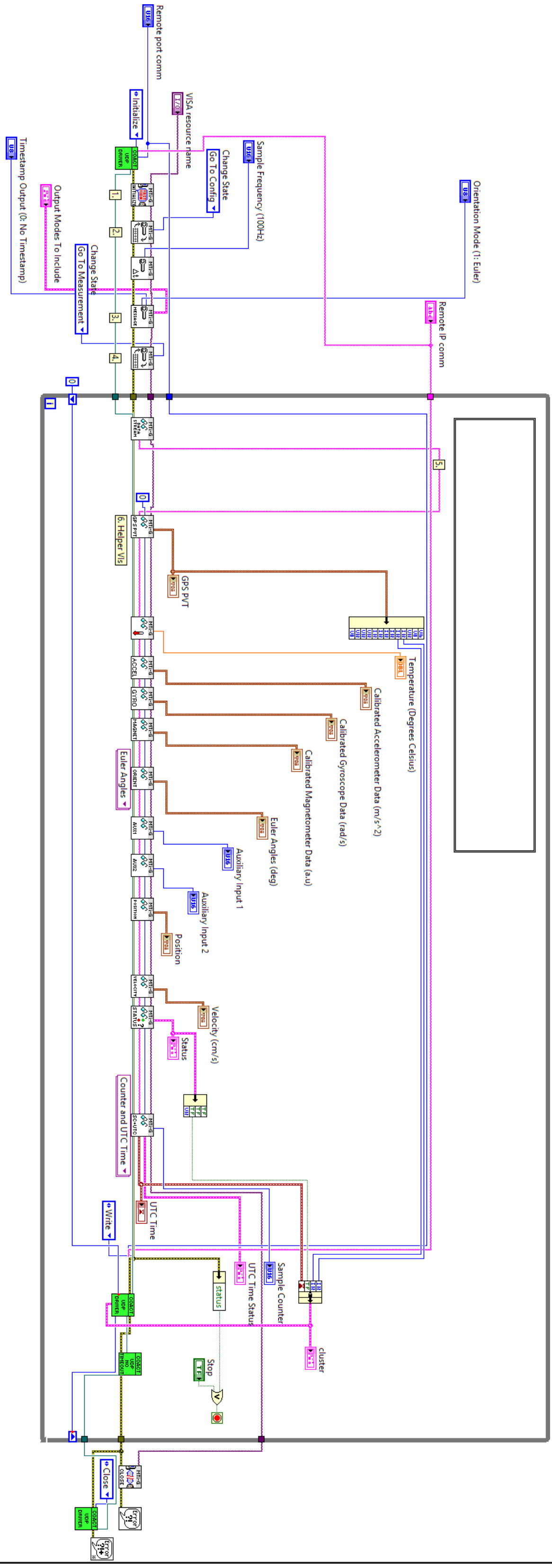
Remote port comm
Initialize
VISA resource name
Change State
Go To Config
Sample Frequency (100Hz)
Timestamp Output (0: No Timestamp)
Output Modes To Include
Change State
Go To Measurement
Orientation Mode (1: Euler)
Remote IP comm
1.
2.
3.
4.
5.
6. Helper VIs
GPS PVT
Temperature (Degrees Celsius)
Calibrated Accelerometer Data (m/s^2)
Calibrated Gyroscope Data (rad/s)
Calibrated Magnetometer Data (a.u)
Euler Angles
Euler Angles (deg)
Auxiliary Input 1
Auxiliary Input 2
Position
Velocity (cm/s)
Status
Counter and UTC Time
UTC Time
UTC Time Status
Sample Counter
status
Stop
cluster
Write
Close

Figure D.8: Block diagram of the GPS.vi file.

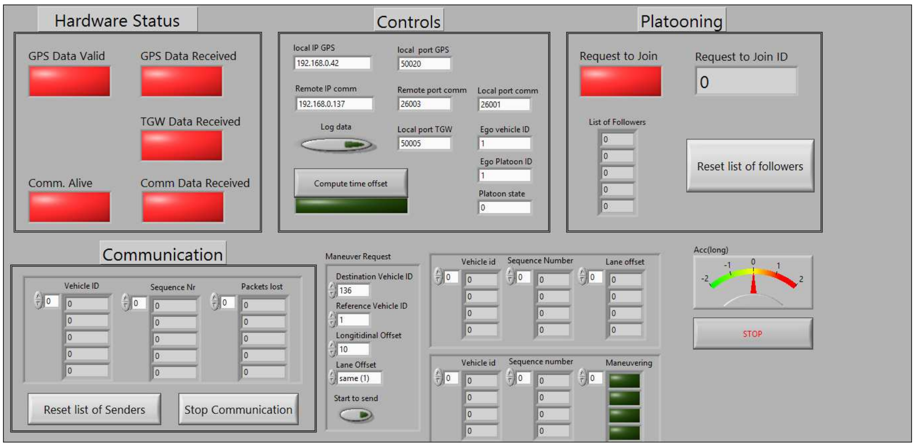
Hardware Status
GPS Data Valid
GPS Data Received
TGW Data Received
Comm. Alive
Comm Data Received
Controls
Log data
Compute time offset
Platooning
Request to Join
List of Followers
Reset list of followers
Communication
Vehicle ID
Sequence Nr
Packets lost
Reset list of Senders
Stop Communication
Maneuver Request
Start to send
Vehicle id
Sequence Number
Lane offset
Vehicle id
Sequence number
Maneuvering
Acc(long)
-2
-1
0
1
2
STOP

local IP GPS: 192.168.0.42
local port GPS: 50020
Remote IP comm: 192.168.0.137
Remote port comm: 26003
Local port comm: 26001
Local port TGW: 50005
Ego vehicle ID: 1
Ego Platoon ID: 1
Platoon state: 0
Request to Join ID: 0
Destination Vehicle ID: 136
Reference Vehicle ID: 1
Longitidinal Offset: 10
Lane Offset: same (1)

Figure D.9: Front panel of the main application.

Appendix E

Auxiliary results for Chapter 7

E.1 Further details on the Additional Communication module

One of the main topic in cooperative control is to manage the relative distance between one vehicle and its predecessor. The radar measurements are used on-board such to control the vehicle dynamics (see Fig. E.1); however, if a problem occurs on the radar measurement (i.e. relative distance Electronic Control Unit failure) or another vehicle is between the follower and the leader, the absolute position of the predecessor has to be known, such to compare it and the absolute position of the considered vehicle, in order to compute the relative distance between the vehicles as the *difference* of two absolute position (see Fig. E.2). Then, the position information collected by GPS are more and more important if we consider two following vehicles moving on a road in the presence of corners. In so doing, Vehicle-to-Vehicle (V2V) communication plays a major role in sharing the predecessor GPS position. Then, an arising problem is the effect due to the packet delays in V2V when computing the relative distance between vehicles. Moreover, another hot topic is the position accuracy measured on the GPS receiver.

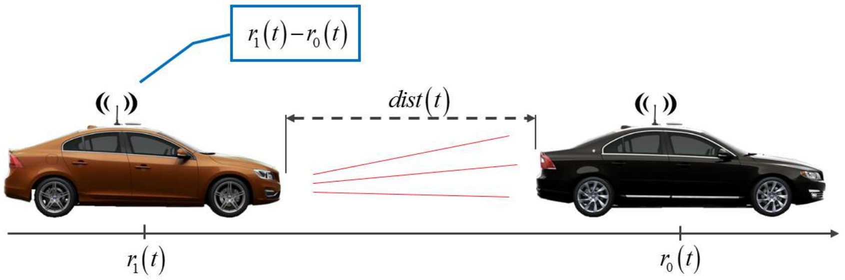

Figure E.1: Relative distance between the centers of mass of two following vehicles computed at time ”t” in an on-board sensors configuration; we use radar technology.

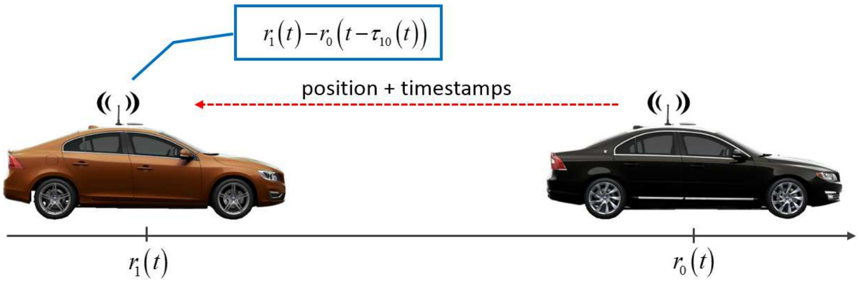
$r_1(t)-r_0(t-\tau_{10}(t))$
position + timestamps
$r_1(t)$
$r_0(t)$

Figure E.2: Relative distance between the centers of mass of two following vehicles computed at time "t" in a V2V configuration; we use GPS receivers, V2V technology and radar.

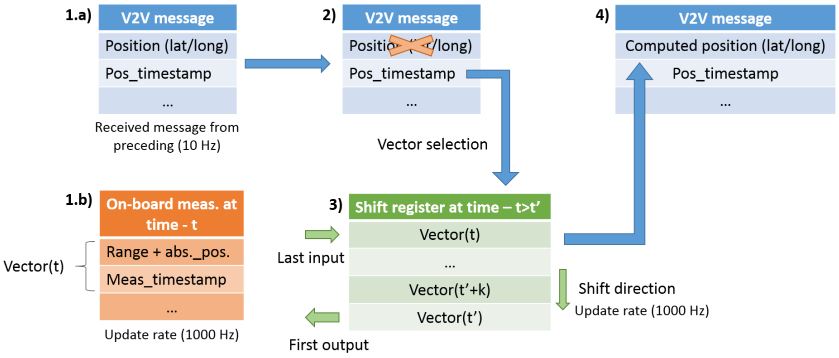
1.a)
V2V message
Position (lat/long)
Pos_timestamp
...
Received message from preceding (10 Hz)
2)
V2V message
Position (lat/long)
Pos_timestamp
...
Vector selection
4)
V2V message
Computed position (lat/long)
Pos_timestamp
...
1.b)
On-board meas. at time - t
Vector(t)
Range + abs._pos.
Meas_timestamp
...
Update rate (1000 Hz)
3)
Shift register at time – t>t'
Last input
Vector(t)
...
Vector(t'+k)
Vector(t')
First output
Shift direction
Update rate (1000 Hz)

Figure E.3: Reconstruction of the predecessor absolute position in the presence of a low accurate GPS measurements.

E.1.1 Position reconstruction with low level accuracy measurements

In order to avoid the usage of low level position measurements accuracy to compute the distributed coupling protocol (4.6), we developed a software module in the main application running on the RTH of the follower nr.1 and follower nr.2, i.e. the *Additional Communication* module (see Fig. 6.2): this software module lets the follower nr.1 of computing on-board the absolute leader position, using both the on-board GPS measurements (we assume the on-board GPS has an high level accuracy in position measuring), the on-board radar measurements and timestamps measurements from the leader (see Fig. E.4). In Fig. E.3 we find a general description of the path followed by the *Additional Communication* module to reconstruct the predecessor position. In particular, the follower nr.1 receives a message via V2V and containing the leader information (step 1.a)): the information about the position of the leader inside the message is discarded due to the low level accuracy (step 2)). A parallel task runs in order to compute on-board the predecessor position (step 1.b): this timestamped information is stored in a shift register that keeps in memory it for a precise time interval (larger than

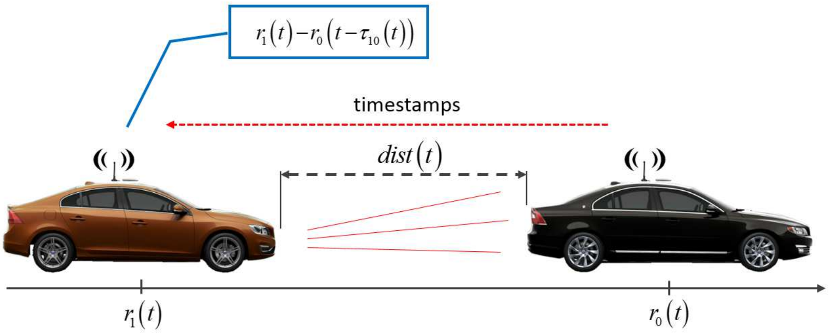

Figure E.4: Relative distance between the centers of mass of two following vehicles computed at time "t" in a V2V configuration (low level GPS accuracy on the leader); we use GPS receivers and V2V technology.

the maximum admissible communication delay) before deleting it. Then, the computed predecessor position is selected in the shift register according to the timestamp value in the received V2V message (step 3)) such to have the right predecessor position (step 4)) at the desired timestamp.
In order to validate this software module, received GPS information from the leader vehicle to the follower nr.1 are compared with the output of the **Additional Communication** module. A comparison between *measured* and *computed* leader position is in Fig. E.5. Moreover, in Fig. E.7 is shown the distance between the measured (with low accuracy) and computed leader position. More in detail, we compute the position errors in Fig. E.6, top and down panel respectively. Finally, we have the computed packet delay in Fig. E.8.

Remark E.1.1. In Fig. E.5, we underline that the measurements switch on different constant values (i.e. blue line), and the computed value (i.e. red line) follow this switching behaviour with a fixed time delay (i.e. about 6 [ms]): this is due to the time the **additional communication** module needs for computing the packet delay $\tau_{ij}(t)$. This delay can be compensated with a fixed constant time.

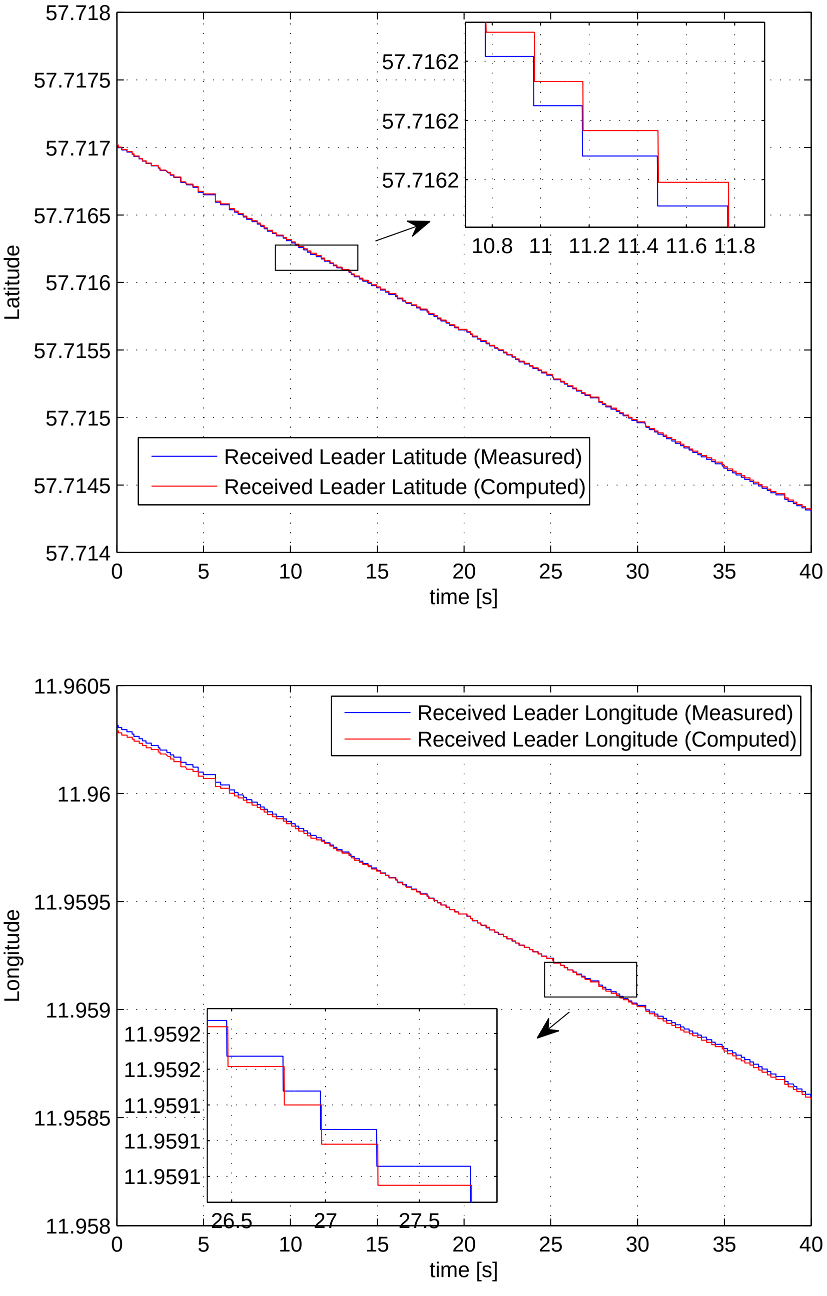

Figure E.5: Comparison between measured and computed received leader position information.

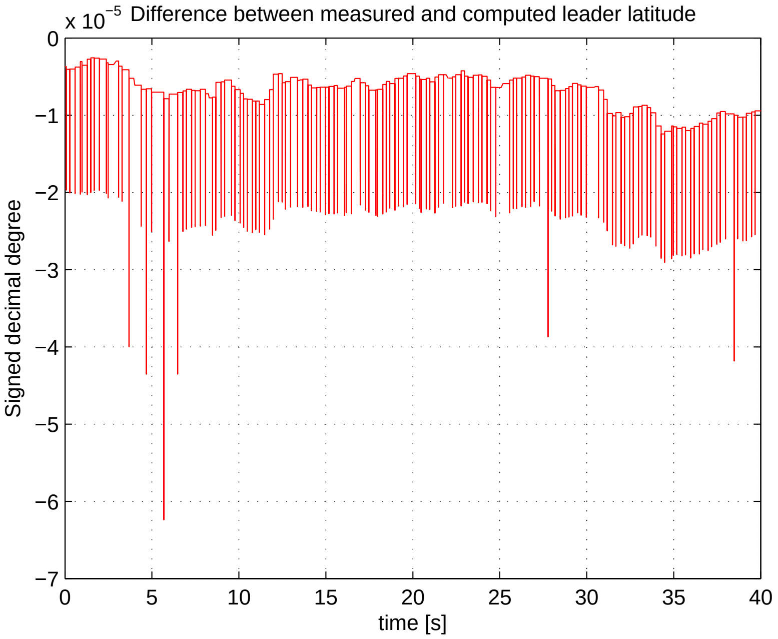

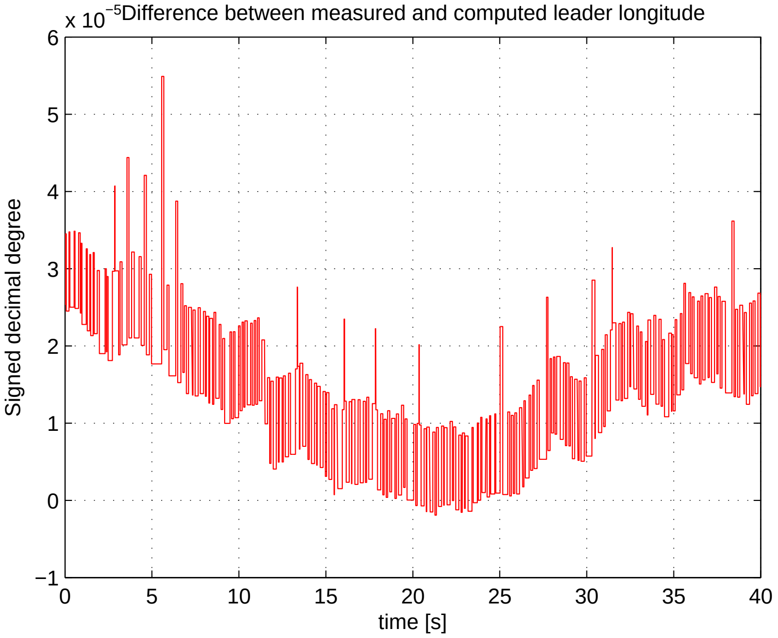

Figure E.6: Leader difference position error.

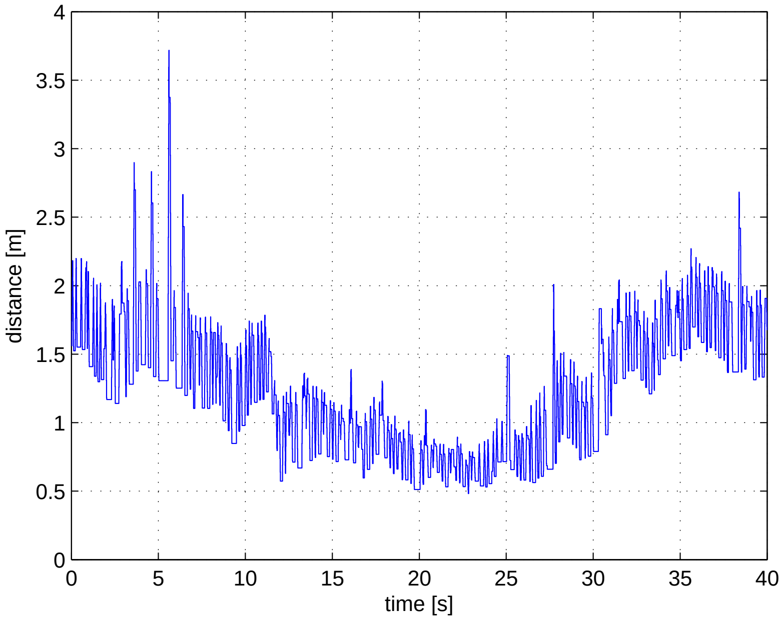

Figure E.7: Relative distance between measured and computed leader position.

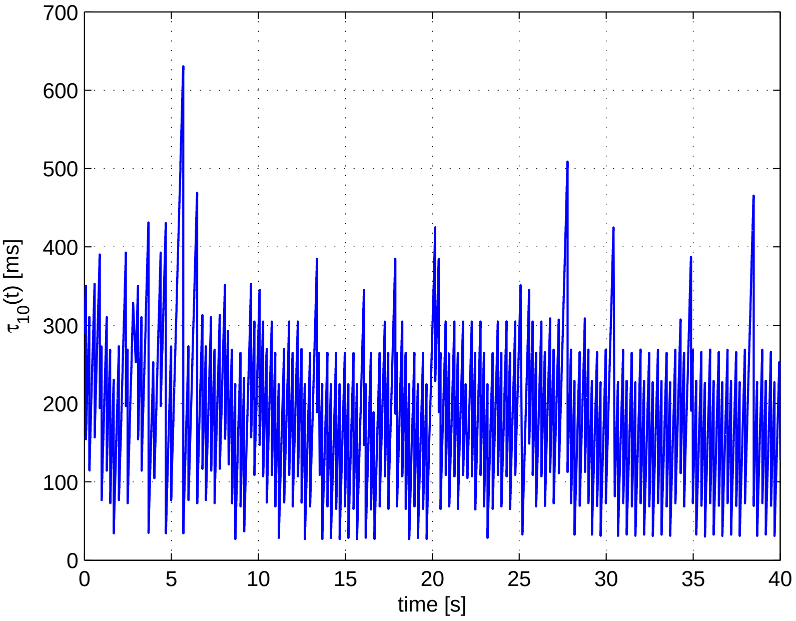

Figure E.8: Received packet delay.